Spring 1991

Two-Dimensional Heat Loss From a Building Slab Including Convective Effects in Saturated Soil

William W. Rust III
Old Dominion University

TWO-DIMENSIONAL HEAT LOSS FROM A BUILDING SLAB INCLUDING CONVECTIVE EFFECTS IN SATURATED SOIL

by

William W. Rust, III
B.S.M.E., February 1972, Purdue University
M.E. (Mechanical Engineering), December 1981, Old Dominion University

A Dissertation Submitted to the Faculty of
Old Dominion University in Partial Fulfillment of the
Requirements for the Degree of

DOCTOR OF PHILOSOPHY

MECHANICAL ENGINEERING

OLD DOMINION UNIVERSITY
March 1991

Approved By:

A. Sidney Roberts, Jr. (Director)

Surendra N. Tiwari

Robert L. Ash

John J. Sweits

Ronald N. Jensen

ABSTRACT

TWO-DIMENSIONAL HEAT LOSS
FROM A BUILDING SLAB INCLUDING CONVECTIVE EFFECTS
IN SATURATED SOIL

William W. Rust, III
Old Dominion University, 1991
Director: A. Sidney Roberts, Jr.

The heat loss from a building slab was investigated. The continuity equation, Darcy's Law and the energy equation were formulated to include the temperature dependence of viscosity and density of water. The governing equations and appropriate boundary conditions were transformed into dimensionless variables. A finite difference numerical scheme was constructed based on the Gauss–Seidel method by lines and solved iteratively in alternating directions. A correlation between the geometrical characteristics of the domain, the convective surface heating parameters, and the total nondimensional slab heat loss in two dimensions was discovered. Furthermore, the correlation was extended to three–dimensional slabs and produced good agreement with analyses by other workers using different methods. Numerical results were validated by comparison with a proprietary finite element solver in two dimensions. Moreover, a scaled laboratory simulation of building slab heat loss was conducted. The agreement between the numerically predicted heat loss and the experimental results was good for solid media. For porous media, the

apparent thermal conductivity for both dry and saturated media was measured and found to be in consonance with data produced by others. The observed dye tracer positions in the flow visualization confirmed the predicted positions. The results of the experiments indicated that: the volume averaged method of computing apparent thermal conductivity of the porous media was inadequate and experimentally determined conductivity should be used; and, the time required for a particle to transit a fixed path in the porous media is independent of the thermal conductivity of the media. Finally, the numerical model was extended to include surface evaporation at the earth interface. Surface evaporation increased slab heat transfer by approximately ten percent compared to a non-evaporating surface condition.

DEDICATION

This work is dedicated to my family, without whose support this would not have been possible: to my wife, Marcella, and our children, Mary, Catherine and Anne; and to Marcella's parents, Dr. and Mrs. J. W. Shreve. Finally, I dedicate this to my mother, Mrs. Kathleen Rust and to the memory of my late father, Mr. Walt Rust.

ACKNOWLEDGEMENTS

I would like to express my appreciation to my advisor, Dr. A.S. Roberts, Jr., for his unflagging support and guidance through the course of this project. I furthermore would like to thank the members of the guidance committee, Dr. Robert L. Ash, Dr. Surendra N. Tiwari, Dr. John J. Swetits, and Mr. Ronald N. Jensen for their assistance and helpful suggestions. I appreciate the assistance of Dr. Joseph H. Rule for his technical advise on the experiment construction, Dr. A.O. Akan for reviewing the manuscript of Chap. 3, and Dr. Arthur Taylor for reviewing the manuscript of Chap. 4. I am grateful to the American Society of Heating, Refrigerating, and Air Conditioning Engineers for the award of a 1989 ASHRAE Grant-in-Aid in support of this research project.

TABLE OF CONTENTS

LIST OF TABLES

LIST OF FIGURES

NOMENCLATURE

a	=	Ratio defined by Eq. (5.18) or a slab plan dimension
b	=	Slab plan dimension
A	=	Cylinder cross sectional area
$\overline{A}_{void}$	=	Average void area in cross section of Reprsentative Elementary Volume (REV)
Bi	=	Biot number = hL/λ
c	=	Specific heat
c_p	=	Specific heat at constant pressure
d	=	Diameter of glass beads
Da	=	Darcy number
$\mathbf{e}$	=	Unit vector aligned with force of gravity
$\mathbf{g}$	=	Gravity acceleration vector
g	=	Acceleration of gravity
h	=	Heat transfer or film coefficient
K		Fluid Conductance or proportionality constant
k	=	Permeability, m^2, defined by Ergun formula = $d^2n^3/(175(1-n)^2)$
L	=	Characteristic length of slab
l	=	Length dimension
$\hat{\mathbf{n}}$	=	Surface normal vector
n	=	Porosity
n_a	=	Average areal porosity

n_a = Areal porosity

P = Pressure

Q = Total heat loss transmitted through media

q = Total heat flux per unit width of Slab transmitted thorough media = Q/w

q_{crust} = Heat Flux (W/m^2) released from crust

q_{cfs} = Crustal Flux strength = $\pi q_{crust} L/\lambda\Delta T$

q_{vf} = Volumetric flow rate

Ra = Rayleigh number = $Lk\rho_f^2 c_f g\beta\Delta T/(\lambda_{eq}\mu)$

r = Cooling factor, defined by Eq. (5.25)

Ste = Stefan number = $c_p\Delta T/h_{fg}$

T = Temperature

t = Time

U = Heat loss coefficient, W/m^2–deg K

U = Velocity in X direction

u = Nondimensional velocity in X direction = U/V_0

V = Volume

V = Velocity in Y direction

V_{pore} = Volume averaged pore velocity

v = nondimensional velocity in Y direction = V/V_0

V_0 = reference velocity = $\lambda/(\rho c)_f L$

w = width of slab

X = Horizontal direction

x = Nondimensional horizontal direction = X/L

Y = Vertical direction

y = Nondimensional vertical direction = Y/L

z = Datum height

Greek

β = Coefficient of thermal expansion

Γ = Boundary of region

γ = Specific weight

Δ = Difference

Δ_i = Defined by equation (4.16)

ϵ = Random Number

Θ = Nondimensional temperature

= $(T - T_2)/(T_1-T_2)$

λ = Thermal conductivity

λ_{eq} = Volume averaged thermal conductivity

ν = Kinematic viscosity

μ = Dynamic viscosity

ρ = Density

τ = Characteristic time

ω = Humidity ratio

Ω = Relative Humidity

Φ = Pressure potential function

φ = Mechanical potential function

ψ = Streamfunction

German

$\mathfrak{R}$ = $k(\rho_r c)_f gL/\lambda_{eq}\nu_r$

Subscripts

d	=	Dynamic
eq	=	equivalent or apparent
i,j,k	=	indices
f	=	fluid
p	=	periodic
r	=	reference
s	=	Static or steady
w	=	Water Table
$_1$	=	interior temperature
$_2$	=	exterior temperature
$_\infty$	=	Free stream condition

Superscripts

*	=	Indicates nondimensional variable or operator

Chapter 1

INTRODUCTION

1.1 Motivation for Building Research

Buildings currently consume thirty-six percent of the annual energy production in the United States. Furthermore, building fossil fuel consumption has placed an annual carbon load of 500 million tons on the atmosphere (Bevington and Rosenfeld, 1990). The long term effects of atmospheric carbon on global climatic patterns is cause for concern.

The national economy is very sensitive to fuel shortages. The fossil fuel supply is limited, and scarcity of fuel supplies has become more noticeable through the past several decades. By 1970, two percent of coal reserves and fourteen percent of the world's petroleum reserves had been exhausted with demand continuing to climb (File and Considine, 1977). Moreover, a major source of fuel is located in areas of the world where political instability is common. By 1990, the United States had experienced two fuel embargoes, two fuel related recessions, and a fuel related war.

The conservation of fuel requires a thorough understanding of the process of building heat loss if meaningful energy reduction is to be accomplished. For example, the national contribution of building heat loss in direct earth-contact is estimated to be approximately one to three quadrillion kilojoules annually (Claridge, 1988). Earth-coupled

heat loss from a building is an important mode which is frequently overlooked. However, as architectural and mechanical improvements are made to the building envelope, the heat lost to the ambient from below grade will become a larger fraction of the total. The motivation for this work is, therefore, to gain additional insight into the process of earth-coupled building heat transfer.

1.2. Thrust and Objectives

The thrust of this study will be to examine building earth-coupled heat loss under steady conditions, specifically focusing on the slab type of construction. Since the presence of water in soil has a strong impact on soil thermal properties (Hart and Couvillion, 1986), the effects of water and water movement will be included in the analysis.

The main objective is, therefore, to predict the steady heat loss from a building slab under a variety of physical conditions. To accomplish this objective, a literature review is performed in Chap. 2, thus defining the scope of the problem.

The solution of earth-coupled heat loss from a slab is dependent on the way the problem is cast mathematically. To retain broad applicability, the interaction of heated surfaces subject to fluctuating weather conditions at the earth surface is examined in Chap. 3. Appropriate mathematical modeling simplifications are justified based on geophysical conditions.

To capture the essence of the steady heat transfer problem from the building slab, the porous nature of soil and its ability to conduct water must be explored. A brief review of porous media literature and

terminology is introduced in Chap. 4. The governing fields equations are placed in nondimensional form suitable for numerical computation.

The nonlinear field equations developed in Chap. 4 must be solved numerically. Chapter 5 examines the numerical methods for solving the field equations subject to the appropriate boundary conditions. Solutions of test cases are compared to other methods of solution. A Shape Factor method for solving slab heat loss problems is introduced and developed.

The results of Chap. 5 are verified by experimental simulation in Chap. 6. The methods used to construct the experiment and to collect data are presented. Good agreement was obtained between the experimental and numerical results.

Chapter 7 extends the mathematical model to the more general case of an earth surface that permits the evaporation of water. Numerical results for the case under study indicate an increase in heat loss due to surface evaporation.

Chapter 8 is an overview of findings in this report and concluding remarks.

1.3 Presentation

To facilitate the presentation of this topic, especially for the benefit of the reader who is unfamiliar with porous media terminology, the material is introduced and discussed in a contiguous manner in each chapter. Detailed supporting calculations are presented in the appendices. Graphical representations are presented as concisely as possible, and all units are nondimensional unless otherwise noted. Horizontal and vertical distances and coordinates of points in the

computational plane have been normalized with respect to a characteristic slab dimension (slab length). Mathematical symbols are defined directly in the text or the list of Nomenclature.

Chapter 2

THE BUILDING EARTH-COUPLED HEAT LOSS PROBLEM

2.1 Literature Review

In general, the computation of heat transfer to the earth must include the effects of water. One method often employed is to lump the thermophysical properties of water into the properties of soil. A second method is to explicitly include the contribution of the motion of the water in the soil to the heat transfer process. The second method is much more complex, especially when water transport as vapor is modeled. The heat transfer literature that can be applied to earth-coupling therefore consists of diverse works roughly falling into three categories: Design Oriented Earth-Coupled Heat Transfer (no water motion); Saturated Porous Media Heat Transfer (includes water motion); and, Partially Saturated Porous Media Heat Transfer (includes diffusion effects of vapor and air). The relevant literature from these areas will be reviewed to provide guidance in capturing the features that are important in modeling heat loss from buildings through the earth. An archetypical building design condition will be established so that numerical modeling and simulation is possible.

2.1.1 Design Oriented Earth-Coupled Heat Transfer

The computation of ground or earth-coupled heat loss has been attempted with varying degrees of success. An extensive review of the

literature of earth-coupled heat transfer was done by Claridge (1988). Several methods cited offer a heuristic approach for two general types of construction, i.e., slab-on-grade or basement construction. Seasonal heat loss from slabs can be estimated using the formula developed by Wang (1979) and Bligh et al. (1978) (ASHRAE, 1989) which states that the heat loss is directly proportional to the temperature difference between the mean ambient temperature and the room temperature and a loss coefficient (which is a function of climatic conditions) per unit length of perimeter. Dubin and Long (1978) state that the heat loss from a slab is essentially concentrated around the edge of the slab. No method was suggested for computing the loss. However, a nomogram for suspended floors was presented.

Lachenbruch (1957) used Green's Functions to solve the three-dimensional periodic problem for a slab-on-grade by using graphical techniques. Kusuda et al. (1983) and Kusuda and Bean (1984) computerized the solution by Lachenbruch but experienced difficulties with the discontinuity at the wall. Delasante et al., (1983) resolved the temperature discontinuity at the wall by assuming a linear temperature profile across the wall. Their results agreed with those of Kusuda and Bean (1984) when the depth defined to evaluate the heat flux from the slab was the same depth as Delesante's (1983) wall thickness (Claridge, 1988).

Bahnfleth and Pedersen (1990) conducted a three-dimensional numerical study on an "L" shaped slab. For this set of computations, they found that the correct parameter for measuring heat flux was the ratio of area to perimeter. They also conclude that soil thermal conductivity and ground surface conditions had a strong influence on

slab flux, but far field boundary conditions were relatively unimportant. Bahnfleth and Pedersen (1990) suggest that an arbitrary three-dimensional plane slab can be modeled by using a two dimensional slab with the same area/perimeter ratio.

Slab-on-grade heat loss can also be a heat gain in warmer seasons. Qualitative observations by Cleveland and Akeridge (1990) of a slab on grade house in Georgia indicate that heat gain through an uninsulated slab is a significant factor. Thermal Monitoring experiments on a full scale building simulation in Tennessee are in progress to determine the effectiveness of edge insulation for slab-on-grade construction (Christian et al., 1990).

Basements add another element of complexity to the way heat flux must be calculated. Boileau and Latta (1968) developed a steady state solution method based on heat flux following approximately circular paths from basement floors and walls. Mitalas (1982, 1983) used heat flux computed from a finite element program and constructed shape factors for basement geometry and used regression coefficients to fit the computed data (Claridge, 1988).

Krarti et al. (1985) used a convective condition inside the house and a periodic sinusoidal condition on the ground surface to study seasonal effects. The solution is decomposed into a steady solution and a periodic solution determined by physical parameters and a so-called disturbance depth (Claridge, 1988).

Krarti and Claridge (1988) developed a method of solving basement problems using the "Interzone Temperature Profile Estimation" (ITPE). This method consists of representing the soil surface temperature by a Fourier Series with as many terms as necessary to adequately represent

actual conditions. The ground coupling configuration is an analytic expression for the shape of the structure. The ground coupling configuration (based on physical size and shape of the ground structure) is chosen and a series of Fourier coefficients are calculated. These coefficients are used to derive heat loss functions for each harmonic. This eventually yields the heat loss for the ground structure as a function of time.

Shen et al. (1988) compute the ground losses by defining the ground temperature as the sum of a steady state and a periodic temperature. The heat flux is then the sum of the steady state flux and the periodic heat flux adjusted by an appropriate phase angle for each point in the field. Nondimensional thermal quantities were formed using various combinations of outside temperature, deep ground temperature, and inside temperature, but this proved to be of little use. Climatic data was still required for the numerical simulations.

Buildings clearly lose heat to the environment by earth-coupled effects. Of the methods described above, each uses the heat conduction equation to derive a solution for a particular subterranean structure. The effect of water is recognized a component that strongly influences the thermal conductivity, density and heat capacity of soil. Yet, on the whole, the transport of water during the heat transfer process is neglected. Bahnfleth and Pedersen (1990) cite Eckert and Pfender (1978), noting that there is weak coupling between heat and mass transfer in soil under typical conditions near a building.

2.1.2 Saturated Porous Media Heat Transfer

The general development of the theory of porous media flow can be traced to experimental work by Darcy (1856) in unconsolidated sand beds. Darcy's experimental work was placed on a sound theoretical foundation by Hubbard (1940). Cheng (1978) traces the continuing work in fluid flow and geothermal heat transfer as reviewed by Elder (1966), Bear (1972) and Witherspoon et al. (1975) and Combarnous and Bories (1975). Fulks et al. (1971) develops the equations for fluid motion in a porous media. Bear (1972) uses microscopic and macroscopic analysis of porous media and develops the three conservation equations. Cheng (1978) also uses a direct application of volume averaging to devise the conservation equations for porous media. Ene and Polisevski (1987) developed a method of homogenization whereby initial and boundary value problems for a domain with periodic structure (porous media) are determined by means of asymptotic expansions of the governing equations in terms of a small parameter. This method is applied to saturated media and multiphase flow.

A large body of work exists studying the flow of saturated fluid in porous media, particularly when dealing with the stability of a fluid when heated from below. The onset of convection was originally studied by Bernard (1900) for a fluid film (Drazin and Reid, 1981). Lapwood (1948) was the first to apply this analysis to saturated porous media. Combarnous and Bories (1975) establish the criteria for the onset of circulation in a porous media. Ene and Polisevski (1987) apply the homogenization technique to Lapwood's problem and arrive at his classical result.

Other configurations have been considered. Bejan (1987) shows the results of natural convection in an infinite saturated porous media for heated horizontal and vertical plane surfaces and cylinders. Gebhart et al. (1988) present the solution of Cheng and Chang (1976) and employ similarity methods to solve a semi-infinite natural convection problem in saturated porous media when heated from the top surface.

In another application, ground heat loss from a two dimensional solar pond was calculated for uniform ground water motion by Duyer and Bober (1984). The location of the water table beneath the solar pond strongly affected the heat loss from the pond.

2.1.3 Partially Saturated Porous Media Heat Transfer

The more general problem of flow of different phases and species in porous media is extremely complex. Numerous assumptions are required concerning the behavior of the components in the media to afford even an attempt at solution. The work on the flow of air and water and the effects of moisture migration is reviewed by Couvillion and Hartley (1986). The equations governing the flow of two or more species are determined by assuming isotropic soil: density of liquid water is constant but the vapor and gas properties are functions of temperature; and the mass of water vapor is neglected. These assumptions are based on previous studies by Philip and De Vries (1957). De Vries (1987) developed the theory of heat and mass transfer based on the moisture potential and the hydraulic conductivity of the medium being dependent on the moisture content and temperature of the media. Also, the thermal conductivity must be known as a function of moisture content and temperature. Couvillion and Hartley (1986) applied these criteria to

earth-coupled heat transfer problems, particularly with respect to the movements of drying fronts, and found qualitative agreement with experimental results. Agreement was improved by choosing correlation coefficients to tune the predicted results to the data.

2.2 Problem Statement

Based on the literature review of Sec. 2.1, the effect of buoyantly induced flow in saturated soil on earth-coupled heat transfer needs to be analyzed. Due to the complexity of the general problem (Claridge, 1988), the physical parameters under consideration will be reduced in order to focus on the buoyant flow.

Slab-on-grade building construction will be analyzed because this is type of building is very prevalent. Computationally, a two-dimensional domain will be considered and is depicted in Fig. 2.1. The remote earth thermal boundaries will be considered to be adiabatic. Heat transfer at the slab and earth surface air interfaces will obey Newton's Law of Cooling, while the interior building and exterior ambient temperatures will be held constant. Justification for the choice of thermal boundary conditions will be presented more fully in Chap. 3.

To focus attention on the slab contribution to buoyantly induced thermal flow and heat transfer, change of phase of water by evaporation or freezing will be excluded inside the soil mass. Furthermore, all boundaries in Fig 2.1 will be considered impermeable to the flow of water. This condition will be relaxed in Chap. 7 to study the effects of earth surface evaporation on slab heat transfer.

A solution to the building slab earth-coupled heat loss problem specified above will be sought in the following chapters.

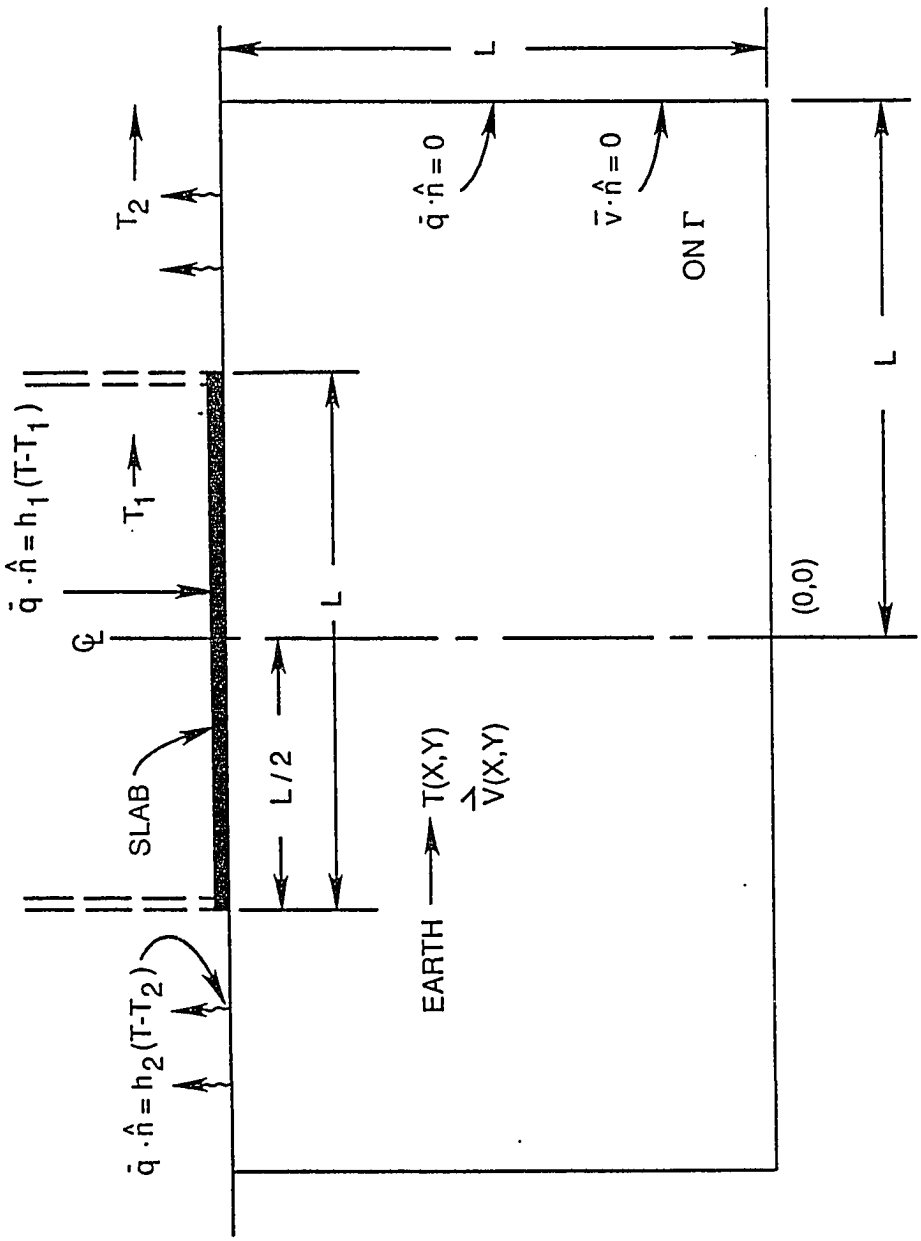

Fig. 2.1 Boundary conditions for the slab-on-grade heat loss problem.

Chapter 3

A TREATISE ON THE INTERACTION BETWEEN HEATED SURFACES, THE EARTH AND THE ENVIRONMENT

3.1 Introduction

A building may have almost any configuration and is subject to extremely diverse weather conditions. To begin a systematic investigation of the problem, simplifications will be made to isolate the salient characteristics of earth-coupled heat transfer without unduly limiting the applicability of the solution.

The design configuration chosen for this study of earth-coupled heat transfer is the slab-on-grade. The is a very common method of building construction. It is much less expensive than basement excavation for the same footprint area. The slab is usually reinforced with a perimeter footing to support the walls. This type of construction is used extensively for commercial and residential construction. As a matter of necessity, the slab-on-grade method may be dictated by the presence of a water table that is close to the ground surface. A basement constructed under these conditions would be subject to leakage and therefore impractical.

Having chosen the slab as the archetypal class of construction for analysis, the problem of how the slab communicates thermally with the environment remains to be addressed. As a mathematical abstraction, the

boundaries may be considered to be infinite. Although there are certain analytical advantages in selecting a boundary infinitely far away, this is a serious limitation for a numerical computation.

Often, the subterranean domain is truncated by selecting an isothermal boundary, an adiabatic boundary or a boundary that is a combination of both conditions. The type of boundary and its location are selected *a priori*, based upon the judgment of the analyst. For example, as previously discussed in Chap. 1, Shen et al. (1988) experienced difficulty in relating ambient temperature, interior temperature, and deep ground temperatures to heat flux without using climatic data. Kusuda and Achenbach (1963) used a symmetry plane and constant deep ground temperature to numerically compute heat loss from a fallout shelter. Solar and convective surface heat losses were also considered. Bahnfleth and Pedersen (1990) noted the insensitivity of heat transmission to far field conditions. Surface conditions were found to be important. An interesting aspect of the Bahnfleth and Pedersen (1990) study was the examination of the effect of building shadow on slab heat loss. This effect was usually negligible, but for some soil conditions (especially including surface evapotranspiration), building shadow could affect heat transfer from the slab by as much as twenty per cent. In an experiment by Yoshino et al. (1990), an unheated, two room house was constructed with windows facing south. The floor level was 1.3 m below ground level with horizontal insulation installed on the east side of the house, 1.3 m wide and 0.3 m below the earth surface. One of the effects noted was that incident solar radiation at the earth surface had little effect on the interior conditions.

Numerical and physical experiments have yielded some interesting and often puzzling results. To further illuminate the process of heat transfer from a slab and to lend credence to subsequent model construction, the following discussion is undertaken to place assumptions on as firm a footing as possible.

3.2 Discussion

The purpose of this discussion is to establish generalizations for the behavior of the earth to the extent that this affects the building slab heat transfer. The method used to perform the analysis will be to postulate a set of propositions and to show that the propositions are true. Some propositions are based on hypothesis, but reflect the current scientific understanding of the subject.

3.2.1 Proposition I

The earth is in a steady periodic condition when viewed from a geological perspective.

One common test of whether a object exposed to heating conditions has reached a stationary state is whether sufficient time has elapsed with respect to the time constant of that object. In fact, the physical age of the earth is an indication of this. Lord Kelvin first computed the age of the earth in 1862. He assumed that after the earth condensed, it originally existed in a homogeneous molten state. His calculations indicate that the age of the earth was between 20–40 million years (Badash, 1989). The discovery of radioactivity at the turn of the Twentieth Century and the production of heat by radioactive decay gave geologists a new method of evaluating geologic age.

Radioactive dating methods have place the currently accepted age of the earth at 4.5 billion years (Badash, 1989). This is a huge number compared to that calculated by Lord Kelvin's cooling model.

Another indication that the earth is in a steady, periodic condition is the sensitivity of the planet to changes in surface conditions. An apparent discontinuity in global weather occurred most recently at the boundary of the Cretaceous and the Tertiary periods, 65 million years ago. Also known as the K–T Boundary, this period is important because mass extinction of thousands of species occurred, including the dinosaurs. Although the exact cause of the K–T Boundary is under contention, evidence indicates that the time duration is very short in the geological sense (Alvarez and Asaro, 1990). One may conclude that the life is very sensitive to abrupt changes in the environment exceeding the usual seasonal period.

3.2.2 Proposition II

A rectangular coordinate system will adequately describe the slab–on–grade problem.

The radius of the earth (6371 km) (Courtillot, 1990) is large compared to the scale of a building and curvature may be neglected. Furthermore, the azimuthal component of heat flux is negligible compared to the radial component. This is true because temperature along the surface of the earth varies by about 120K at most, while the temperature difference between the surface and the center of the earth is 5000 K (Courtillot, 1990).

Carslaw and Jaeger (1959) indicate that a radial geothermal gradient exists on dry land from between 10 and 50 C/km and 40 C/km

under water. The average flux to the surface has an average value of 1.2×10^{-6} cal/cm^2–sec (5.0×10^{-2} W/m^2).

Based on the above information, the earth is essentially in a steady periodic state. This condition is used by Shen et al. (1988) to perform heat loss calculations. Furthermore, the earth may be considered to be locally one–dimensional and flat. Crustal heat flux is present which will be considered constant in a particular local area.

3.2.3 Proposition III

A building slab may be idealized as a plane on the earth surface.

The two dimensional temperature field resulting from a constant temperature slab, Eq. (A.1.15), as derived in Appendix A.1 is

$$\Theta(x,y) = \frac{1}{\pi} \arctan \frac{y}{x^2+y^2 - .25} \qquad \text{(A.1.15)}$$

Figure 3.1 is the isothermal map of Eq. (A.1.15) for selected values of constant temperature.

3.2.4 Proposition IV

There is an adiabatic surface beneath every constant temperature finite length slab located on a semi–finite plane with constant opposing heat flux.

The earth generates heat by radioactive decay. Heat flux reaching a particular section on the surface is the result of a source at a greater depth. The crustal heat flux will be considered to be uniform near the surface in order to demonstrate that the proposition is valid.

Superposition is used to determine the temperature field surrounding the slab and is

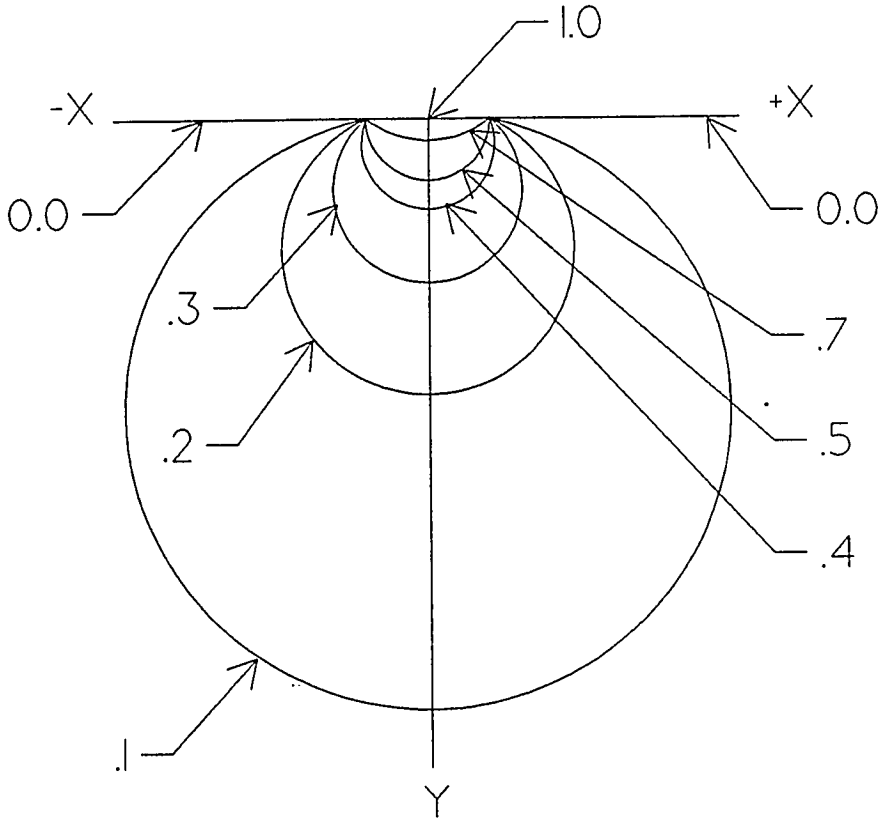

Fig. 3.1 Isothermal map for constant temperature slab in a semi – infinite domain.

$$\Theta(x,y) = \frac{1}{\pi} \arctan \frac{y}{x^2+y^2-.25} + \tilde{q}\, y \qquad (A.2.7)$$

The derivation of the solution is presented in Appendix A.2.

With Eq. (A.2.7), one may find the equation of isothermal surfaces and lines of heat flux for the problem as given by Eqs. (A.2.12) and (A.2.17).

The crustal flux strength may be defined as

$$q_{cfs} = \pi\tilde{q} = \pi q_{crust} L/\lambda\Delta T \qquad (3.1)$$

then Eq. (A.2.17) becomes

$$\frac{dy}{dx} = -\left[\frac{2xy}{q_{cfs}(x^2+y^2-.25)^2+x^2+(q_{cfs}-1)y^2-.25}\right]^{-1} \qquad (3.2)$$

The lines of flux are determined by solving Eq. (3.2) numerically by using a Euler explicit marching method. Figure 3.2, a flux map, shows the position of the flux lines under the slab for a unit crustal flux strength. Notice that flux lines originating from the slab are turned back and end at the outside surface (dashed curves). An interface exists between the crustal lines of flux and slab lines of flux. Since no lines of flux emanating from the slab cross the interface line, the interface line effectively represents an adiabatic surface. Therefore, by considering the interaction of the two fields, a problem with infinite boundaries may be treated as a finite problem with adiabatic subterranean boundaries.

There are a multitude of choices for the crustal flux strength. Each crustal flux strength will yield a unique family of curves that are solutions to Eq. (3.2). The maximum distance that the heat flux from the slab can penetrate to the exterior earth surface is determined by the

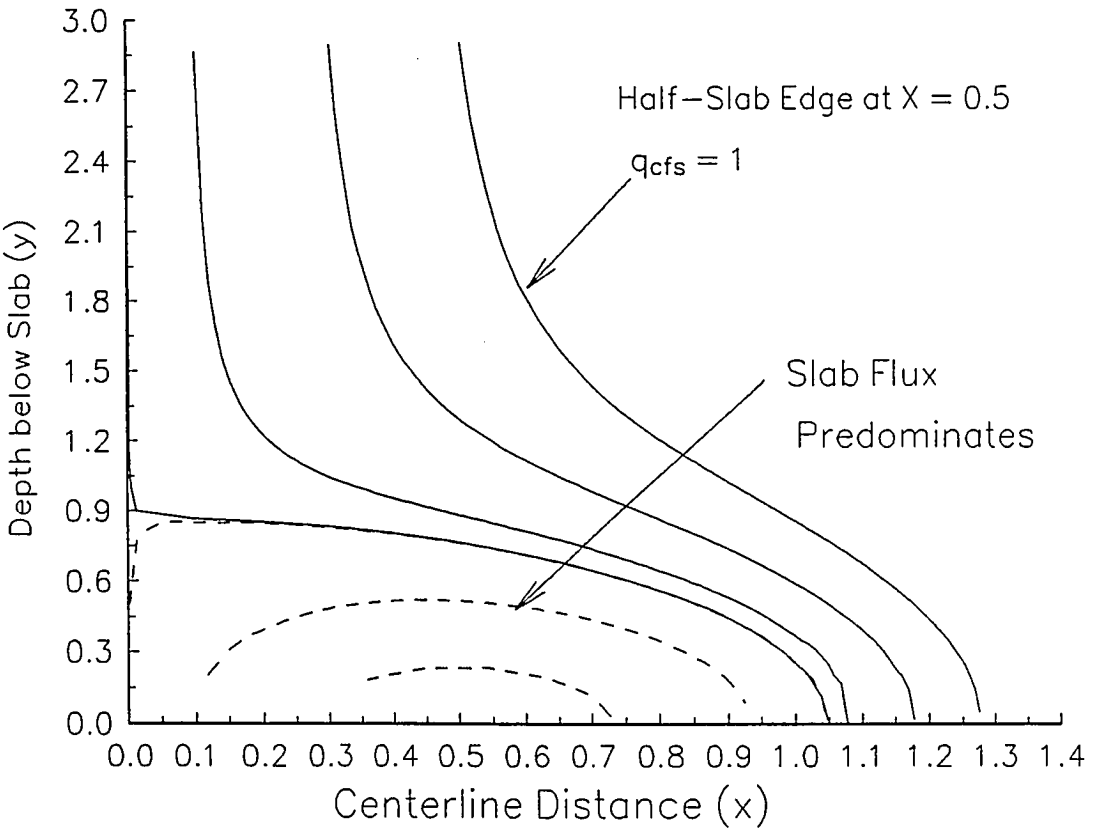

Fig. 3.2 **Constant temperature slab flux envelopment by opposing crustal flux of unit strength.**

crustal flux strength and vise versa. Figure 3.3 shows the relationship of the maximum horizontal distance that slab heat flux will penetrate to the outside earth surface as a function of the crustal flux strength. The computational domain for the problem is uniquely determined by the crustal flux strength.

3.2.5 Proposition V

A steady state heat flux passing through a two or a three-dimensional body may be considered as a one-dimensional problem

Suppose an arbitrary shaped body subject to a surface heat flux. The body may be treated as a control volume with an outward pointing normal. Then

$$\iint_A (\mathbf{q} \cdot \hat{\mathbf{n}}) dA = 0 \tag{3.3}$$

Since the control volume is arbitrary, then

$$\mathbf{q} \cdot \hat{\mathbf{n}} = 0 \tag{3.4}$$

A family of surfaces may be constructed satisfying this equation. Two other families of surfaces that are mutually orthogonal to each other and the family of surfaces in described by Eq. (3.4) may be determined. This may be demonstrated from the Gauss' theorem:

$$\iiint_{Vol} (\nabla \cdot \mathbf{q}) dV = \iint_A (\mathbf{q} \cdot \hat{\mathbf{n}}) dA = 0 \tag{3.5}$$

Again, since the integral is arbitrary, then

$$\nabla \cdot \mathbf{q} = 0 \tag{3.6}$$

The scalar product is commutative, therefore,

$$\mathbf{q} \cdot \hat{\mathbf{n}} = \hat{\mathbf{n}} \cdot \mathbf{q} \tag{3.7}$$

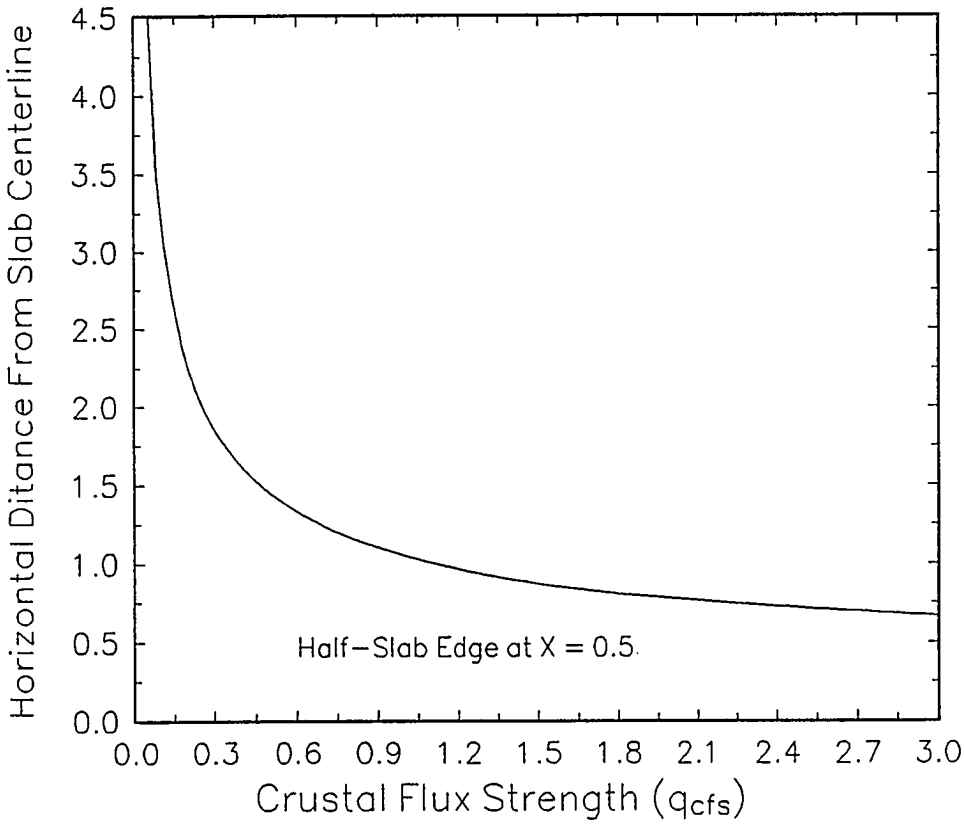

Fig. 3.3 **Slab flux horizontal penetration distance versus crustal flux strength.**

This indicates that the gradient operator in Eq. (3.6) can be expressed in terms of the direction normal to the family of surfaces satisfying Eq. (3.4). Any mapping which directs $\hat{n}$ along the gradient operator may be considered one-dimensional.

3.2.6 Proposition VI

The net periodic heat flow through any point in a one-dimensional body is zero.

Subject to the conditions stipulated in Appendix A.3, this proposition allows for the analysis of steady conditions in terms of seasonal averages without undue concern for the effects of the periodic component.

3.3 Final Observations

A constant temperature surface segment is an idealization of the real building slab of negligible thickness. The constant temperature surface is not physically attainable because of the thermal discontinuity at the left and right hand edges. The presence of the edge discontinuity causes an infinite gradient at the edge point, and the flux cannot be computed. The total heat transferred across the surface cannot be computed for the same reason. However, since the temperature field is continuous and differentiable everywhere else in the plane, this constant temperature surface can be considered a limiting case for a convectively heated slab which is the usual situation in a typical building.

This point is discussed further as the model is developed in Chaps. 4 and 5.

Chapter 4

FLUID FLOW AND HEAT TRANSFER IN POROUS MEDIA

4.1 Introduction

Earth-coupled heat loss is an important mode of energy transfer from a building as discussed in Chaps. 2 and 3. The earth under the building is usually porous and may contain a substantial amount of water. The physics of porous media fluid flow and ground water hydrology and heat transfer encompasses a large body of literature. This branch of fluid mechanics is, however, very specialized, and has developed a terminology that may be unfamiliar to a substantial percentage of engineers trained in other disciplines. The following exposition is intended to provide the reader who is not familiar with porous media fluid flow a brief overview of some important concepts that are used regularly in the porous media literature. The following treatment is simplified to accomplish this purpose.

4.2 Background

Henry Darcy made contributions to physics as an investigator in fluid flow in pipes and the flow of water in sand beds. As an engineer in the city of Dijon, France, he had need of information about the use of sand as a filter for the water in the municipal fountain distribution system. To discover this information, he conducted a series of

experiments in which he filtered water through a column of sand packed into an iron pipe. The volume of water discharged in a given amount of time was recorded for various physical parameters. At the conclusion of his work, Darcy found that the volumetric flow of water through the sand bed was directly proportional to the difference in manometer heights when measured at the inlet and exit of the filter bed, the cross sectional area of the bed, and inversely proportional to the length of the filter bed. This was expressed as

$$Q_{vf} = -KA(h_2 - h_1)/l \tag{4.1}$$

where K is the proportionality constant, A is the cross sectional area, l is the length of the path of water through the sand and h_1 and h_2 are the manometer heights of the inlet and outlet, respectively (Darcy, 1856). The subscripts, vf (volumetric flow rate), will be used to distinguish between use of the letter Q for volume flow and heat flow since this symbol has historically been used to represent both quantities. Darcy also recognized that the relationship was no longer valid for velocities which exceeded the range of ten centimeters per second.

Hubbert (1940) demonstrated that Darcy's Law can be considered a special case of

$$q_{vf} = -(K/g)\ \nabla\ \varphi \tag{4.2}$$

where q_{vf} is the volumetric flow rate per unit area and

$$\varphi = gz + \int dP/\rho + v^2/2 \tag{4.3}$$

is the energy per unit mass of fluid (also known as the mechanical energy potential). For ground water flow, $v^2/2$ is negligible and density is a very weak function of pressure. Consequently, φ may be written as

$$\varphi = gz + P/\rho \tag{4.4}$$

In terms of head, φ may be written as

$$\varphi' = z + P/\gamma \tag{4.5}$$

where γ is the specific weight of the fluid. In terms of φ', Darcy's Law becomes

$$q_{vf} = -K \nabla\varphi' \tag{4.6}$$

Fulks et al. (1971), defined for a porous media the porosity and derives the continuity equation and momentum equation for a fluid flowing in a porous medium. Bear (1972) extended the analysis to include the energy equation in porous media along with the equations for temperature varying density and viscosity. Combarnous and Bories (1975) discuss these equations and also give the criteria for establishing buoyant flow.

4.3 Discussion of Selected Porous Media Terminology

A porous medium is a solid material that has interconnected voids interspersed throughout. Although the distribution of the voids within the solid matrix is arbitrary, the void volumes must be interconnected in some manner. Otherwise, the fluid would not be able to penetrate the medium and no flow would be possible.

There are two basic methods employed to solve flow problems through a porous media. The first method is a microscopic investigation of the flow of fluid in the pores of the media. Considering the fluid as a continuum, the equations of fluid motion and the detailed knowledge of the geometric boundaries of the pores and initial conditions are required to produce a solution. The scope of this problem is immense.

Although this is theoretically possible to accomplish, only simple shapes can be managed (Bear, 1972).

The second method is macroscopic. This technique abandons the notion that interpore flow can be analyzed. Instead, the local fluid properties at a point in the matrix are averaged over a small encapsulating volume of space, and the average value is considered to act at the particular point. The disadvantage of this method is that when information is averaged, there is a net loss of information about the properties in the individual pore spaces. The benefit of this approach is that flow field can be solved by invoking volume averaging.

A volume averaged property, $\mathcal{V}$, is an extension of the customary averaging method and may be expressed as (Cheng, 1978)

$$\mathcal{V} = \frac{1}{V}\int_V Y \, dV \tag{4.7}$$

The porosity of the material is the ratio of the volume of the voids included in the total volume to the total volume of material. The porosity of a material can vary as a function of position within the material. Therefore, it becomes necessary to define porosity at a point. This is done by selecting a small sample volume of material that encloses the particular point P, which is large when compared to the volume of an individual pore space but is small when compared to the characteristic dimension of the the domain. This is called a Representative Elementary Volume (REV). The REV has the property that small changes in the size of the REV do not affect the computed value of the porosity at point P.

$$n(P) = \lim_{\mathcal{V}\to REV} V_{void}/\mathcal{V} \tag{4.8}$$

where V is the volume of space under consideration and V_{void} is the void volume contained within V.

The areal porosity, n_a, can be defined in a similar manner.

$$n_a = A_{void} / A \tag{4.9}$$

This quantity is not very useful because the porosity can vary with the orientation of the plane one selects for the computation. A more useful quantity is the average areal porosity, n_a, which will be defined as the average void area, $\bar{A}_{void}$, to the total cross-sectional area, A, for a cylinder of material of length, s.

$$n_a = \bar{A}_{void} / A \tag{4.10}$$

where,

$$\bar{A}_{void} = \frac{1}{s}\int_0^s A_{void}\, dl \tag{4.11}$$

Alternately,

$$V_{void} = \bar{A}_{void} \cdot s \tag{4.12}$$

and

$$V = A \cdot s \tag{4.13}$$

Therefore,

$$n_a = n \tag{4.14}$$

The average areal porosity is equal to the volumetric porosity.

The velocity at a point can be treated similarly. The volume average velocity at a point in the media can be represented in terms of the average pore velocity in the REV as

$$V = n\, V_{pore} \tag{4.15}$$

This follows immediately from the continuity equation since for any cross-sectional area,

$$Q_{vf} = V \cdot A = V_{pore} \cdot A_{void} \tag{4.15.1}$$

$$V \cdot A = V_{pore} \cdot n \cdot A \tag{4.15.2}$$

The permeability of porous media is a property that measures the ability of the media to conduct a fluid. The permeability of porous media is analogous to the thermal conductivity or electrical specific conductivity of the material (Hubbert, 1940).

4.4 Conservation Equations for Porous Media

Deriving the Conservation equations for a fluid in porous media may be accomplished by summing mass, momentum and energy for a REV. Volume averaging of properties, Eq. (4.7), is then applied to the conservation equations to obtain the desired result. The general conservation equations for porous media include the possibility of a multitude of different chemical species flowing in the media such as water, air, oil, or dissolved minerals. Moreover, the porous media properties of porosity, permeability, and thermal conductivity may be directional (Bear, 1972). For the problem of heat transfer for a building slab on saturated soil, only the flow of liquid water will be considered. Moreover, there is no compelling reason to select a porous media in which one direction is preferred over any other. Therefore the media properties will be chosen to be isotropic and homogeneous throughout. Combarnous and Bories (1975) give the following conservation equations where the velocities are volume averaged through the media.

Mass:

$$n\frac{\partial \rho}{\partial t} + \nabla \cdot (\rho \mathbf{V}) = 0 \tag{4.16}$$

Momentum:

$$(\rho/n)\frac{\partial \mathbf{V}}{\partial t} + (\rho/n^2)(\mathbf{V} \cdot \nabla)\mathbf{V} = -\nabla P + \rho \mathbf{g} - \mu/k\mathbf{V} \tag{4.17}$$

Energy:

$$\nabla \cdot (\lambda_{eq} \nabla T) - \nabla \cdot [(\rho c)_f \mathbf{V} T] = \frac{\partial}{\partial t}(\rho c)_{eq} T \tag{4.18}$$

Properties with the subscript "eq", i.e., λ_{eq} and $(\rho c)_{eq}$, represent an equivalent property for the REV in which the fluid and porous media have been lumped together by the volume averaging method to form a composite.

For the steady problem, all time derivatives are zero. Furthermore, ground water flow velocities are small and terms of the second degree are neglected. Equation (4.17) reduces to an equivalent form of Darcy's Law:

$$\mathbf{V} = -(k/\mu)(\nabla P - \rho g) \tag{4.19}$$

The mass continuity equation becomes

$$\nabla \cdot (\rho \mathbf{V}) = 0 \tag{4.20}$$

If the specific heat in Eq. (4.18) is considered constant, then the term $\nabla \cdot [(\rho c)_f \mathbf{V} T]$ in Eq. (4.16) reduces to $(\rho c)_f \mathbf{V} \cdot \nabla T$ and the energy equation becomes

$$(\rho c)_f \mathbf{V} \cdot \nabla T = \lambda_{eq} \nabla^2 T \tag{4.21}$$

These are the field equations that describe steady flow in a isotropic, homogeneous porous media with constant thermal conductivity.

4.5 Buoyant Flow in Porous Media

The conservative Eqs. (4.19)–(4.21) must be put into a form that will facilitate the computation of buoyant flow in the media. Suppose that a thermal gradient exists in a fluid. A corresponding density gradient is also created as well as a net imbalance in the gravitational body force. Elements of the fluid that are less dense will tend to be displaced by fluid of greater density. A reference state may be established for some location in the fluid where a static condition

exists. This may be expressed as a special case of Darcy's Law.

$$0 = -(k/\mu)(\nabla P_s - \rho_r g) \tag{4.22}$$

where P_s is the static pressure at the reference density. Subtracting this from Eq. (4.19) yields

$$\mathbf{V} = -(k/\mu)(\nabla(P - P_s) - (\rho - \rho_r)g) \tag{4.23}$$

The conservation equations are not in a form that may readily be solved. Since the energy equation is nonlinear, an analytic solution is not possible for most situations. It is necessary to prepare the equations for numerical treatment. Nondimensionalization of the governing equations is a very useful method for obtaining a numerical solution. Scaling will be chosen for the problem of slab earth-coupled heat loss based on the length of the slab, L. There is no free stream velocity in this problem so the reference velocity must be defined in terms of thermophysical properties. The following nondimensional quantities are defined:

$$x = X/L \tag{4.24}$$

$$y = Y/L \tag{4.25}$$

$$v = V/V_0 \tag{4.26}$$

where

$$V_0 \equiv \lambda_{eq}/(\rho c)_f L \tag{4.27}$$

Also,

$$\Delta T = T_1 - T_2 \tag{4.28}$$

$$\Theta = (T - T_2)/(T_1 - T_2) \tag{4.29}$$

$$P_d = P - P_s \tag{4.30}$$

and

$$\mathbf{V}^* = \mathbf{V} \cdot L \tag{4.31}$$

Using these expressions to change variables, the continuity equation and

the energy equation become

Mass:

$$\nabla^* \cdot \mathbf{v} = 0 \tag{4.32}$$

Energy:

$$\mathbf{v} \cdot \nabla^* \Theta = \nabla^{*2} \Theta \tag{4.33}$$

Nondimensionalization of Eq. (4.23) yields

$$\mathbf{v} = -(k/\mu)(\nabla P_d - (\rho - \rho_r)\mathbf{g})/V_0 \tag{4.34}$$

It is helpful to cast this equation into a more suitable form by normalizing as many variables as possible. By defining the following quantities

$$\mathbf{e} = \mathbf{g}/g \tag{4.35}$$

$$\rho^* = \rho/\rho_r \tag{4.36}$$

$$P^*_d = P_d/\rho_r g L \tag{4.37}$$

$$\nu = \mu/\rho \tag{4.38}$$

$$\nu^* = \nu/\nu_r, \tag{4.39}$$

Eq. (4.34) is expressed as

$$\mathbf{v} = -k(\rho_r c)_f g L(\nabla^* P^*_d - (\rho^* - 1)\mathbf{e})/\lambda_{eq} \nu^* \nu_r \tag{4.40}$$

Let

$$\mathfrak{R} = k(\rho_r c)_f g L/\lambda_{eq} \nu_r \tag{4.41}$$

The governing equations in nondimensional form, after dropping the asterisk notation for convenience, become

Mass:

$$\nabla \cdot \mathbf{v} = 0 \tag{4.42}$$

Energy:

$$\mathbf{v} \cdot \nabla \Theta = \nabla^2 \Theta \tag{4.43}$$

Darcy's Law:

$$\mathbf{v} = -\mathfrak{R}\ (\nabla P_d - (\rho - 1)\mathbf{e})/\nu \tag{4.44}$$

By taking the divergence of Darcy's Law, Eq. (4.44), and setting to zero, the continuity equation is satisfied automatically. For water, density and viscosity will be considered to be functions of temperature (Sun Zu-Shung et al., 1970, Kwok and Chen, 1987). The resulting expression is

$$\mathfrak{R}\, \nabla^2 P_d = -\frac{\partial \nu}{\partial \Theta}\,(\mathbf{v}\cdot\nabla\Theta) + \mathfrak{R}\,\frac{\partial \rho}{\partial \Theta}\,(\nabla\Theta\cdot\mathbf{e}) \tag{4.45}$$

or equivalently,

$$\mathfrak{R}\, \nabla^2 P_d = -\frac{\partial \nu}{\partial \Theta}\,\nabla^2\Theta + \mathfrak{R}\,\frac{\partial \rho}{\partial \Theta}\,(\nabla\Theta\cdot\mathbf{e}) \tag{4.46}$$

Equations (4.43) – (4.46) are the field equations for the flow of buoyantly induced flow with temperature varying density and viscosity.

4.6 The Stream Function

In two dimensions, a stream function may be defined such that

$$u = \frac{\partial \psi}{\partial y}\ ,\ \text{and}\ v = -\frac{\partial \psi}{\partial x} \tag{4.47}$$

These functions identically satisfy the continuity equation. By cross differentiating Darcy's Law and using the definitions in Eq. (4.47) one obtains

$$\nabla^2\psi = \frac{\partial \nu}{\partial \Theta}\,\left(v\frac{\partial \Theta}{\partial x} - u\frac{\partial \Theta}{\partial y}\right)/\nu + \mathfrak{R}\,\frac{\partial \rho}{\partial \Theta}\,\frac{\partial \Theta}{\partial x}/\nu. \tag{4.48}$$

The flow is fully described in terms of P_d, Θ, and $\mathbf{v}$. Although no additional information is gained by using the stream function, streamlines are useful as an aid in visualizing the flow in the porous media.

4.7 The Boussinesq Approximation and the Rayleigh Number

The fluid and its viscosity and density as functions of temperature must be known to utilize the porous media field equations. To check the

validity of the above expressions, the commonly used expressions for viscosity and density variation may be substituted where appropriate. Viscosity is usually considered to be constant while density variation in buoyant flow situations is often described by using the Boussinesq approximation. The Boussinesq approximation is a first order Taylor series which describes density as a function of temperature. In nondimensional variables, the approximation is

$$\rho = 1 - \beta\Delta T(\Theta - \Theta_r) \tag{4.49}$$

where β is the coefficient of thermal expansion for the liquid.

A coordinate system for Eqs. (4.44) – (4.46) and (4.48) must be selected. For customary rectangular coordinates with x to the left and y upwards,

$$\mathbf{e} = -\mathbf{j}\ , \text{ and } \nabla\Theta \cdot \mathbf{e} = -\frac{\partial\Theta}{\partial y} \tag{4.50}$$

Using Eq. (4.50), the density relationship in Eq. (4.49) and the following relationships

$$\nu^* = \nu = 1 \tag{4.51}$$

$$\frac{\partial\rho}{\partial\Theta} = -\beta\Delta T \tag{4.52}$$

$$\frac{\partial\nu}{\partial\Theta} = 0 \tag{4.53}$$

$$\Phi = \Re\, P_d \tag{4.54}$$

and substituting into (4.45) yields

$$\nabla^2\Phi = \Re\beta\Delta T\,\frac{\partial\Theta}{\partial y} = Ra\,\frac{\partial\Theta}{\partial y} \tag{4.55}$$

where the Ra is the Rayleigh number.

$$Ra = k(\rho_r c)_f g L\beta\Delta T/\lambda\nu_r \tag{4.56}$$

Equation (4.55) is equivalent to the expression given by Ene and Polisevski, 1987.

Substituting the same relations into Eq. (4.48) results in

$$\nabla^2\psi = -\Re\beta\Delta T\frac{\partial\Theta}{\partial x} \tag{4.57}$$

or

$$\nabla^2\psi = - \text{Ra} \frac{\partial\Theta}{\partial x} \tag{4.58}$$

This agrees with the formulation given by Himasekhar and Bau (1988).

There are several interpretations of the Rayleigh number in porous media literature. Combarnous and Bories (1975) classify Eq. (4.57) as the filtration Rayleigh number. Kladas and Prasad (1989) further define a filtration Rayleigh number in terms of the product of the Darcy number and the fluid Rayleigh number.

$$\text{Ra} = \text{Da}\ \text{Ra}_f \tag{4.59}$$

where the Darcy number is the permeability divided by the square of the pore size. This distinction is helpful when high velocities in porous media cause wall channeling in the media. In ground water flow induced by thermal effects, however, this distinction is unnecessary. All references to the Rayleigh number will refer to the filtration Rayleigh number, defined by Eq. (4.56).

Chapter 5

THE COMPUTATIONAL PROBLEM

5.1 A Brief Overview of Method and Results

A basic scientific investigation begins with a hypothesis that is to be verified or refuted by analysis or experiment. This work investigates the contribution of liquid water as an agent for the removal of heat from a building slab. Since a nonlinear analytic solution is not expected for even the simple geometry being considered here, the solution of the above equations must be undertaken by computer. One inherent drawback of numerical methods is that a vast amount of information is obtained about a specific case. Generalizations and behavior trends are detected by parametric study.

After refining the computer algorithm discussed in the following sections and using the parameters expected in field conditions, nondimensional heat flux ($q/\lambda\Delta T$) calculations clearly indicated that the presence or absence of water in the media made a negligible difference. This result appeared to contradict the intuitive conception of the ability of wet earth to conduct heat. The only way to resolve this discrepancy was to perform an experiment and determine more information about the process. Details of the experiment are discussed in Chap. 5.

The experimental results, which agreed qualitatively with those predicted by the computer solution, were based upon a constant

filtration Rayleigh number (composed of properties of water at an intermediate reference temperature and a volume averaged thermal conductivity). Buoyant circulation was evident. The experimentally determined heat transfer for saturated porous media was approximately an order of magnitude higher than that of dry porous media and the numerical porous media flow solution. Also, the fluid velocities were experimentally observed to be much larger than the computed values. It was obvious that corrections to the modeling were needed.

The first correction made was to presume that the numerical value of $q/\lambda\Delta T$ was correct. With this assumption, an experimental value for porous media thermal conductivity could be found and used in the Rayleigh number to replace the volume averaged value. When the velocity field was recomputed, better overall agreement was reached with the experiment. This was an encouraging result, although not completely satisfactory.

Water is an anomalous liquid that has a density maximum at 4 C. Viscosity decreases sharply over the temperature range under study of between 0 C and 20 C. To examine the effect of the temperature variation of these properties, reformulation of the governing equations was necessary. Chapter 4 develops the details of this analysis. Again, recomputation of the velocity field showed a substantial improvement in the streamline positions and essentially agreed with the experimental observations. The magnitude of the velocity field was lower than observed, however.

Improving the model to allow for temperature variation in the properties gradually improved the agreement with observations of the scale model. The porous media (i.e., 1 mm glass beads) average porosity

was measured by displacement of water and is accurate to within one per cent. The only remaining property in question is the permeability. The permeability was determined by use of the Ergun Formula, (see list of Nomenclature and Chap. 6) which is an empirical formula valid for beds of randomly packed spherical particles. Correction of the previously computed value of permeability by the velocity deficit brought the computed results into consonance with the experimental observations. The probable cause for this is due to the difference in permeability and porosity of the media adjacent to the wall of the test cell compared to the central region of the porous media. The wall effect will be discussed at greater length in Chap. 6.

The governing equations for buoyant flow in porous media were derived in Chap. 4. These equations must be solved in the domain of interest, which for this problem is the convectively heated slab-on-grade. This chapter will discuss the methods employed in the numerical solutions, test special case problems with the code and compare these results with solutions produced by other means and finally, perform a parametric study that allows the problem of heat flow from a two-dimensional slab to be solved without resorting to numerical methods.

5.2 Boundary Conditions

The conditions one would expect to find in the interior of a building is a convectively heated ground floor where heated air is distributed by an air handler. The outside earth surface is also subject to an assortment of weather conditions. The primary exchange of heat is by convection between the air and the earth. Solar radiation is

of a periodic nature, and the average long term effect on the steady slab flux may be neglected in accordance with Proposition VI. Proposition IV allows the selection of a finite, adiabatic subterranean boundary. The thermal boundary conditions can therefore be written as

$$\mathbf{q} \cdot \hat{\mathbf{n}} = h\ (T - T_\infty) \text{ on slab or air/earth interface} \tag{5.1}$$

$$\mathbf{q} \cdot \hat{\mathbf{n}} = 0 \text{ on } \Gamma \text{ elsewhere.} \tag{5.2}$$

When applied to the slab with a constant heat transfer coefficient, the equations then become

$$\lambda \frac{\partial T}{\partial Y} = -\ h_1(T - T_1), \text{ on slab} \tag{5.3}$$

$$\lambda \frac{\partial T}{\partial Y} = h_2(T - T_2), \text{ on earth, and} \tag{5.4}$$

$$\nabla T \cdot \hat{\mathbf{n}} = 0 \text{ on } \Gamma \text{ elsewhere.} \tag{5.5}$$

These conditions are illustrated in Fig. 5.1. Using the definitions in Chap. 4, the boundary equations are transformed into nondimensional variables and become

$$\frac{\partial \Theta}{\partial y} = Bi_1\ (1 - \Theta_1) \text{ on slab,} \tag{5.6}$$

$$\frac{\partial \Theta}{\partial y} = Bi_2\ \Theta_2 \text{ on earth, and} \tag{5.7}$$

$$\nabla \Theta \cdot \hat{\mathbf{n}} = 0 \text{ on } \Gamma \text{ elsewhere.} \tag{5.8}$$

The boundaries for fluid flow are considered to be impermeable and correspond to the thermal boundaries. At the lower boundary, this condition would be characteristic of some strata of rock or clay at a given depth beneath the surface. An impermeable earth surface physically represents a membrane or an asphalt covering over the earth surface. This condition will be relaxed in Chap. 7 to study the effects of evapotranspiration on slab heat loss.

The vertical surfaces surrounding the slab will also be taken to be impermeable. This condition could be physically justified based on the

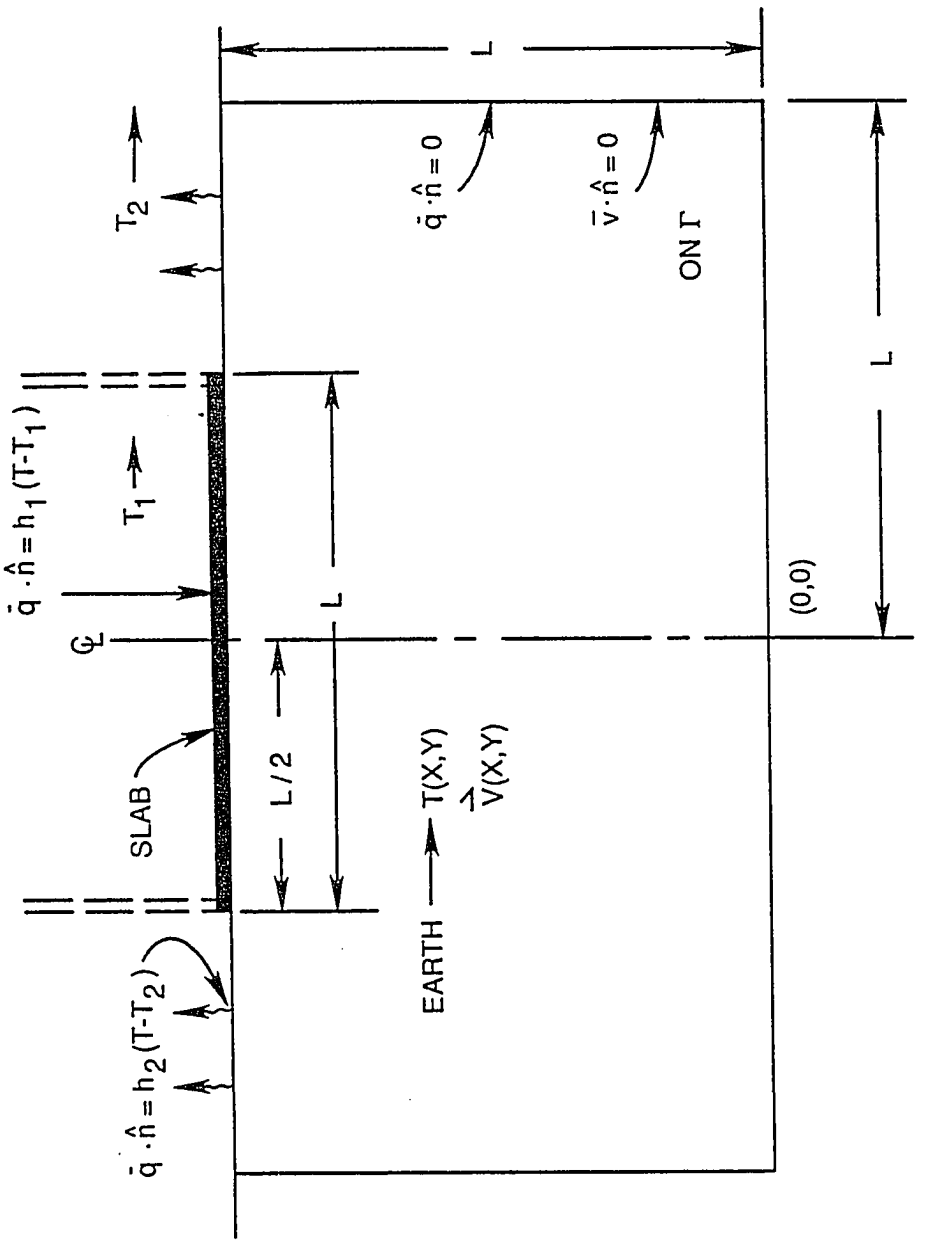

Fig. 5.1 Boundary conditions for the two-dimensional slab-on-grade.

fact that most residential structures are situated in a developed area and symmetry planes will exist between the properties. Thermally induced fluid flowing from a slab and from its "image" slabs will circulate in direct opposition to each other. This opposing flow may be represented by an impermeable surface. Therefore, to study the case of natural convection induced by the slab, impermeable surfaces will be considered to exist at all boundaries. This may be expressed as

$$\mathbf{v} \cdot \hat{\mathbf{n}} = 0 \text{ on } \Gamma. \tag{5.9}$$

5.3 Difference Equations

The field equations and boundary conditions for the problem may be approximated by using difference equations instead of differential equations. The differential equations are valid at all points in the domain while the difference equations are applied to a select set of points in the domain and on the boundary. The accuracy of the scheme depends on how many points are selected and how the differential equation is approximated. This method is known as the finite difference method, and the following difference operators are defined (Anderson et al., 1984):

$$\overline{\delta}_x u_{i,j} = u_{i+1,j} - u_{i-1,j} \tag{5.10}$$

$$\delta_x^2 u_{i,j} = u_{i+1,j} - 2u_{i,j} + u_{i-1,j} \tag{5.11}$$

These difference operators are utilized to form approximations to derivatives of $u_{i,j}$ to within the specified accuracy as follows:

$$\frac{\partial u}{\partial x}_{i,j} = \overline{\delta}_x u_{i,j}/2\Delta x + O(\Delta x^2) \tag{5.12}$$

$$\frac{\partial^2 u}{\partial x^2}_{i,j} = \delta^2_x u_{i,j}/\Delta x + O(\Delta x^2) \tag{5.13}$$

Derivatives used in boundary conditions were computed using a second

order accurate polynomial fitting approximation:

$$\frac{\partial u}{\partial x}_{i,j} = (-3u_{i,j} + 4u_{i+1,j} - u_{i+2,j})/2\Delta x + O(\Delta x^2) \qquad (5.14)$$

The central difference Eqs. (5.12) and (5.13) approximate the derivatives at a point by the values of the point and the surrounding points. In two dimensions, there are five points involved in the approximation, thus the term five point molecule is used to describe the configuration. The problem at hand is steady state, therefore no time derivatives are necessary. For a given rectangular domain divided into N equal units in the x direction and M equal units in the y direction, there are (N+1)(M+1) points requiring solution, which may be specified by a set of field equations or a boundary condition of interest. The problem involves two coupled sets of equations which must be solved simultaneously to account for the transfer of heat and mass.

5.4 Solution of the Finite Difference Equations

One goal of this study to compute the total heat transmitted through the convectively heated slab. The temperature and pressure field must be found by an appropriate solving scheme. Once the temperature field has been computed to within the desired order of accuracy, the total heat transmission across the plane of the slab is determined by integrating the surface flux. As a consequence of performing the integration, the original numerical accuracy of the approximating method is reduced. This drawback may be overcome by either increasing the accuracy of the approximating functions or by using mesh refinement until the required error limit is achieved. The general approach selected for the slab problem employs a second order

accurate approximation (Eqs. (5.12) and (5.13)) for the field equation derivatives. The boundary derivatives are approximated by Eq. (5.14).

A polynomial fitting approximation at the boundary has interesting properties. The flux component normal to the surface is modeled very effectively. In a finite difference approximation, however, a flux path adjacent to the boundary one-half mesh step in width exists that is neglected by this kinematic approach. The importance of this path and its contribution to slab heat transfer was investigated by comparing the kinematic boundary results with the conservation equation boundary results for the one-half mesh step region.

Comparison of methods and results incorporating the two boundary approximations were mixed. The conservation equation boundary method produced closer agreement to the final result with a coarse mesh than the kinematic boundary condition. However, the kinematic boundary conditions (used with a Gauss-Seidel method by lines solver) produced a more robust algorithm that converged for a greater range of parameters than other schemes using the conservation equation boundaries. Furthermore, the process of mesh refinement reduced any initial course mesh accuracy advantage enjoyed by the conservation boundary conditions. The kinematic boundary was selected for use because it was found to be effective when applied to porous media flow and heat transfer in the regime under investigation.

As previously stated, several numerical solving schemes were investigated such as explicit and fully implicit. The most effective method in this application was found to be the Gauss-Seidel by lines (GSL) with successive over-relaxation. The sweep directions were

alternated with each line. This method has several advantages over the fully implicit method or an explicit method, such as:

1. Smaller memory requirements. The fully implicit method requires simultaneous solution of an (N+1)(M+1) set of points. By taking maximum advantage of the banded nature of the matrix for the five point molecule, the storage requirements are proportional to a fraction of $((N+1)(M+1))^2$. The GSL method casts the governing equations into tridiagonal form. The boundary points are not tridiagonal, but may be reduced to tridiagonal by one additional step. Memory requirements are reduced to four times the maximum of N or M.

2. Rapid transport of boundary information through the domain. The fully explicit method solves for the value at a point in terms of the surrounding points. The GSL method solves for the values along an entire line in terms of the conditions of the adjacent lines and the boundary conditions. By alternating the direction of the lines, the latest boundary information is transmitted into the domain and is available for the next iterative step.

3. Stability of the algorithm is enhanced. The tridiagonal system is diagonally dominant and inherently stable. The mesh size may be selected to be coarse for the initial estimate of the solution. Naturally, for any fixed point iterative scheme, the value of the parameters will determine whether the procedure will converge. Divergence is easily corrected by decreasing the initial mesh size. Once a tentative solution is found, mesh refinement by linear interpolation is employed to improve accuracy. Appendix B–1 gives a detailed derivation of the difference equations. Appendix B–2 is a discussion of the logic flow chart and presents the code used to

calculate the earth-coupled porous media heat transfer problem specified by Eqs. (4.43), (4.44), (4.45), and Eqs. (5.6)—(5.8). For brevity, the code will be referred to as "SLAB" in the following discussion.

5.5 Comparison of Results and Error Analysis

Numerical solution of partial differential equations is an exercise in cost-to-benefit ratio optimization. The desired solution should be produced with the lowest computational cost to within the degree of accuracy that is required. The primary concern here is slab heat transfer under convective conditions where the thermophysical properties must be estimated or averaged. A numerical solution to within two percent of the exact value is acceptably accurate for this analysis. However, if the exact solution was known, then an approximate solution would be unnecessary. In general, the exact solution is not known, but for the special cases with known solutions, the algorithm may be tested and compared for accuracy. The presumption is that if the algorithm converges to the exact solution for the known case, then by inductive reasoning, it will converge to a solution where the exact solution is not known.

The following comparisons are made to determine the accuracy of SLAB. To illustrate the solution dependence on mesh size, Case I compares the SLAB constant surface heat flux conduction solution to the exact solution at various locations along the surface. To demonstrate the apparent insensitivity of surface temperatures to flow in the porous media, Case II compares the constant flux exact solution to the porous media constant flux solution produced by "FIDAP", a commercially prepared code. Finally, Case III is a surface temperature comparison of

the finite element method and the finite difference method. Case III solutions generated by SLAB and FIDAP are produced for the porous media problem with a constant convection condition at the surface. All of these comparisons are for the same domain with insulated lower boundaries as shown in Fig. 5.1. All temperatures and positions in the following discussion have been normalized.

5.5.1 Case I (Comparison with Exact Solution)

A two-dimensional square, solid plate insulated on sides and bottom is subjected to a unit heat flux at the upper surface. Flux is absorbed along the left half of the plate ($0.0 < x < 0.5$), and rejected along the right half of the plate ($0.5 < x < 1.0$). The value of the total heat ($q/\lambda\Delta T$) flowing through the plate is exactly 0.500. The conduction temperature profile along the upper surface ($0.0 < x < 1.0$) is given by

$$\Theta_{surface} = \frac{4}{\pi^2} \sum_{n=1}^{\infty} \frac{1}{n^2} \sin(n\pi/2)\cos(n\pi x) \qquad (5.15)$$

where the zero reference temperature is chosen at the point $x = 0.5$. Table 5.1 compares surface temperature values calculated by Eq. (5.15) and SLAB for a 16 X 16 mesh and a 32 X 32 mesh. The geometric mean error ratio is 1.0254 for 16 X 16 points and 1.0108 for the 32 X 32 point mesh when iterations were halted at a maximum successive difference of 2E-5 at all points in the temperature field.

5.5.2 Case II (Comparison of Porous Media FIDAP and Exact)

FIDAP (Version 4.5) is an all purpose incompressible fluid mechanics and heat transfer code developed by Fluid Dynamics International, Inc., 1600 Orrington Avenue, Suite 400, Evanston Illinois

60201. This code employs a fully implicit, finite element scheme and is capable of computing porous media flow using the Darcy's Law as the momentum field equation. Two cases were solved with FIDAP and compared with SLAB for constant heat flux of unity.

FIDAP performed the computation for the porous media problem very effectively. For the constant flux case, the FIDAP surface temperatures were not directly comparable with the solution found above because the temperatures were computed based on a reference temperature of zero. Adjusting the temperature profile to the same reference temperature for a 16 X 16 mesh produced an average difference of 0.035 percent between FIDAP porous media solution and the solid media theoretical solution. Table 5.2 compares the solid plate theoretical surface temperatures with the porous media solution produced by FIDAP. Again, the comparable results are insensitive to the nature of the nature of the media.

5.5.3 Case III (Comparison of Porous Media SLAB and FIDAP Solutions)

For a constant Biot number of thirty across the top surface, a comparison of FIDAP and SLAB for 16 X 16 mesh showed good agreement at the exterior points but differed slightly on alternate sides of the midpoint of the hot and cold regions. Figure 5.2 compares the surface temperature profiles produced by FIDAP and SLAB.

Proceeding to employ the SLAB code, the porous media internal field patterns for a convectively heated slab, Bi = 30, are calculated. Figure 5.3 compares the streamline patterns in the media for the case of constant viscosity and the Boussinesq density approximations with the streamline pattern for the case where a second degree polynomial was used to describe the density and viscosity of water. Figure 5.4 is a

Table 5.1 Temperature comparison of exact constant flux conduction solution with SLAB solution for two mesh sizes

Node	Distance	Temperature		
	x	Exact	16 X 16	32 X 32
0	.0000	.3712	.3757	.3741
1	.0625	.3673	.3718	.3702
2	.1250	.3554	.3599	.3582
3	.1875	.3350	.3396	.3376
4	.2500	.3051	.3099	.3076
5	.3125	.2641	.2696	.2665
6	.3750	.2088	.2157	.2113
7	.4375	.1321	.1433	.1356
8	.5000	6E–8	.0000	.0000

Table 5.2 Temperature comparison of exact constant flux solution with FIDAP porous media solution

Node	Distance	Temperature	
	x	Exact	16 X 16
0	0	.3712	.3725
1	.0625	.3673	.3708
2	.1250	.3554	.3571
3	.1875	.3350	.3349
4	.2500	.3051	.3099
5	.3125	.2641	.2648
6	.3750	.2088	.2068
7	.4375	.1321	.1282
8	.5000	6E–8	–.0085

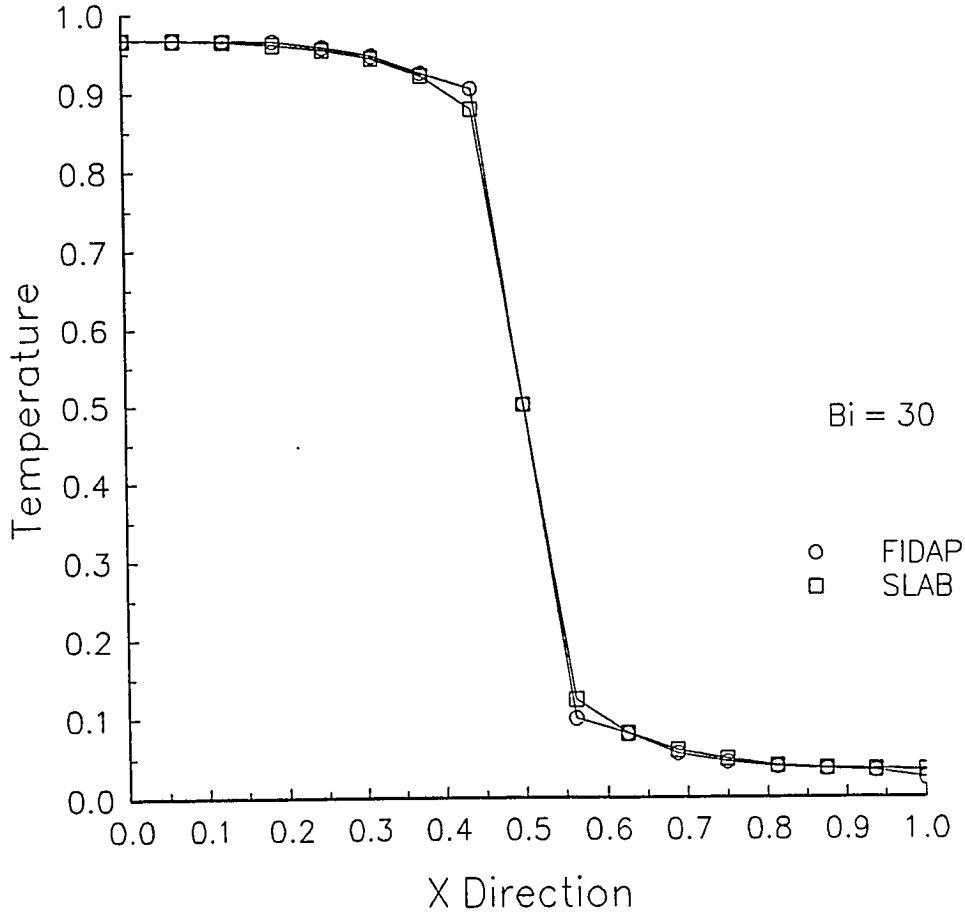

Fig. 5.2 Top surface (y = 1) temperature profile comparison for SLAB and FIDAP codes.

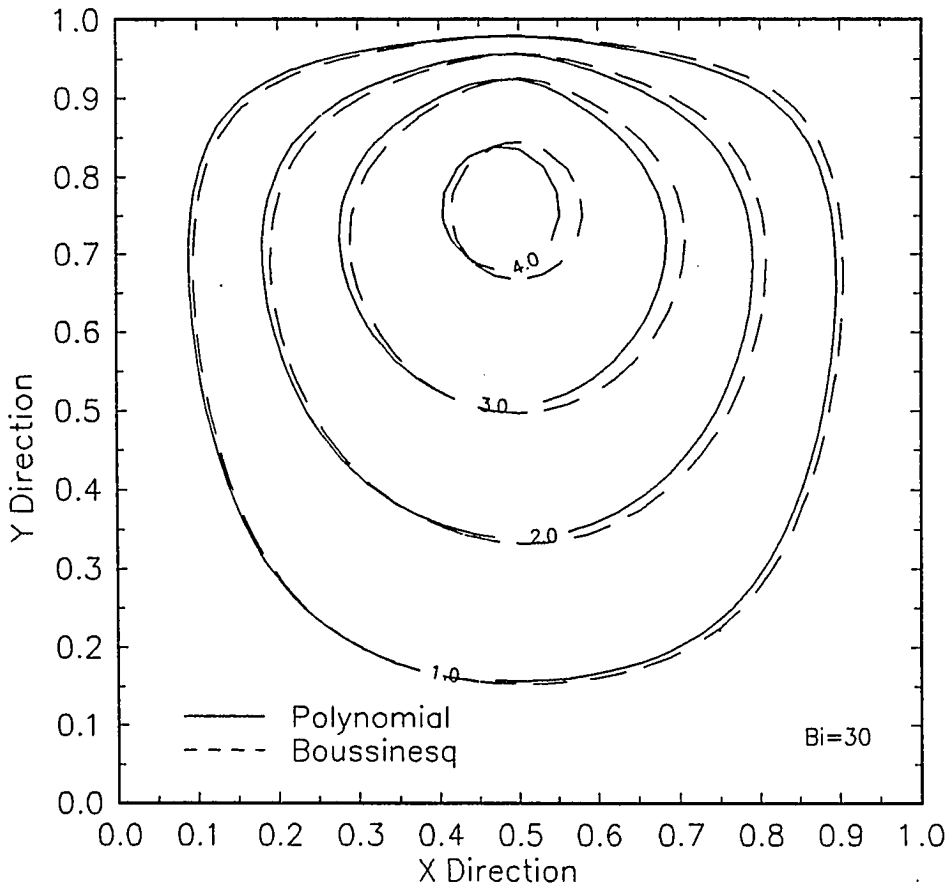

Fig. 5.3 Streamline comparison between polynomial fit density and viscosity and Boussinesq density approximation and constant viscosity.

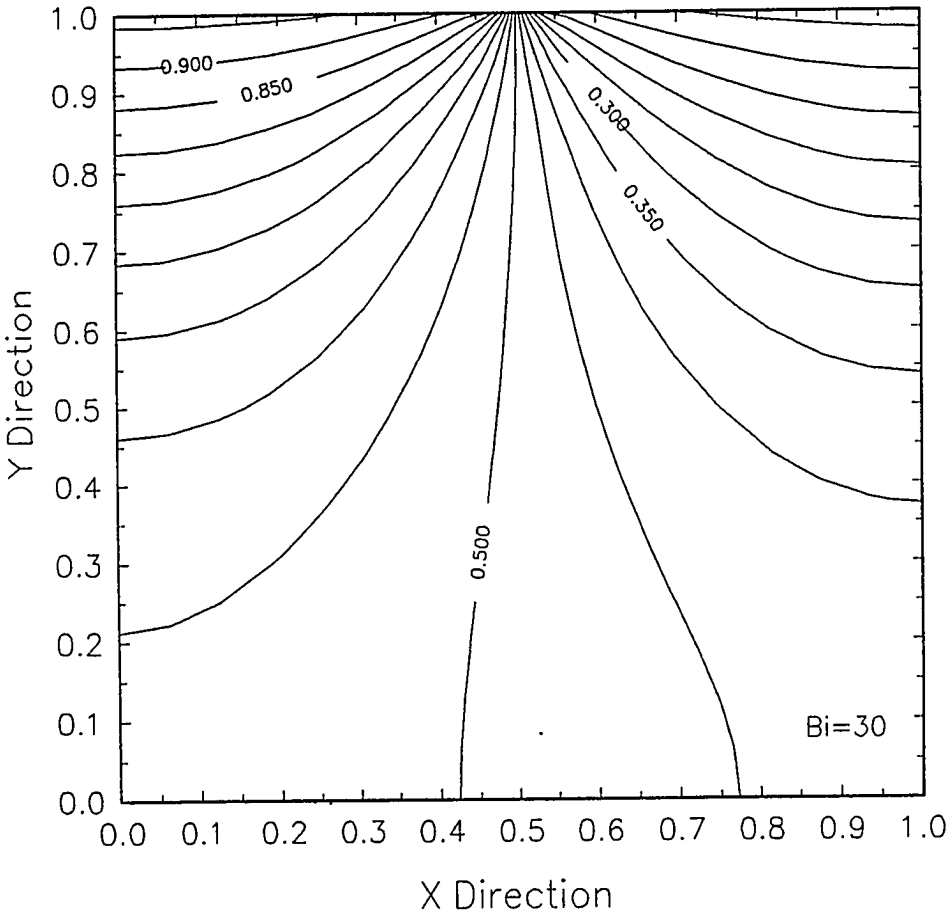

Fig. 5.4 Isothermal map of polynomial fit density and viscosity for streamline pattern shown in Fig. 5.3.

map of the position of the corresponding isotherms for temperature dependent viscosity and density. This map is essentially indistinguishable from the Boussinesq model solution.

5.6 Total Heat Transfer

Total heat transfer must be determined by integrating the local flux across the slab surface. Numerical experimentation has shown that saturated porous media and dry media yield the same value of heat flux for similar boundary conditions. The numerical experimentation has also shown that integrating a second order accurate solver results in a first order accurate integral. Mesh size reduction is one possible method that may be used to improve accuracy of heat flow computations. The sequential reduction of mesh size throughout the domain resulted in a sequence of approximate total heat transfer solutions. The sequence appeared to resemble a geometric series. Using the geometric aspect of the approximate heat flux solutions could improve the overall estimate of the total heat flux from the surface without exhaustive computation.

Table 5.3 is a summary of the total heat flux $(q/\lambda\Delta T)_i$ and the successive differences (Δ_i) for the unit heat flux problem of Sec. 5.5.1 as a function of mesh size. The successive difference is defined as

$$\Delta_i = (q/\lambda\Delta T)_i - (q/\lambda\Delta T)_{i-1} \tag{5.16}$$

where i the index of the number of mesh reductions (mesh size halvings).

Presume that the next term in the mesh reduction series would be represented by the following term

$$(q/\lambda\Delta T)_{i+1} = (q/\lambda\Delta T)_{i-1} + \Delta_i + \frac{\Delta}{a}i \tag{5.17}$$

where

$$a = \Delta_{i-1}/\Delta_i \tag{5.18}$$

The n^{th} term in the series would be

$$(q/\lambda\Delta T)_n = (q/\lambda\Delta T)_{i-1} + \Delta_i \sum_{k=1}^{k=n} a^{1-k} \tag{5.19}$$

This series converges when $a > 1$ and n increases without bound. The limit of the series is

$$(q/\lambda\Delta T)_\infty = (q/\lambda\Delta T)_{i-1} + \Delta_i \frac{a}{i(a-1)} \tag{5.20}$$

The following examples are chosen to illustrate the approximation applied to specific data.

5.6.1 Constant Flux Problem

For the constant flux problem of Sec. 5.5.1, the exact solution is 0.500. The following values are chosen from Table 5.3 for i = 3:

$(q/\lambda\Delta T)_{i-1} = (q/\lambda\Delta T)_2 = 0.48974$

$\Delta_3 = 0.00531$

$a = (0.01058)/(0.00531) = 1.99242$

$(q/\lambda\Delta T)_\infty = 0.50040$

This is a much better estimate of the exact answer than $(q/\lambda\Delta T)_3 = 0.49505$.

5.6.2 Constant Convection Problem (Bi = 10)

Consider the convectively heated rectangular plate with a breadth to depth ratio (H/D) of 2 that is heated on the upper surface between $0.0 < x < 0.5$. and cooled between $0.5 < x < 1.0$ with equal heat transfer coefficients. If the Biot number is set at 10, then the data in Table

Table 5.3 Total heat flux versus mesh size for unit surface flux

i	Mesh Size	$(q/\lambda\Delta T)_i$	Δ_i
0	8 X 8	.45832	—
1	16 X 16	.47916	.02084
2	32 X 32	.48974	.01058
3	64 X 64	.49505	.00531

Table 5.4 Heat flux versus Mesh size for convectively heated surface (Bi = 10)

	Mesh Size	$(q/\lambda\Delta T)_i$	Δ_i
0	8 X 4	.5518	—
1	16 X 8	.6396	.0877
2	32 X 16	.6907	.0512
3	64 X 32	.7183	.0276
4	128 X 64	.7326	.0143

5.4 is generated by SLAB. For the case cited in Table 5.4 and i = 4,

$$(q/\lambda\Delta T)_3 = 0.7183$$

$$\Delta_4 = 0.0143$$

$$a = 1.930$$

$$(q/\lambda\Delta T)_\infty = 0.747$$

So, by inductive reasoning, $(q/\lambda\Delta T)_\infty = 0.747$ is closer to the exact answer than $(q/\lambda\Delta T)_3 = 0.7183$.

5.6.3 Constant Convection Problem (Bi = 30)

Figure 5.5 illustrates the total heat flux as a function of mesh size as calculated by SLAB for the convectively heated surface similar to the problem in Sec. 5.6.2 except the Biot Number is thirty instead of ten. This figure graphically illustrates the heat flux asymptotically approaching a limiting value. The total heat flux $q/\lambda\Delta T$ is computed at three locations, hot and cold upper surfaces and a plane through the midpoint of the domain, to check for internal convergence. Although a slight flux difference exists across the hot and cold surface, this difference diminishes with decreasing step size. This is due to the steepness of the temperature gradient at the midpoint.

5.7 The Domain Shape Factor

Proposition V provides the theoretical basis for viewing the slab-on-grade problem as a potentially one-dimensional problem if the correct coordinate transformation is found. For a convectively heated slab, this computation is not a simple matter. However, an approximate method may be employed by devising a domain shape factor to investigate the correlation between the physical and thermal parameters of the

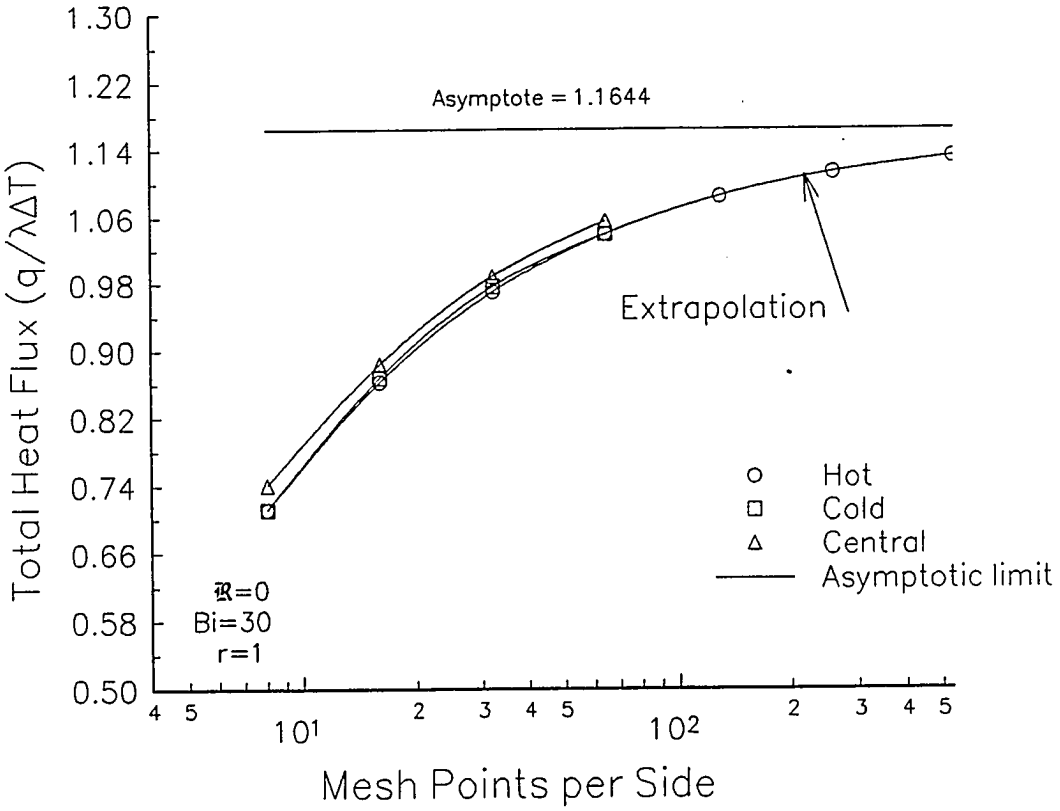

Fig. 5.5 Heat flux versus mesh points per side for a square, two-dimensional domain.

problem (Rust and Roberts, 1990). The original hypothesis motivating this method is justified by proposition VI stated in Chap. 3.

Assume a convectively heated half slab is situated on the upper surface of the domain. The slab half-length is L_1. The lower boundaries are adiabatic. The heat transferred from the slab is carried away by the ambient convection at the earth surface, which is a distance L_2 from the slab wall. The heat transfer coefficients on the slab and earth surface and the interior and exterior temperatures are h_1 and h_2, and T_1 and T_2 respectively. The heat transmitted through the air-earth interfaces and a strip of earth a differential thickness wide can be found by a standard resistance technique. Figure 5.6 shows the slab and its orientation on the domain. The differential strip is shown with a length, ξx, that is proportional to the distance along the slab from x = 0. The proportionality or shape factor, ξ, is to be determined. The differential heat rate through the elementary strip may be expressed in terms of the series path for heat flow as

$$dQ = w(T_1 - T_2)\left[\frac{\xi x}{\lambda} + \frac{1}{h_1} + \frac{1}{\epsilon h_2}\right]^{-1} dx \qquad (5.21)$$

where ϵ is defined to be of O(1),

$$\epsilon = L_2/L_1 \qquad (5.22)$$

Integration of this expression yields

$$Q/\lambda w\Delta T = q/\lambda\Delta T = \ln(1 + \xi Bi_1/(1+r))/\xi \qquad (5.23)$$

where

$$Bi_1 = h_1L_1/\lambda,\ q = Q/w, \text{ and} \qquad (5.24)$$

$$r = L_1h_1/L_2h_2 \qquad (5.25)$$

The shape factor, ξ, is implicitly defined in terms of known parameters. The quantity $q/\lambda\Delta T$ may be computed for a specific geometry and a

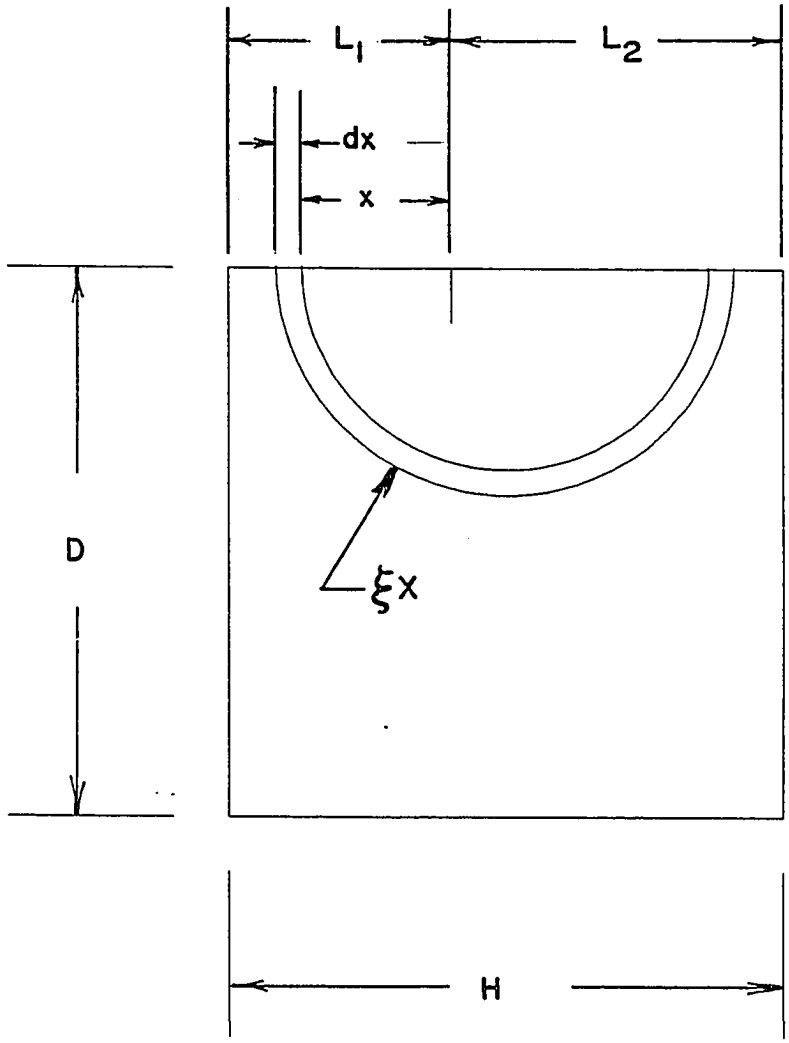

Fig. 5.6 Half-slab orientation and differential strip.

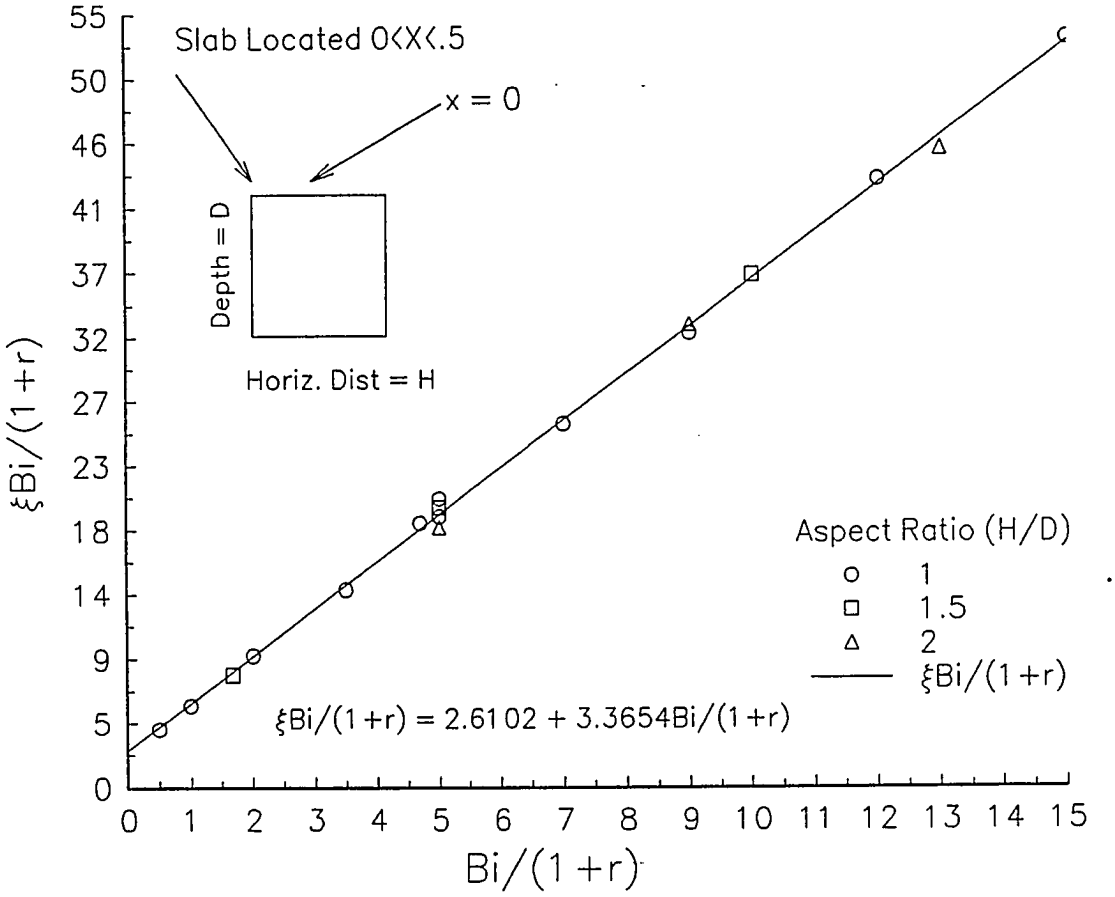

Fig. 5.7 Shape factor parametric study.

corresponding shape factor determined. Figure 5.7 is a shape factor parametric study for various rectangular domains and Biot numbers. From Fig. 5.7, a best fit relationship is found, namely,

$$\xi = 3.3654 + 2.6102\ (1 + r)/Bi \qquad (5.26)$$

The following example will illustrate the use of the shape factor.

5.7.1 Shape Factor Example Problem

A slab–on–grade building is heated to 20 C by forced hot air with an average heat transfer coefficient of 3 W/m^2–deg K. Winter ambient temperature is –10 C. If the building slab's short dimension is 10 m and the soil has a thermal conductivity of 3 W/m–deg K, find the total heat loss from the building per foot of width.

5.7.2 Solution Method

5.7.2.1 Compute Bi for the half–slab.

$$Bi = hL/\lambda = \frac{3\ W/m^2\text{–deg K} \cdot 5\ m}{3\ W/m\text{–deg K}} = 5$$

5.7.2.2 Geological Data. Since no geological information is stated in the problem, assume L_2 is large and

$$r \cong 0$$

5.7.2.3 Shape Factor. Find the shape factor from Eq. (5.26) or use Fig. 5.6.

$$\xi = 3.3654 + 2.6102 \cdot (1 + 0)/Bi$$

$$\xi = 3.887$$

5.7.2.4 Heat Flux. Use Eq. (5.23) to calculate the heat flux.

$$q/\lambda\Delta T = \ln\ (1 + 3.887 \cdot 5)/3.887 = 0.776$$

Solving for q yields

$$q = 0.776 \cdot 3 \text{ W/m-deg K} \cdot 30 \text{ C} = 69.85 \text{ W/m}$$

For the full length (both sides of the symmetry plane) of the slab, the total heat lost per unit length of slab is $q_{total} = 2q$.

$$q_{total} = 139.7 \text{ W/m}.....\text{Ans.}$$

5.8 Extending the Shape Factor Method to Other Applications

The energy loss from the slab has been determined to be a function of the conductivity of the soil, the average temperature difference between the interior and exterior of the structure, and the Biot number for the slab. This method may be extended to a wider variety of situations by including additional factors as required. The treatment of slab insulation, the effect of a water table located in proximity to the slab, and the extension of the method to three dimensions are discussed in the following paragraphs. These extensions are compared to results obtained by other computational methods found in the literature.

5.8.1 Additional Slab Insulation

Additional slab insulation may be included in the computations by adjusting the film coefficient, h, to represent a loss coefficient, U, that includes the thermal characteristics of the insulation.

$$U = \left[\frac{1}{h} + \frac{\Delta x}{\lambda_{ins}} \right]^{-1} \tag{5.27}$$

The loss coefficient, U, replaces the film coefficient in the Biot number.

5.8.2 Presence of a Water Table

For fully saturated soil, the correction for a water table is not necessary provided the apparent thermal conductivity of saturated soil is used. However, for a water table located relatively close to the slab, two soil zones are present. The effect of the water table on the slab may be treated as a one-dimensional problem superposed on the two-dimensional problem. With the soil conductivity known in the unsaturated region, the heat loss to the water table may be expressed as

$$Q = U\ A\ \Delta T, \text{ where}$$

$$U = \left[\frac{1}{h} + \frac{\Delta x}{\lambda_{ins}} + \frac{\text{depth}_{\text{water table}}}{\lambda_{soil}} \right]^{-1}$$

This quantity is added to the heat loss to the ambient computed with the shape factor method.

5.8.3 Extension to Three-dimensional Slabs

Three-dimensional effects of slab heat loss may be computed by applying the shape factor method. Again, by utilizing the linear superposition of solutions, the three-dimensional problem is decomposed into a pair of separate, two-dimensional, mutually orthogonal problems as outlined below.

Given a slab (a X b) subject to known thermal conditions, find the heat loss to the ambient.

5.8.3.1 Step 1. Decompose the slab into a pair of quasi-two-dimensional problems of (length X width) where (a X b) is the first problem and (b X a) is the second problem.

5.8.3.2 Step 2. Find the heat loss in the "a" direction by finding the

Biot number for the half-slab, Bi = $U(a/2)/\lambda$.

5.8.3.3 Step 3. Find the shape factor in the "a" direction from equation (5.26). Find the heat flux $(q/\lambda\Delta T)_a$ in the "a" direction from equation (5.23).

5.8.3.4 Step 4. Repeat Step 2 and 3 using the "b" direction.

5.8.3.5 Step 5. Find the total heat loss in the "a" and "b" directions.

$$Q_a = 2 \cdot (q/\lambda\Delta T)_a \lambda (T_1 - T_2) \cdot b$$

$$Q_b = 2 \cdot (q/\lambda\Delta T)_b \lambda (T_1 - T_2) \cdot a$$

The total heat loss from the slab is the sum

$$Q = Q_a + Q_b$$

5.8.4 Comparison of Two-dimensional Methods with Slab Insulation and Water Table

Krarti and Claridge (1988) propose and solve the following time dependent problem in two dimensions using the ITPE method they developed. The steady state heat loss solution to this problem will be found using the shape factor method and compared to the steady state solution of the ITPE method.

5.8.4.1 Two-dimensional problem and ITPE solution. Compute the two-dimensional heat loss from a uniformly insulated 8 m X 16 m slab-on-grade with a U-factor of 0.645 W/m^2-deg K. A Water table is located 5 m below the building foundation at Madison, WI. Soil thermal conductivity is 1 W/m-deg C. Krarti and Claridge (1988) use the following data to solve this problem with the ITPE method where "t" is

time and "ω" is angular frequency.

Earth surface Temperature, T_s:

$$T_s = 7.8 + 15.2 \cos(\omega t) \text{ (deg C)}$$

Water Table Temperature, T_w:

$$T_w = 11.4 \text{ C}$$

Building Space Temperature, T_i:

$$T_i = 21.0 + 2 \cos(\omega t) \text{ (deg C)}$$

The computed total annual heat flux by the ITPE method is

$$Q(t) = 405 + 78 \cos(\omega t + 1.83) \text{ (Watts)}$$

Using these data, the heat loss will be computed using the shape factor method. In this example, an insulated slab and a water table under the slab are considered. This problem must be solved by using superposition of the total heat loss to the ambient with the total heat loss to the constant temperature water table.

5.8.4.2 Shape factor solution.

5.8.4.2.1 Compute Bi for the half-slab. The U-factor is the combined surface conductance of the slab and the insulation.

$$Bi = UL/\lambda = \frac{0.645 \text{ W/m}^2\text{-deg K} \cdot 4 \text{ m}}{1 \text{ W/m-deg K}} = 2.58$$

5.8.4.2.2 Find the Shape factor assuming r = 0.

$$\xi = 3.3654 + 2.6102 \cdot (1 + 0)/2.58 = 4.377$$

5.8.4.2.3 Use Eq. (5.23) to calculate the heat flux.

$$q/\lambda\Delta T = \ln [1 + 2.58 \cdot (4.377)]/2.58 = 0.5732$$

5.8.4.2.4 Solve for the total flux from the slab.

$$Q_1 = 2q\lambda\Delta T \cdot w \text{ (w is width of the slab)}$$

$$Q_1 = 2 \cdot (0.5732) \cdot (1 \text{ W/m-deg K}) \cdot (16 \text{ m}) \cdot (21 - 11.4)(C)$$

$$Q_1 = 242.1 \text{ W to ambient.}$$

5.8.4.2.5 Compute Heat loss to ground water table assuming a linear path.

$$q_2 = \left[\frac{1}{0.645 \text{ W/m}^2\text{-deg K}} + \frac{5 \text{ m}}{1 \text{ W/m-deg K}} \right]^{-1} \cdot (21 - 11.4)(C)$$

$$q_2 = 1.465 \text{ W/m}^2$$

$$Q_2 = q_2 A = (1.465 \text{ W/m}^2) \cdot (8 \text{ m} \cdot 16 \text{ m}) = 187.6 \text{ W to water}$$

table.

5.8.4.2.6 The total average heat flux is the sum of the solutions.

$$Q = Q_1 + Q_2 = 429.7 \text{ W}$$

The shape factor value is six percent higher than the value given by Krarti and Claridge (1988) using a transient method. The cooling factor, r, cannot be determined from the information given in the published problem, which if known would probably improve agreement.

5.8.5 A Three-dimensional Comparison

Krarti et al. (1990) extended the ITPE method to three-dimensions. Average heat loss per unit area for a variety of slab-on-grade rectangular geometries were computed and tabulated along with the results from Mitalas (1987). For the sake of comparison, the following data were used:

λ = 0.9 W/m-deg C (soil thermal conductivity)

U = 0.45 W/m^2-deg C (combined surface conductance)

T_2 = 20 C (inside temperature)

T_1 = 10 C (outside surface temperature)

These data will be used to compute the slab heat loss per unit area as outlined in Sec. 5.8.3. Table 5.5 is a comparison of the ITPE slab loss method computed by Krarti et al. (1990) and the shape factor method

for a unit area of surface. The shape factor method is within the band of difference of the results of Mitalas quoted by Krarti et al. (1990) and the ITPE method cited in Table 5.5.

5.9 Closure

The two-dimensional, steady heat transfer from a building slab has been computed by the SLAB code developed for this purpose. A comparison of output data from this code with a commercially developed code and the exact solution has shown good agreement within the required accuracy. A shape factor method has been developed to predict heat loss from a convectively heated slab that produces accurate results over a wide range of conditions.

The SLAB code, suitably modified for the experimental model, will be employed in Chap. 6 to predict heat transfer and flow conditions in porous media. The suitability of the approximations embedded in the governing equations and the numerical approximations will be examined in the light of experimental measurements.

Table 5.5 Slab heat loss comparison using ITPE method and shape factor method

Dimension (m X m)	Heat Loss (W/m^2)		Difference (%)
	ITPE	Shape Factor	
2 X 2	3.725	3.493	–6.2
4 X 4	2.700	2.925	+8.3
6 X 6	2.500	2.536	+1.4
4 X 10	2.525	2.470	–2.2
10 X 10	2.030	2.030	0.0
10 X 20	1.850	1.748	–5.5

Chapter 6

POROUS MEDIA HEAT TRANSFER EXPERIMENT

6.1 Introduction

Heat transfer has been computed subject to the approximations employed in the formulation of the governing equations and subsequent numerical approximations. Several features of slab heat transfer were revealed, especially the apparent insensitivity of total heat transfer, $q/\lambda\Delta T$, to the saturation state of the media. To validate this result requires that measurements be performed by experiment.

The experiment was designed to emulate as much as possible a steady, two-dimensional slab on grade over a saturated soil. A scaled down experiment was deemed most appropriate because: steady conditions could be maintained; two-dimensional effects and adiabatic boundaries could be achieved more easily; flow visualization was possible without environmental hazard; response time was in hours instead of years; and finally, the cost of a small scale experiment was realistic.

There are certain sacrifices that must be made when performing scaled experiments. In some cases, similitude in thermal and dynamic parameters cannot be achieved simultaneously. For porous media, scaling accentuates the wall effects where the media contacts the container. The thickness of the media is limited to a few centimeters because flow visualization requires a relatively thin section so that tracer dye may

be seen. Moreover, physical construction was required which would allow for aspect ratios to be changed if desired.

The following sections will discuss the design and construction of the experimental apparatus, the procedures followed to measure total heat transfer and the resolution of discrepancies in the porous media thermal conductivity, porosity and permeability.

6.2 Experimental Apparatus

Heat transfer is energy crossing a boundary by means of a temperature difference, and for the analysis herein, will be considered to be a linear rate process. To measure heat transfer by conduction, a temperature gradient must be detected in some way. In a scaled model, this is not easy to obtain with accuracy. Heat transfer may be measured by phase change which occurs isothermally at atmospheric pressure. Ice is an ideal candidate for a phase change substance because the temperature range between the ice point and room temperature is the approximate temperature range experienced by a typical slab exposed to winter conditions. The experimental apparatus takes advantage of melting ice as a measure of slab heat transfer. The apparatus was made of plexiglas to observe the flow field and designed to be free of mechanical penetrations that disturb the flow field.

Figure 6.1 is a schematic of a 1/100 scale model of the two dimensional half-slab apparatus. The section designated as the test cell is essentially a tank with inside dimensions of 100 mm X 100 mm X 12.5 mm and made of 6 mm thick, clear plexiglas. A machined brass fitting was mounted in both vertical end walls of the test cell so that plastic tubing could be attached to fill the test cell with liquid or to inject

dye as required. The fittings were designed to minimize the protrusion into the porous media flow field. The test cell upper surface was made sufficiently flat to accommodate a gasket seal.

The upper section of the apparatus consists of one assembly which provides the heating and cooling required to induce circulation in the porous medium test cell. The upper assembly consists of two chambers: one chamber is to contain ice and the other chamber is to contain room temperature water. The outer walls of the upper assembly were also constructed of 6 mm plexiglas. The central partition between the chambers was constructed of a double thickness of 6 mm plexiglas with a 1.6 mm brass vent tube (not shown) inserted vertically on the centerline. The floor of the ice chamber and the warm water chamber were identical. Each floor consisted of a brass plate, approximately 110 mm X 25 mm X 1.2 mm, with thermocouples soldered into the plate along the centerline. The ice chamber was also equipped with a spill tube in the outside wall which was attached to the plexiglas by means of a brass fitting.

The heating assembly and the test cell filled with porous media were placed in a clamping device. The position of the test cell with respect to the upper heating assembly could be adjusted to vary the ratio of the cooling and heating surface areas exposed to the fluid circulating in the porous media. Solid media could be easily substituted for the porous media test cell by merely replacing the test cell with a specimen of the desired material.

After the upper heating assembly and the test cell were clamped together and checked for leaks, the entire assembly was leveled and insulated with styrofoam panels. Auxiliary plexiglas draft shields were

placed on both sides of the test cells so that heat gain from the ambient would be reduced while visually observing or photographing the flow pattern.

The cooling effect was produced by manually placing crushed ice at -12 C in the ice chamber, the floor of the ice chamber being at the top of the test cell. Room temperature water was circulated from storage tanks to the adjacent heating chamber by siphon tubes. The head needed to power the siphon tubes was provided by small 30 W in-line reciprocating pump which maintained a differential of about 75 mm of water. An interesting feature of this arrangement was that the water level in the heating chamber always remained fixed at the average level of the two storage tanks, provided that the siphon tubing was matched by length and diameter. This eliminated the need for level control in the heating chamber.

The sub-surface soil was simulated in the experiment by using one mm diameter glass beads. This size was chosen because the permeability of the bead pack and dimensions of the model produced similitude with common soils and a full scale slab through the parameter $\mathfrak{R}$ (Eq. (4.41)) or the Rayleigh number (Eq. (4.56)). The Rayleigh number for typical soil and thermal conditions found in practice has a magnitude that is within the range of validity of Darcy's Law (Bear, 1972).

6.3 Procedure

Water serves as an excellent substance for detecting heat gain by phase change. Ice at -12 C is loaded manually into the ice chamber and is removed as water at the cold plate temperature by careful siphoning. The rate of heat absorption is measured by collecting the water from the

ice chamber as a function of time. Since the enthalpy of water is known at the plate temperature (T_c), the heat transferred is

$$\dot{Q} = \dot{m}\,(h_{T_c} - h_{-12C}), \text{ where} \tag{6.1}$$

$$h_{-12C} = -h_{sl} + c_{p_{ice}}(0 - 12)(C)$$

and $\dot{Q}$ is the total rate of heat absorbed by the ice, $\dot{m}$ is the mass rate of discharge of water, and h is the enthalpy of water in the solid or liquid phase at the designated temperature, provided that steady conditions are present. Steady conditions are determined by monitoring temperatures and discharge rate. These data may be collected for a variety of materials and compared with the theoretical predictions if the heat flow through the material can be isolated from the ambient gain. The method of isolating the desired quantity is discussed below.

The total heat gain is the sum of the individual contributions from all sources. This may also be thought of as a linear combination of terms in the form

$$\dot{Q} = \sum \dot{Q}_k = \sum U_k \Delta T_k \tag{6.2}$$

where the subscript designates the source of the heat gain. For the experimental apparatus, steady-state heat is gained from the ambient through the insulation around the ice chamber, from the warm chamber to cold chamber flowing through the plexiglas partition, and from the media directly to the cold plate.

$$\dot{Q} = \dot{Q}_{wall} + \dot{Q}_{plexiglas} + \dot{Q}_{media} \tag{6.3}$$

Supposing that the media heat loss coefficient is known, then the unknown coefficients may be found. This is accomplished by clamping a block of insulation of known conductivity in place of the test media. Furthermore, two independent sets of data may be obtained if the warm chamber is filled with ice in one instance and ambient temperature water

in the other. Thus,

$$\Delta T\ \mathbf{U} = \mathbf{Q} - \mathbf{Q}_m \tag{6.4}$$

where bold indicates a matrix quantity. Solving for $\mathbf{U}$,

$$\mathbf{U} = \Delta T^{-1}\ (\mathbf{Q} - \mathbf{Q}_m) \tag{6.5}$$

The U coefficients will remain constant provided that the apparatus insulation configuration and the method of loading the ice chamber is not changed. Various material of known and unknown thermal conductivity may be tested in the apparatus and the results compared with the computed values of $q/\lambda\Delta T$. The SLAB code was adapted to the experiment by setting the slab and earth surface temperatures to the corresponding experimentally observed plate temperatures. The partition wall between the hot and cold chamber was represented as a nondimensional wall of thickness 1/8 and centered at the slab/earth interface. A linear temperature profile was imposed across the wall. Repeating the procedure developed in Chap. 5 for the constant temperature surface with linear wall resulted in the total integrated heat flux of:

$$q/\lambda\Delta T = 1.035 \tag{6.6}$$

This is the net total heat transfer from the warm plate through the media to the cold plate for the specific dimensions of the test apparatus.

6.4 Apparatus Characteristics

An experimental apparatus should be sensitive to changes in the controlled variables but minimize the intrusive effects when measuring the desired quantities. After experience was gained conducting the porous media heat transfer experiments, several equipment characteristics became apparent that were not foreseen in the design of the

apparatus. Before proceeding with the discussion of results of the experiment, these characteristics will be discussed as well as the measures used to overcome ambiguities or difficulties.

6.4.1 Measuring Instruments

Various instruments were required to conduct this experiment. Mass was measured with a triple beam balance to within ±0.05 grams. Volume was measured with a 250 milliliter graduated cylinder to within ± 1 ml. Temperature was measured with three devices: a Fluke type K thermocouple reader accurate to ± 0.5 F or ± 0.5 C; a Supco PT-200 type J dual probe thermometer accurate to within ± 0.5 F or ± 0.5 C; and an alcohol thermometer accurate to ± 1 F. Critical distances were measured to ± 0.1 mm or 0.001 inch with micrometers or calipers. Where a choice of measurement scale was offered, selection was based on the most accurate. For temperature, all measurements are in degrees Fahrenheit. To minimize chance of error, all data will be reported in the units in which they were measured. Intermediate calculations will be performed in measured units and converted to be consistent with the SI units at the last step.

6.4.2 Temperature Measurement

The conditions being measured are valid assuming that a steady periodic state is maintained, and therefore the periodic component will not affect the steady value (see Chap. 3). The manual stirring of the ice was performed at regular time intervals thus emulating the steady periodic condition. The exact amount of agitation during any particular interval is essentially random. How random agitation of the ice chamber

and the ±1/2 deg F sensitivity of the thermocouple reader affects experimental accuracy is discussed below.

The ice chamber agitation and measuring process was simulated by a computer model. The average value of two series of numbers were compared

$$T_{avg} = \frac{1}{n} \sum_{i=1}^{n} T_i \tag{6.7}$$

$$T_{avg,exact} = \frac{1}{n} \sum_{i=1}^{n} T_{i,exact} \tag{6.8}$$

such that each term obeys this rule:

$$| T_i - T_{i,exact} | < 1/2, \text{ where} \tag{6.9}$$

$$T_{i,exact} = T_i + \epsilon, \text{ and}$$

$$\epsilon = \text{random number}, -1/2 < \epsilon < 1/2 \tag{6.10}$$

The result of several simulations indicate that rounding accuracy improves as the number of samples increases as indicated in Table 6.1. The averaging process provides a means of increasing accuracy that will be taken advantage of in the following analysis.

6.4.3 Improvements to the Apparatus and Data Corrections

As experience was gained collecting data, it became obvious that improvements were needed to increase accuracy. The spill tube discharge was erratic and the temperature of the discharge water was not precisely known because no thermocouples were located at the tube inlet (see Fig. 6.1). This defect was corrected by fabricating a siphon tube with slots cut along the perimeter of the suction end so that ice would not block the flow. The slotted end of the tube rested directly on the cold plate in the ice chamber, and the other end was placed in a jig so that the

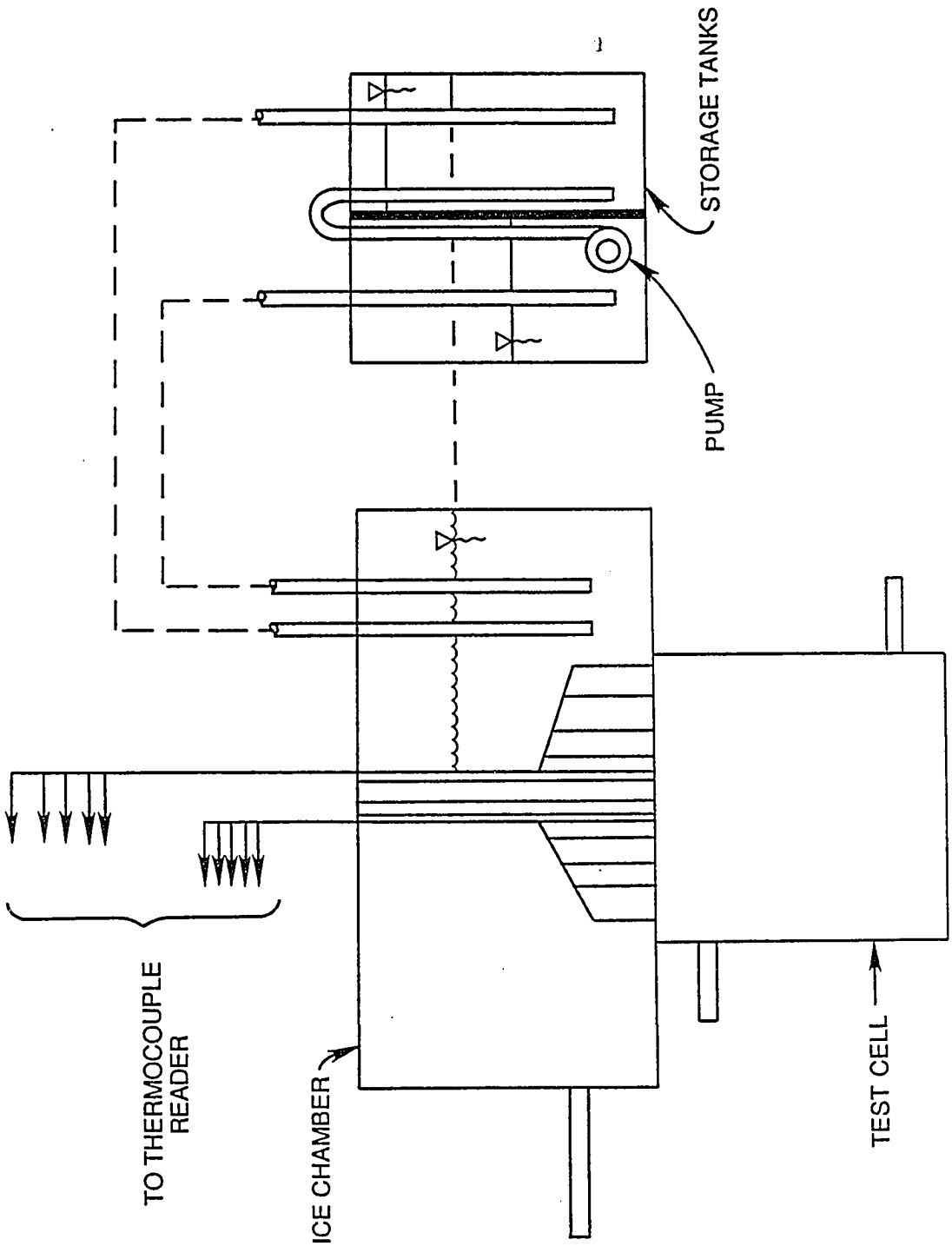

Fig. 6.1 Schematic diagram of test apparatus.

discharge end of the tube would remain fixed at a preset height relative to the cold plate elevation. This increased the uniformity of the discharge and assured that the water temperature was exactly that of the cold plate. A correction to discharge temperature data measured previously with the spill tube is taken to be the average of the cold plate and the ice point, 32 F.

Additional insulation over the clamping device was found to be necessary to reduce heat gain to the ice chamber. Adding extra insulation reduced the number of intrusions into the ice chamber needed to maintain steady conditions. A correction was found for data taken before the added insulation was installed.

The water storage tank was intended to act as a thermal reservoir and was expected to remain in thermal equilibrium with the room. This was not the case, however. The in-line pump acted as a small heat source and created a new tank equilibrium temperature that was slightly different than the average room temperature. The analysis of heat gained by the ice chamber required that ambient room and tank temperatures be taken into account.

6.4.4 The Thermal Conductivity of Glass

Although glass is a common material, it exhibits a wide range of thermal properties as shown in Appendix C. The use of solid glass as a test specimen was desirable because the test porous media was composed of glass spheres. The comparison of solid media and porous media properties in the saturated and dry condition would be informative. This required that the thermal properties of the glass specimen be verified.

The following transient thermal comparison test was devised to find the correct values of thermal conductivity.

Step 1. Two identical, rectangular shapes were fabricated from plexiglas and glass. The physical and thermal properties of the plexiglas were known from published data and would serve as the standard. Each material was imbedded in identical blocks of styrofoam so that the exposed surface was flush with the styrofoam. Thermocouples were attached to opposite sides of the plastic and glass with equal amounts of aluminum tape so that the temperature of the exposed surface and the insulated surface could be measured.

Step 2. Each test unit was in turn chilled to a uniform temperature of -10 C along with a dummy block of styrofoam. The dummy block of styrofoam was used to cover the exposed test unit surface so the unit could be removed from the freezer without undue heating. The dummy block of styrofoam was removed from the test unit at time zero thus creating a step change in temperature at the exposed surface. The change in the difference in temperature between the exposed surface and the insulated surface were recorded as a function of time.

Step 3. The one-dimensional transient heat equation

$$\frac{\partial \Theta}{\partial t^*} = \frac{\partial^2 \Theta}{\partial x^{*2}} \tag{6.11}$$

subject to

$$\Theta = (T - T(1,0))/(T_\infty - T(1,0)) \tag{6.12}$$

$$\Theta(x^*,0) = 0 \tag{6.13}$$

$$\Theta_\infty = 0, \; t < 0 \tag{6.14}$$

$$\Theta_\infty = 1, \; t \geq 0 \tag{6.15}$$

$$\frac{\partial \Theta}{\partial x^*} = \frac{hw}{\lambda} (\Theta_\infty - \Theta), \; x^* = 0 \tag{6.16}$$

$$\frac{\partial \Theta}{\partial x^*} = 0, \quad x^* = 1 \tag{6.17}$$

was solved numerically where T_∞ is the ambient temperature, $x^* = x/w$ (w is thickness of material), $t^* = t/\tau$ (t is time), and $\tau = \rho c w^2/\lambda$. Other symbols are defined in the nomenclature.

Step 4. Using the plexiglas as the standard, Eqs. (6.11)—(6.17) were solved to match the measured temperature–time function. These data produced the film coefficient, h. The film coefficient was used with various thermal data for glass listed in Appendix C. Equations (6.11)–(6.17) were solved using the properties of glass listed in Appendix C until a match was found with the measured transient response. The values given by Hodgman et al. (1963) fit the overall measured response data within two percent. Other property data for glass differed significantly from the measured response data. The agreement with Hodgman et al. (1963) is sufficient to conclude that the thermal conductivity of the glass specimen is 1.046 W/m–deg K.

6.5 Solid Media Results

Temperature data fields are averaged as described in Sec. 6.4.2. Mass discharge rate is found from the least squares fit of the cumulative sum of the discharge as a function of time. Table 6.2 is a summary of reduced observations for data collected on three separate occasions. These data are averaged from field observations and will carry an extra digit of precision which will later be rounded to the appropriate experimental accuracy.

Applying the corrections stated in the previous section, loss coefficients were desired that would best satisfy all the observed data within the range of uncertainty. Table C.2 in Appendix C lists the raw

Table 6.1 Accuracy for a given sample size

Sample Size	Accuracy
1	±0.5
25	±0.13
50	±0.03
500	±0.01

Table 6.2 Temperature-discharge Data for solid media

Material	Discharge, gm/hr	T_2, °F	T_i, °F	T_{room}, °F	T_{tank}, °F	Date
Glass	36.95	36.62	66.57	68.62	67.29	3 Mar 90
Glass	35.40	37.67	65.44	67.31	65.89	4 Mar 90
Plexiglas	34.74	34.60	65.85	68.17	66.50	8 Mar 90

calibration data measured in this experiment. Assuming the computed value, $q/\lambda\Delta T = 1.035$, the initial loss coefficients (heat gain) for the ice chamber walls and the inter-chamber partition were estimated using the temperature of the warm bath (loaded with ice) at 35.5F.

$U_1 = 0.2471$ BTU/hr-deg F

$U_2 = 0.0786$ BTU/hr-deg F

By refining the initial estimate iteratively, the following coefficients were found that best described the aggregate data. By correcting the warm bath temperature (while loaded with ice) to 38.0 F and using the data from Table 6.2,

$U_1 = 0.2423$ BTU/hr-deg F

$U_2 = 0.0888$ BTU/hr-deg F

Applying a correction for the less well-insulated apparatus data,

$U_1' = 0.2850$ BTU/hr-deg F

$U_2 = 0.0888$ BTU/hr-deg F

With these values in Table 6.2, the thermal conductivity is computed using $q/\lambda\Delta T = 1.035$ from Eq. (6.6) to be

$\lambda = .19$ W/m-deg K, for plexiglas medium data of 8 Mar 1990,

$\lambda = 1.09$ W/m-deg K for glass medium data of 3 Mar 1990, and

$\lambda = 1.06$ W/m-deg K for glass medium data of 4 Mar 1990.

6.6 Porous Media Results

In the previous sections, the experimental method was discussed that would verify the numerical computations. The expression $q/\lambda\Delta T = 1.035$ for the test geometry appears to be correct for the solid media based on the thermal conductivity measurements of Sec. 6.5. The purpose

of this section will be to carry forward this technique to the porous media.

There is a dearth of information on thermal properties of porous media. This precludes a direct test. However, the apparent thermal conductivity of the porous media can be measured in the test apparatus and the results used to calculate the velocity field. Agreement of computed and observed velocity fields would indicate that the apparent thermal conductivity was correct. The apparent thermal conductivity will be computed in this section and the velocity field comparisons will be made in Sec. 6.7. The data in Table 6.3 were recorded for the porous media tests.

To illustrate the calculation procedure, the thermal conductivity for the dry porous media (consisting of 1 mm glass beads) is computed. The total heat gain is measured by the mass of water discharged per unit of time multiplied by the change in enthalpy for water between -12 C and the corrected discharge temperature. From this total is deducted the heat gain from the ambient and the warm tank. Moreover, the walls of the test cell are plexiglas and the heat gain from the warm plate to the cold plate through the walls must also be deducted from the total. The thermal conductivity is found by dividing the remaining heat rate per unit width (w) by (1.035 X ΔT).

Step 1. Compute total heat rate. (see Eq. 6.1))

$$Q = \dot{m}\Delta h = (44.25 \text{ gm/hr}) \cdot (.34873 \text{ BTU/gm at } 36 \text{ F})$$

$$Q = 15.4318 \text{ BTU/hr}$$

Step 2. Compute individual gains.

$$Q_1 = U_1(T_{room} - 32) = (.2850 \text{ BTU/hr-deg F}) \cdot (71.72 - 32)\text{F}$$

$$Q_1 = 11.3222 \text{ BTU/hr}$$

$$Q_2 = U_1 \cdot (T_{tank} - 32) = (.0888 \text{ BTU/hr-deg F}) \cdot (70.22 - 32)\text{F}$$

$$Q_2 = 3.3939 \text{ BTU/hr}$$

$$Q_{wall} = 1.035 w \lambda \Delta T = 1.035 \cdot (.472 \text{ in.})(\text{ft}/12 \text{ in.}) \cdot (.11 \text{ BTU/hr-deg F}) \cdot (67.69 - 40.02) \text{ F}$$

$$Q_{wall} = 0.1239 \text{ BTU/hr}$$

Step 3. Compute the net heat gain.

$$Q_{net} = Q - Q_1 - Q_2 - Q_{wall}$$

$$Q_{net} = 0.5839 \text{ BTU/hr}$$

Step 4. Compute the thermal conductivity.

$$k = Q_{net}/w\lambda\Delta T = (0.5839 \text{ BTU/hr})/[(.5 \text{ in.})(\text{ft}/12 \text{ in.}) \cdot (1.035) \cdot (67.69 - 40.02) \text{ F}]$$

$$k = 0.49 \text{ BTU/hr-ft-deg F or } 0.85 \text{ W/m-deg K.}$$

Experimental measurements of apparent thermal conductivity of 2.38 mm spherical bead packs composed of different materials and interstitial gases present in the media were performed by Duncan et al. (1989). Several interesting observations were noted as follows: that the series and parallel thermal resistance techniques investigated for computing apparent thermal conductivity of the gas-saturated media were inappropriate in predicting the measured conductivities; and, that the presence of the gas environment affected the apparent thermal conductivity significantly. Using an entirely different apparatus, bead size, thermal configuration and gases than those reported here, Duncan et al. (1989) measured the thermal conductivity of the bead pack under vacuum to be 0.47 W/m-deg K; under nitrogen at 100 KPa to be 0.81 W/m-deg K and 0.72 W/m-deg K for argon at 100 KPa. The apparent thermal conductivity with air in the porous media of 0.85 W/m-deg K compares favorably with that of Duncan et al. (1989) for nitrogen gas in the media.

The saturated porous media results follow the identical procedure as the dry media except that the siphon tube and additional insulation was used while conducting the experiments. One additional fact must be considered while analyzing the data. The properties of water are referenced to 10 C in the nondimensional property polynomials (Eqs. (C.1) and (C.2)). To achieve an accurate representation of the velocity field, the correct plate temperatures (referenced to 10 C) must be used. In other words, at a cold plate temperature of 0 C (32 F) and a hot plate temperature of 20 C (68 F) the nondimensional plate temperatures are 0.0 and 1.0 for the cold and hot plates respectively. In this case $q/\lambda\Delta T$ = 1.035. For these experiments, the cold plate and hot plate are not necessarily 0 C and 20 C respectively. This is not a serious obstacle, however. For example, plate temperatures of 5 C (39 F) and 15 C (59 F) are equivalent to the nondimensional temperatures are 0.25 and 0.75 for the respective plates. The numerical computation yields $q/\lambda\Delta T = 0.5175 = 1.035\cdot(.75 - .25)$. The correct temperature relationships must be maintained for the properties of water

$$q/\lambda\Delta T = 1.035\cdot(\Theta_1 - \Theta_2) \tag{6.18}$$

Repeating the calculations for saturated porous media data in Table 6.3 yields

λ = 2.86 BTU/hr–ft–deg F or 4.95 W/m–deg K for saturated porous media test of 11 April 1990.

λ = 2.81 BTU/hr–ft–deg F or 4.86 W/m–deg K for saturated porous media test of 24 April 1990.

λ = 2.85 BTU/hr–ft–deg F or 4.93 W/m–deg K for saturated porous media test of 25 April 1990.

λ = 3.73 BTU/hr–ft–deg F or 6.45 W/m–deg K of 75% saturated porous media test of 25 April 1990.

Hart and Couvillion (1986) have displayed measured soil thermal conductivity for granular soils with densities between 1600–1900 Kg/m^3 to be within the following ranges: for dry soil, 0.39–0.81 W/m–deg K; and for saturated soil, 3.46–7.0 W/m–deg K. The glass beads in the test cell have a density of 1850 Kg/m^3 with the thermal conductivities 0.85 and 4.94 W/m–deg K and are within the range given by Hart and Couvillion (1986).

The behavior of the 75% saturated soil is surprising in that λ is larger, and needs further investigation. It is presumed that the effect is created by the tremendous difference between the enthalpy of liquid and vapor water similar to the principle of the heat pipe.

6.7 Photographic Streaklines and the Velocity Field

The purpose of the velocity field investigation is to verify the computed values of temperature and velocity by the SLAB code and the appropriateness of using the measured apparent thermal conductivity. In conjunction with the calorimetric experiments described previously, flow visualization was desired. This was accomplished by injecting a small quantity of bromothymol blue dye into the bead pack and photographing the position of the dye as it circulated with the fluid. That the fluid circulated can be seen from the sequence of representative photographs shown in Fig. 6.2. The initial position of the dye is shown in Photograph 6.1. The nondimensional temperature for the warm plate was 0.920 and for the cold plate was 0.263. Photograph 6.2 was taken after 1.20 hours had elapsed. Photograph 6.3 was taken after 2.42 hours had

elapsed and also shows the injection of a second dye tracer. Photograph 6.4 is taken after a total elapsed time of 9.25 hours. The leading edge of the initial dye trace has been displaced to the upper corner of the cell while the leading edge of the second dye tracer has overtaken and merged with the trailing edge of the initial injection.

The visual observations of the dye trace displacement qualitatively agree with the expected results. It is presumed that the flow field is uniquely determined for a given set of physical parameters, and that if the physical parameters are known, then quantitative agreement between the predicted and observed displacements may be achieved.

The nondimensional velocity field has been computed and is a function of position. By following the displacement of a particle of dye, the velocity may be computed as

$$v = \frac{ds}{dt} \tag{6.19}$$

where $s(x,y)$ is the displacement of a particle of flowing fluid measured along its path, $s(x,y)$. Conversely, the transit time between two points $s(x_1,y_1)$ and $s(x_2,y_2)$ is specified in terms of a known velocity field as

$$\Delta t = \int_{s(x_1,y_1)}^{s(x_2,y_2)} \left[1/|v(x,y)| \right] ds \tag{6.20}$$

For a velocity field that is known at discrete points, $P(i,j)$, with magnitudes, $v(i,j)$, and direction angles, $\alpha(i,j)$, with the horizontal axis, a first order approximation for the transit time along a small incremental path length, Δs, yields

$$\Delta t = \min\{\Delta y/|v(i,j)\sin(\alpha(i,j)|,\ \Delta x/|v(i,j)\cos(\alpha(i,j)|\} \tag{6.21}$$

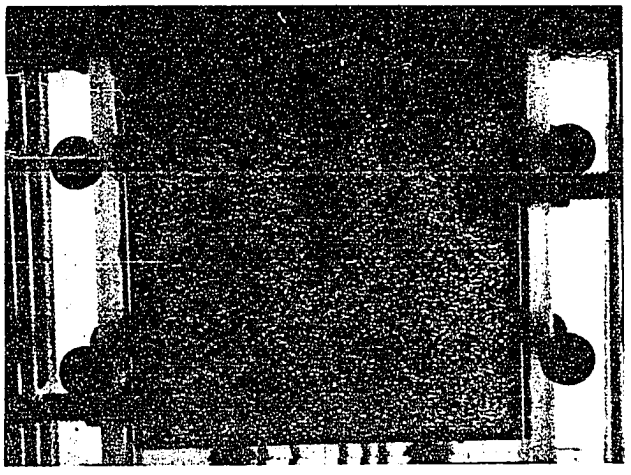

Photograph 6.1 Initial dye injection.

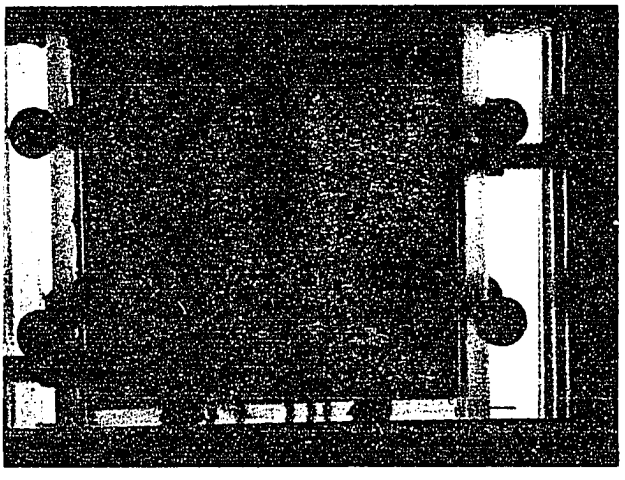

Photograph 6.2 Buoyancy induced dye motion.
Elapsed time: 1.2 hours.

Fig. 6.2.1 Sequential photographs of dye injected into 1 mm glass bead porous medium heated and cooled from the top.

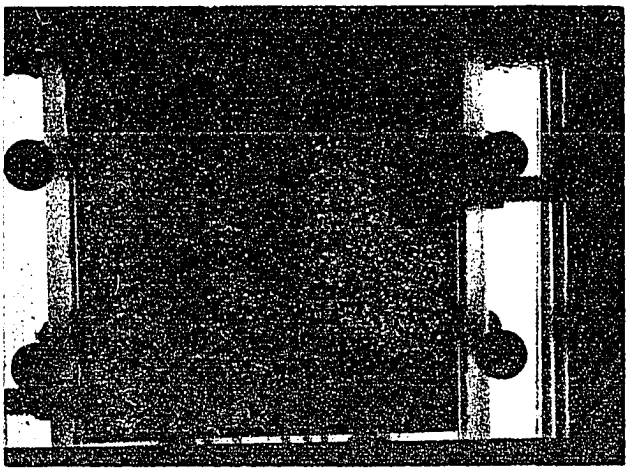

Photograph 6.3 Buoyancy induced dye motion, second injection.
Elapsed time: 2.42 hours.

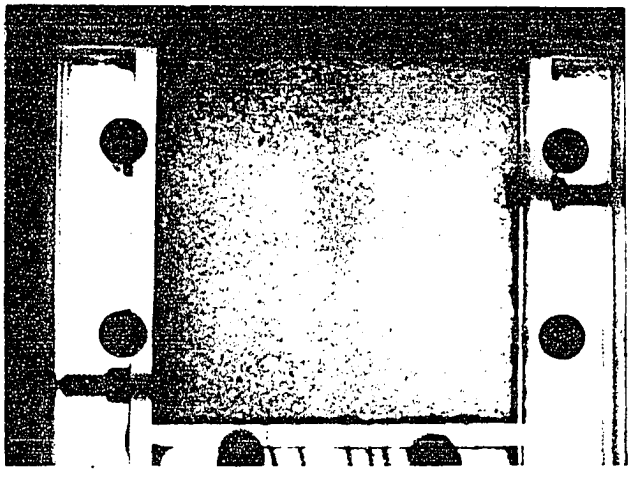

Photograph 6.4 Buoyancy induced dye motion.
Elapsed time: 9.25 hours.

Fig. 6.2.2 Sequential photographs of dye injected into 1 mm glass bead porous medium heated and cooled from the top.

The position of a particle located at $P_1(i,j)$ with the above velocity will move to a new location $P_2(i+\delta_x, j+\delta_y)$ in time Δt. The nearest neighboring point to P_2 is chosen as the starting point to compute the next increment of time. Thus the position of the particle may be calculated as a function of time.

In principle, the observed positions of the dye particle with time should match the computed positions with time by taking smaller and smaller increments of distance. There are practical considerations, however. A dye particle is impossible to see in a porous medium so the amount of dye used must be large enough to be visible. This presents a problem as to which particle in the dye streak should be selected to monitor because no particle may be identified specifically. Furthermore, the finite quantity of dye is subject to dispersion and diffusion due to concentration gradients. To minimize these effects, the apparent centroid of the dye tracer was found graphically and used as the reference point for the following analysis.

Although the average porosity of the bed was expected to determine the transit time of the dye, closer examination inveighed against this hypothesis because the predicted transit times were found to be much too long.

For porous media in a container, the porosity and permeability of the bed varies with the distance from the wall. For instance, Khan and Beasley (1989) give porosity of a bead pack as function of ratio of the bed thickness to the particle diameter as

$$n = .4272 - 4.515E\text{-}3(d_{bed}/d) + 7.881E\text{-}5(d_{bed}/d)^2 \qquad (6.22)$$

$1 < (d_{bed}/d) < 28$, and

$n=.3625$ for $(d_{bed}/d) > 28$

The test cell bed to bead diameter ratio of 12.25 yields a porosity of 0.384. The actual, measured porosity for the bead pack was 0.39 prior to packing with extra beads. Additional beads forced into the bed reduced the average porosity to 0.36.

The walls, however must be treated as a different problem. Khan and Beasley (1989) note that flow of liquid in randomly packed beds of uniform spheres is highly preferential near the container wall. This is true because a perfect bed of body–centered or face–centered spheres tangent to a wall produce an average porosity of 0.47. Randomly located voids will increase this value.

The photographic record made of these experiments actually captured the fluid activity near the wall of the test cell. The camera was focused at the interface of the plexiglas wall and the outermost layer or beads. In spite of the relative "thinness" of the cross section, the interior dye position is concealed from view. The dye trace photographs therefore are of a high porosity area.

Another key factor in the motion of the fluid in the porous media is the permeability of the media. The Ergun equation for the permeability of spherical beds is given by Renken and Poulikakos (1989) as

$$k = d^2n^3/(175(1-n)^2) \tag{6.23}$$

This is strongly dependent on porosity and will be assumed valid in the wall region for this analysis.

Equation (4.41) defines $\Re$ as

$$\Re = k(\rho_r c)_f gL/\lambda_{eq}\nu_r$$

The experimental values of all of the parameters composing $\Re$ are constant except for the permeability of the media. The measured thermal conductivity is known from the previous section is taken to be 4.94

W/m–deg K from the last section. The permeability, k, therefore, is the only value not well known in this problem. The goal will be to find a value of porosity such that the photographic data may be matched to the computed velocity field.

A correlation between the mathematical problem in nondimensional form and the real problem is needed. This is done as follows:

In dimensional form the transit time Δt through some small path is

$$\Delta t \cong \frac{\Delta x}{V}, \text{ or}$$

$$\Delta t \cong \frac{\Delta x/L \cdot L}{V/V_0 \cdot V_0} \cong \frac{\Delta x^*}{v^*} \cdot \tau, \text{ or}$$

$$\Delta t \cong \Delta\tau^* \cdot \tau$$

The quantity $\Delta\tau^*$ is the nondimensional time interval computed from the mathematical solution to the porous media problem and depends on $\mathfrak{R}$. The characteristic time, τ, depends on model and fluid properties. The quantity V_0 is a volume averaged reference velocity. The pore velocity is that which is physically observed and is related by Eq. (4.15).

$$V_{0,\text{pore}} = V_0/n$$

$\mathfrak{R}$ is defined when selected values of porosity are chosen: i.e.,

$\mathfrak{R}(.36) = 412$; $\mathfrak{R}(.47) = 1337$; $\mathfrak{R}(.54) = 2569$; and $\mathfrak{R}(.56) = 3211$.

In the process of searching for a suitable value of $\mathfrak{R}$, the following relationship was discovered to within the accuracy of the numerical approximations:

$$\mathfrak{R}_1\Delta\tau_1^* = \mathfrak{R}_2\Delta\tau_2^* \tag{6.24}$$

where $\Delta\tau^*$ is the nondimensional time required to cross a specified distance in the nondimensional domain.

Figure 6.3 illustrates the streamline pattern produced by the SLAB code for $\mathfrak{R} = 3211$. Superposed on the streamline pattern is the outline

of the successive dye positions, and these are numbered sequentially. These dye positions are extracted from the same series of photographs depicted in Fig. 6.2. The streamlines appear to conform to the position of the dye.

The values in Table 6.4, Dye position versus computed and measured time, correspond to the sequence of positions shown in Fig. 6.3. The coordinates listed are for the centroid of the dye trace. The agreement is within an average of seven minutes of the predicted and observed times. Seven minutes uncertainty in time is equivalent to 3 mm uncertainty in displacement. The porosity for these data, 0.56, was chosen in order to give the best fit.

As a consequence of Eq. (6.24), the transit time for a fluid in the media is independent of interstitial fluid properties except viscosity and depends only on the media permeability, porosity and temperature difference driving the fluid. This can be shown by supposing two identical configurations in every respect except that the media thermal conductivities are different.

$$\mathfrak{R}_1 = C/\lambda_1, \text{ and}$$

$$\mathfrak{R}_2 = C/\lambda_2$$

The transit time for the first conductivity is

$$\Delta t_1 = \Delta t_1^* \cdot \tau_1$$

$$\Delta t_1^* = \Delta t_2^* \left(\mathfrak{R}_2/\mathfrak{R}_1 \right) = \Delta t_2^* \cdot (\lambda_1/\lambda_2)$$

Since $\tau = nL/V_0$, and $V_0 = \lambda_1/\rho cL$, then

$$\Delta t_1 = \Delta t_2^* \cdot (\lambda_1/\lambda_2) \cdot \left[\frac{nL}{\frac{\lambda_1}{\rho cL}} \right]$$

$$\Delta t_1 = \Delta t_2^* \cdot \tau_2 = \Delta t_2$$

Table 6.3 Temperature–discharge data for porous media

Condition	Discharge, gm/hr	T_2, °F	T_1, °F	T_{room}, °F	T_{tank}, °F	Date
Dry	44.25	40.02	67.69	71.72	70.22	28 Nov 89
Saturated	46.85	40.19	70.00	73.27	71.95	11 Apr 90
Saturated	52.76	39.17	73.00	77.48	73.67	24 Apr 90
Saturated	54.37	38.93	74.00	77.76	75.00	25 Apr 90
75% Sat.	55.67	38.79	73.00	76.00	73.36	25 Apr 90

Table 6.4 Dye position versus computed and measured times for porosity of 0.56

Position Number	Coordinate (x*,y*)	Computed time, min	Measured time, min
1	(.90,.67)	0.0	0.0
2	(.91,.58)	12.7	18.0
3	(.90,.44)	42.0	42.0
4	(.88,.33)	70.0	72.0
5	(.74,.14)	150.0	135.0
6	(.54,.10)	207.0	195.0

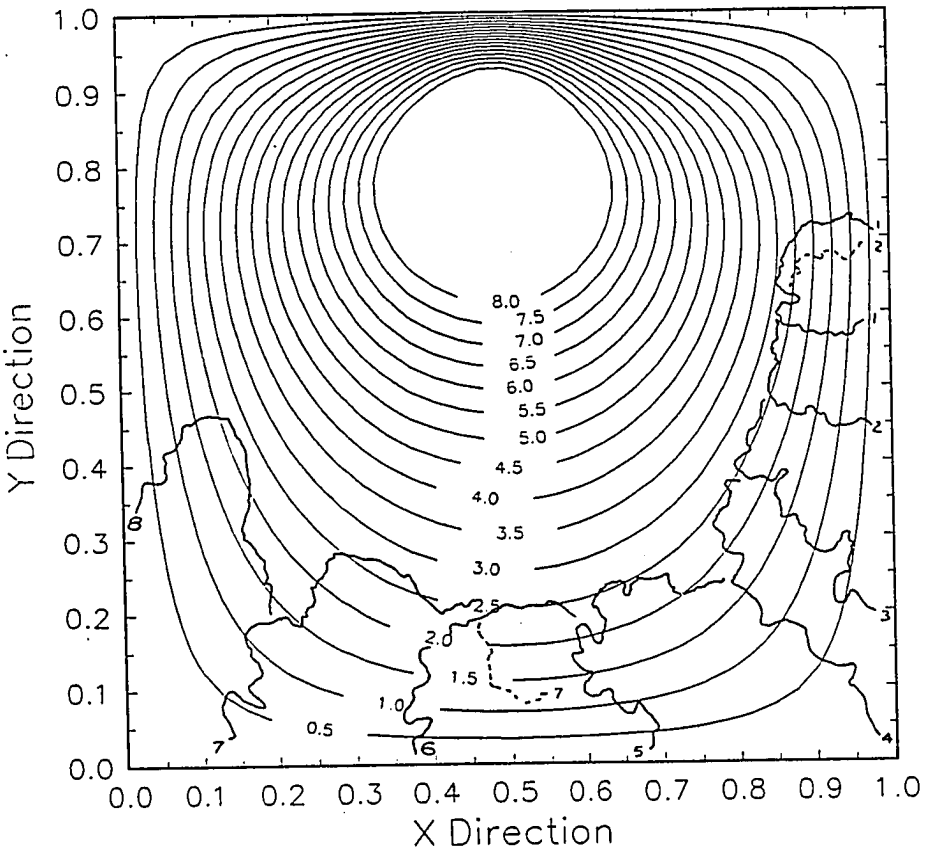

Position	Elapsed Time (hr)
1	0.00
2	0.30
3	0.70
4	1.20
5	2.25
6	3.25
7	4.25
8	5.25

Fig. 6.3 Superposition of streamline pattern and dye positions shown in Fig. 6.2.

This process could be repeated for density, and specific heat as well with the same result. The presumption that the apparent thermal conductivity may be deduced by observing the flow field is incorrect.

6.8 Closure

By performing this experiment to validate the numerical code, a good deal has been learned. The SLAB code does predict the correct value of total heat transfer for a two-dimensional slab if the media thermal conductivity is known. For Porous media, the apparent thermal conductivity of the medium must be known. Also, the streamline plot for the test cell matches the observed pattern. Moreover, if the correct porosity and permeability are available, then the transit time of a fluid percolating through the media by buoyant force may be determined. In the steady state, the transit time is independent of the thermal conductivity, density and specific heat of the interstitial fluid.

Chapter 7

THE EFFECTS OF EVAPORATION ON STEADY SLAB HEAT FLUX

7.1 Introduction

In the preceding chapters, the interaction of water on slab heat transfer has been discussed and developed for the steady problem with an impervious surface. To extend the applicability of slab heat transfer to more situations, the impervious surface should be relaxed to allow evaporation of water. The goal of this analysis will be to find the steady contribution of evaporation of water at the earth surface for saturated soil.

7.2 Surface Conditions in the Steady Problem

In Chap. 3, the groundwork was developed for the analysis of the problem in terms of a steady problem and a periodic problem. The periodic problem does not contribute to the average heat transfer from the slab when viewed from the perspective of long time intervals. Therefore, by following the previous line or reasoning, one hopes to find the essential behavior of the steady problem. Since the media remains saturated, the governing field equations for the problem remain the same. The boundary equations must be modified.

The general formulation of the First Law of Thermodynamics for a control volume may be written as

$$Q - W = \frac{\partial}{\partial t}\int_{\text{Volume}} e\rho dV + \oint_{\text{Surface}} (e + P/\rho)\rho \mathbf{V}\cdot d\mathbf{A} \tag{7.1}$$

Applying this to the air–earth boundary of the domain for the i^{th} microscopic REV (control volume for porous media), terms may be eliminated that are not applicable. Thus,

$$Q_i = \frac{\partial U}{\partial t}i + (\dot{m}\, h_{fg})_i \tag{7.2}$$

where Q is the total heat transfer to the element, U is the average internal energy, $\dot{m}$ is the mass crossing the boundary (neglecting storage), and h_{fg} is the heat of vaporization of water at the surface temperature. All flux terms parallel to the surface will be neglected.

Examining the terms that compose Q in this application, there are: heat conduction into the element; heat convection away from the element; radiation from the surface into the environment; and the incoming radiation from the sun. For an area element ΔA,

$$Q_{cond} = -\lambda\frac{\partial T}{\partial Y}\cdot\Delta A \tag{7.3}$$

$$Q_{conv} = -h_{conv}\Delta A\cdot(T - T_2) \tag{7.4}$$

$$Q_{rad} = -Q(T,T_2) + Q_{solar} \tag{7.5}$$

Linearizing the radiation term and recognizing that $Q_{solar} = Q(t)$, a function of time, the radiation term becomes

$$Q_{rad} = -h_{rad}\Delta A\cdot(T - T_2) + Q(t) \tag{7.6}$$

Combining these terms and defining $h = h_{conv} + h_{rad}$,

$$Q = -\lambda\frac{\partial T}{\partial Y}\cdot\Delta A - h\cdot\Delta A\cdot(T - T_2) + Q(t) \tag{7.7}$$

Following the prescription in Chap. 3, temperature can be expressed as the steady contribution and the periodic contribution of all the terms.

$$T = T_s + T_p \tag{7.8}$$

Using this relationship, the energy Eq. (7.2) may be written for the i^{th}

REV element as the periodic solution and the steady solution per unit of surface area as

$$q(t) - k\frac{\partial T}{\partial Y}p - hT_p = [(\dot{m}/\Delta A)h_{fg}]_p + \rho c\Delta Y\frac{\partial T}{\partial t}p \quad (7.9)$$

$$- k\frac{\partial T}{\partial Y}s - h(T_s - T_2) = [(\dot{m}/\Delta A)h_{fg}]_s \quad (7.10)$$

where q(t) is the incident solar radiation per unit area at the earth surface. Normally, the time derivative of the surface node temperatures are neglected in Eq. (7.9). Since the behavior of the steady problem is of interest here, the periodic boundary will not be considered further. The steady Eq. (7.10) may be made nondimensional using the procedure in Chap. 5, resulting in

$$\frac{\partial \Theta}{\partial y}s + Bi\Theta_s = -L[(\dot{m}/\Delta A)h_{fg}]_s/(\lambda\Delta T) \quad (7.11)$$

The mass flow from the surface is determined by the ability of the air over the earth to absorb moisture which is directly related to the humidity ratio of the air. By using the concept of the mass transfer coefficient (Threlkeld, 1970), the moisture transport for forced convection is given by

$$\dot{m}/\Delta A = h_D(\omega_s - \omega_{ambient}), \text{ and} \quad (7.12)$$

$$h/(h_D c_{p,air}) = .854 \quad (7.13)$$

where h is the convection film coefficient and h_D is the mass transfer coefficient. Combining these equations and noting that $\omega_{ambient} = \omega_2$, and dropping the subscript s for steady state,

$$\frac{\partial \Theta}{\partial y} + Bi\Theta = -1.171(Bi/Ste)(\omega - \omega_2) \quad (7.14)$$

and ω is the humidity ratio of saturated air at the surface of the earth, ω_2 is the average humidity ratio for the particular locality and will be assumed to be equivalent to a relative humidity of 50 percent at 2 C for

comparison purposes. The Stefan number, Ste, is defined as (Zhang and Nguyen, 1990)

$$Ste = \frac{c_{p,air}\Delta T}{h_{fg}} \tag{7.15}$$

7.3 The Humidity Ratio as a Function of Temperature

The humidity ratio is a function of the wet bulb and dry bulb temperatures at any given time. However, by assumption, the earth surface is assumed to be in a saturated condition at some infinitesimal distance away from the soil. The humidity ratio varies continuously through the boundary layer until humidity ratio ω_2 is reached. On the saturation curve of the psychrometric chart, the humidity ratio is a function of the dry bulb temperature only. Using this fact, the humidity ratio can be approximated as a polynomial function of temperature. Using a least squares fit of the psychrometric chart the following expression results

$$\omega(\Theta)(x\ 10^3) = 3.85 + 4.307\Theta + 7.6902\Theta^2 \tag{7.16}$$

$0\ C \leq T \leq 21\ C$, and $\omega(X\ 10^3)$ accurate to $\pm$ 1%

The ambient humidity ratio should be selected to be the mean coincident relative humidity, Ω_2, so

$$\omega_2 = \Omega_2 \cdot \omega(\Theta_2) \tag{7.17}$$

7.4 Mass Flux at the Boundary

Evaporation will remove mass from the domain. For a steady solution, the amount of water evaporated from the domain must be replaced by an equal mass of water entering the domain. For the purposes of comparison with previous cases, the influx of water will be uniformly distributed along the boundary excluding the symmetry plane beneath the slab.

The mass of water evaporated at each surface element is given by Eq. (7.12). Setting this equation equal to the flow rate of water entering each element,

$$\rho \mathbf{V}_i \cdot \hat{\mathbf{n}} = h_D(\omega - \omega_2) \tag{7.18}$$

After normalizing by the unit velocity, V_0, and using the relationship in Eq. (7.13),

$$\mathbf{v}_i \cdot \hat{\mathbf{n}} = 1.171 \cdot Bi \cdot (c/c_{p_{air}}) \cdot (\omega - \omega_2) \tag{7.19}$$

The influx of water at each element is uniformly distributed. Then

$$\mathbf{v}_{\text{on } \Gamma} \cdot \hat{\mathbf{n}} = \frac{1}{D} \int_{\text{evaporation}} \mathbf{v}_i \cdot \hat{\mathbf{n}} \, dx$$

where D is the net linear distance along the boundary, Γ, through which water is entering.

7.5 Slab Heat Loss With Evaporation

Consider a slab heated by convection at 20 C with a Biot number of 30 and a cooling factor of one (as defined in Chap. 6). Utilizing the modeling in the preceding sections, a comparison of heat loss for a permeable surface and an impermeable surface is desired. For the pervious surface, the ambient temperature of 2 C and a relative humidity of 50 percent will be taken as the atmospheric conditions. The impermeable surface atmospheric conditions will be identical except that mass flux terms will be dropped from the computation.

The heat loss for the impermeable surface under the stated conditions was found to be

$$q/\lambda\Delta T = 1.057 \quad \text{(impermeable)}$$

The evaporation process increased the total slab heat loss by 0.095 to

$$q/\lambda\Delta T = 1.158 \quad \text{(permeable)}$$

Figure 7.1 is an isothermal map of the domain temperature field for the permeable surface and is very similar in shape to that of Fig. 4.4 for an impermeable surface.

Figure 7.2 shows the streamline locations for the permeable surface case with liquid water being admitted from the right hand side of the domain. The streamlines become very densely packed near the edge of the slab on the upper surface (0.5, 1.0). The irregular lines near the surface are due to the temperature varying properties of water especially near the density maximum of 4 C.

7.6 Closure

The evaporation of water from the saturated earth surface was found to augment the transfer of heat from the slab by nearly ten percent for the case under study. The evaporation model also predicts a pronounced area of atmospheric moisture removal at the outermost edge of the building slab. With the completion of these outlined calculations, this chapter will be concluded. Additional remarks are reserved for the final chapter, Chap. 8.

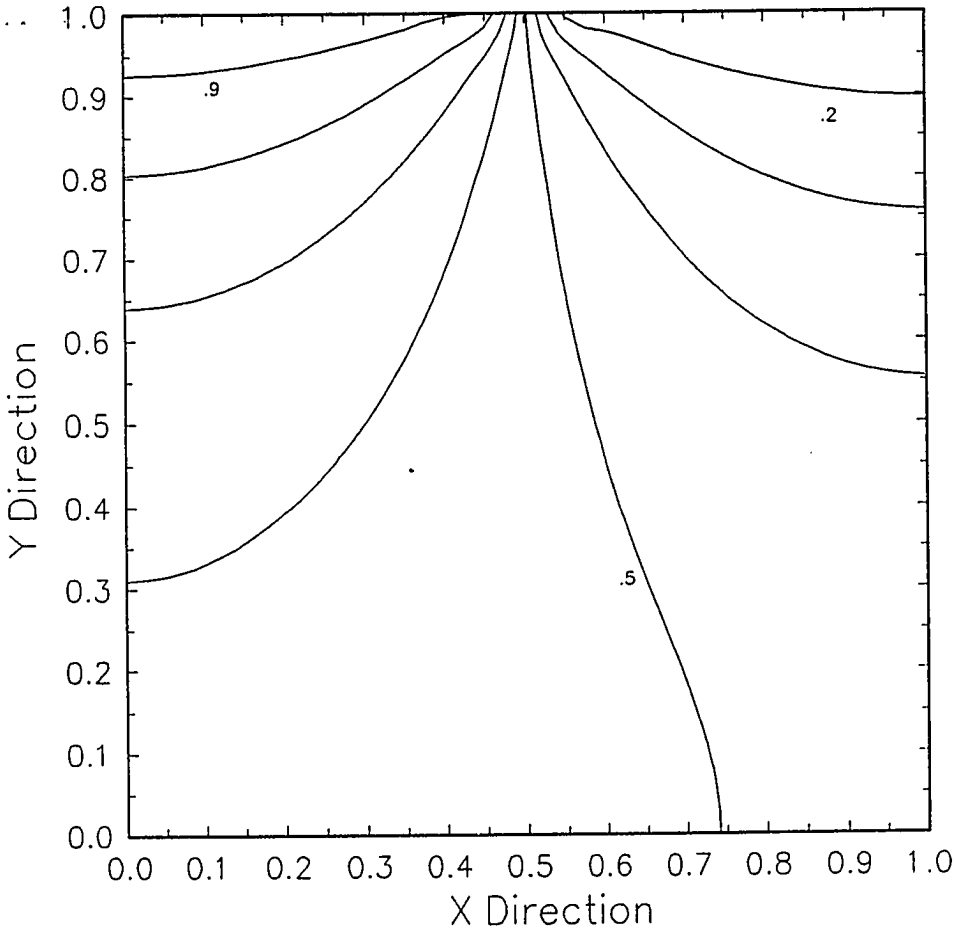

Fig. 7.1 Isothermal map of slab on saturated soil exposed to surface evaporation for Bi = 30, r = 1 and Θ_2 = 0.1.

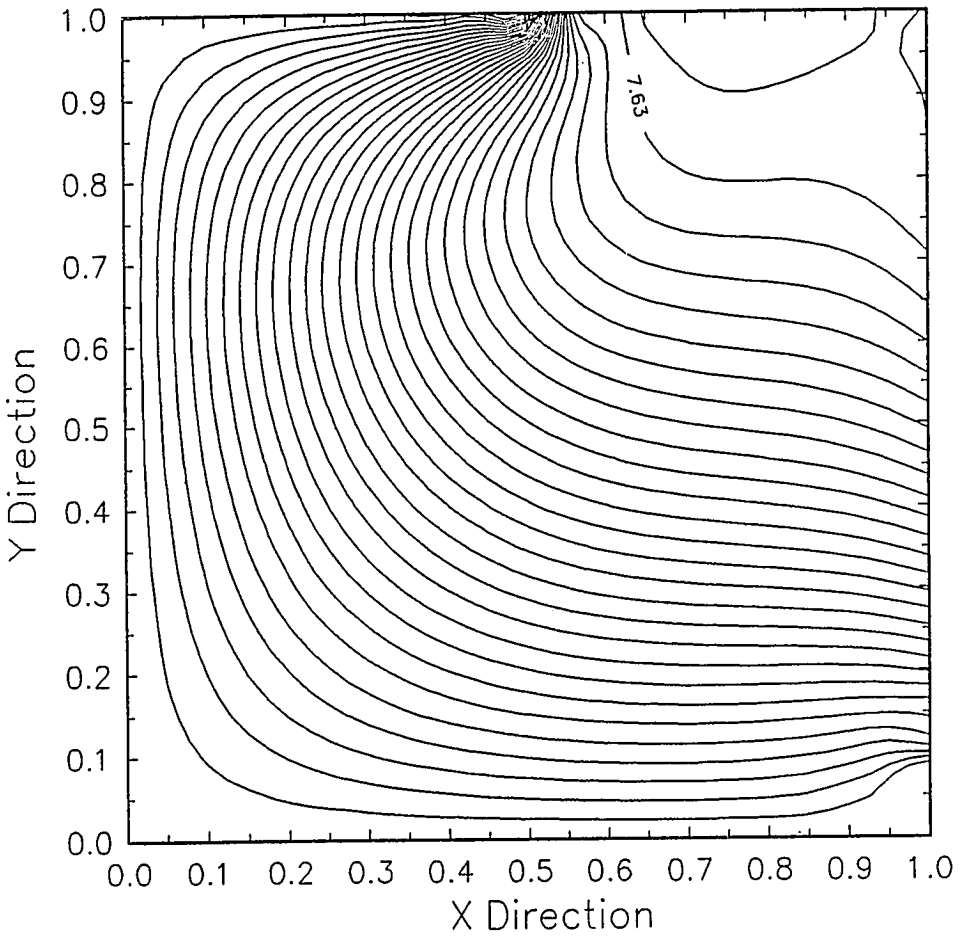

Fig. 7.2 Streamlines near slab for thermally induced flow in saturated soil exposed to surface evaporation for Bi = 30, r = 1 and Θ_2 = 0.1.

Chapter 8

CONCLUSIONS AND RECOMMENDATIONS

8.1 Conclusions

The problem under investigation was to predict the heat loss by a convectively heated building slab to the ambient while including the effects of thermally induced flow in saturated soil. Field and boundary equations describing the flow of energy and fluid in porous media were formulated. The solution of the governing equations subject to the slab boundary conditions was found using an implicit finite difference scheme. The resulting numerical solutions were compared to solutions produced by FIDAP, a finite element fluid mechanics and heat transfer program. Good agreement was found, indicating that the numerical procedure could be extended to more complex thermal and fluid boundaries. For temperature ranges of interest in the building slab earth-coupling problem, the momentum equation as embodied by Darcy's Law (without modification) produced solutions that agreed with experimental observations.

During the progress of the investigation of earth-coupled heat transfer phenomena, several general observations were made concerning the process. These observations are valid for steady-state and are listed below in no particular order of importance. All are logically related; therefore, a logical ordering is appropriate.

1. The far field boundary for an object exchanging heat by earth contact may be treated as adiabatic.

2. It is possible to characterize heat loss from a body in contact with the earth as one-dimensional.

3. The effects of convection in saturated soil on the transfer of heat from the slab ($q/\lambda\Delta T$) was not important. The energy transferred from the slab was dependent on the apparent thermal conductivity of the soil (λ) and this is highly dependent on moisture content.

4. The time required for a buoyant fluid to circulate in a closed region depends on the permeability of the media, the viscosity of fluid, and the temperature difference driving the flow. The transit time does not depend on the apparent thermal conductivity of the media.

5. Two-dimensional slab heat transfer with the environment may be characterized by a shape factor method developed here to relate the geometrical boundaries and surface convective heating conditions to the total heat loss from the slab.

6. Three-dimensional heat loss may be characterized as the superposition of two separate, two-dimensional heat transfer problems which may be solved by using the shape factor method.

7. Earth surface evaporation increases slab heat loss. For the nominal case analyzed in Chap. 7, a ten percent increase in total heat loss was noted with the inclusion of evaporation.

8.2 Recommendations

The formulation of the problem and solution of two-dimensional and three-dimensional problems by a shape factor method has been developed.

There are, however, numerous, related areas that need to be addressed such as:

The ability of water vapor to augment the transport of heat through the soil by diffusion and phase change,

Insulation selection and placement to optimally retard the flow of heat from a slab,

Extension of the shape factor method to include basement structural heat loss and optimal insulation placement,

Effects of the periodic component of the driving weather function on heat loss by earth coupling, and particularly with respect to the role of water and water vapor in the process,

Field validation of the computational predictions.

Christian (1989) lists twenty-one broadly defined building foundations research areas in priority order of importance. The second and third most important items listed are:

> 2. *Simplified Tools*—Simplified tools (e.g., charts, nomographs, or programs for personal computer) that are directly useful to builders and designers need to be developed. These tools should clearly show the energy savings and the economic impact of design decisions. To the greatest extent possible, they should also show the impact of different designs on other performance factors. . . .
>
> 3. *Benchmark Research Models.*—The possibility that a single mathematical model can be general enough, yet not too unwieldy, to handle all energy-related issues for all typical foundations needs to be explored. If such a model were available and were generally acceptable in the buildings community, validation research could be focused and, eventually, this "benchmark" model could provide the simulation data for development of simplified tools.

The SLAB code and the shape factor methods have been produced to answer these priority research questions to the extent discussed in this

dissertation. By pursuing this problem, insight has been gained that may eventually be used to conserve the limited natural resources being consumed by the nation's buildings.

REFERENCES

Alvarez, W., and Asaro, F., 1990, "An Extraterrestrial Impact," Scientific American, Vol. 263, No. 4, October, pp. 78–84.

Anderson, D.A., Tannehill, J.C., and Pletcher, R.H., 1984, Computational Fluid Mechanics and Heat Transfer, Hemisphere Publishing Corporation, Washington, pp. 40–45.

ASHRAE Handbook of Fundamentals, 1989, American Society of Heating Refrigerating and Air Conditioning Engineers, Inc., Atlanta GA, pp. 25.1–25.10.

Badash, L., 1989, "The Age-of-the-Earth Debate, "Scientific American, Vol. 261, No 2, August, p. 96.

Bahnfleth, W.P., and Pedersen, C.O., 1990, "A Three-Dimensional Numerical Study of Slab-On-Grade Heat Transfer,"ASHRAE Transactions, Vol. 96, Pt. 2.

Bear, J., 1972, Dynamics of Fluids in Porous Media, American Elsevier Pub. Co, New York, reprinted by Dover Publications, New York, 1988.

Bejan, A., 1987, "Convective Heat Transfer in Porous Media," Handbook of Single Phase Heat Transfer, S Kakac, R.K. Shah, and W. Aung, eds., John Wiley and Sons, New York, pp. 16.8–16.10.

Bénard, H., 1900, "Les Tourbillons Cellulaires Dans Une Nappe Liquide," Revue Génenerale de Science Pure et Appliqué, Vol. 11, pp. 1261–71 and 1309–28.

Bevington, R., and Rosenfeld, A.H., 1990, "Energy for Buildings and Homes," Scientific American, Vol. 263, No. 3, Sept, pp. 77–84.

Boileau, G.G.. and Latta, J.K., 1968, "Calculation of Basement Heat Losses," Technical Paper No 292, Division of Building Research, NRC, Ottawa, Canada.

Bligh, T.P., Shipp, P., and Meixel,G., 1978, "Energy Comparisons and Where to Insulate Earth Sheltered Buildings and Basements," Earth Covered Settlements, U.S. Dept. of Energy Conference, Fort Worth, TX, May.

Carslaw, H.S., and Jaeger, J.C., 1959, Conduction of Heat in Solids, Oxford University Press, London, p. 83.

Cheng, P., 1978, "Heat Transfer in Geothermal Systems," Advances in Heat Transfer, Vol. 14, Irvine, T.F., and Hartnett, J.P., eds., Academic Press, New York, p. 3.

Cheng, P., and Chang, I.D., 1976, International Journal of Heat and Mass Transfer, Vol. 19, p. 1267.

Christian,J.E., 1989, "The Most Needed Building Foundations Research Products," ASTM STP 1030, American Society for Testing and Materials, Philadelphia, PA, p. 657.

Christian, J.E., Wasserman, D.M., Graves, R.S., McElroy, D.L., Yarbrough, D.W., Childs, K.W., and Childs, P.W., 1990, "ORNL Slab-on-Grade Edge Insulation Experiment: Design, Construction, and Research Plan," Oak Ridge National Laboratory Report ORNL/CON-280, Oak Ridge National Laboratory, Oak Ridge TN, March, p. 3.

Claridge, D.E., 1988, "Design Methods for Earth-Contact Heat Transfer," Advances in Solar Energy, Vol. 4, K.W. Boer, Ed., American Solar Energy Society, Inc., Boulder, CO and Plenum Press, New York, pp. 311-337.

Cleveland, J.P., and Akridge, J.M., 1990, "Slab-On-Grade Thermal Loss in Hot Climates," ASHRAE Transactions, Vol. 96, Pt. 1.

Combarnous, M., and Bories, S., 1975, "Hydrothermal Convection in Saturated Porous Media," Advances in Hydroscience, Vol. 10, pp.231-307.

Couvillion, R.J., and Hartley, J.G., 1986, "Low Intensity Heat and Moisture Transfer in Moist Soils - Current Models," ASHRAE Transactions, Vol. 92, pt 1.

Courtillot, V. E., 1990, "A Volcanic Eruption," Scientific American, Vol. 263, No 4, October, p.92.

Darcy, Henry, 1856, "Les Fountaines Publiques de La Ville De Dijon," Dalmont, Paris, p. 309.

Delasante, A.E., Stokes, A.N., and Walsh, P.J., 1983, "Application of Fourier Transform to Periodic Heat Flow into the Ground Under a Building," International Journal of Heat and Mass Transfer, Vol. 26, pp. 121-132.

De Vries, D.A., 1987, "The Theory of Heat and Moisture Transport in Porous Media Revisited," International Journal of Heat and Mass Transfer, Vol. 30, No. 7, pp. 1343-1350.

Drazin,P.G., and Reid, W.H., 1981, Hydrodynamic Stability, Cambridge University Press, Cambridge, p. 32.

Dubin, F.S., and Long, C.G., 1978, Energy Conservation Standards For Building Design, Construction and Operation, McGraw Hill Book Co., New York, p 152.

Duncan, A.B., Peterson, G.P., and Fletcher, L.S., 1989, "Effective Thermal Conductivity within Packed Beds of Spherical Particles," ASME Journal of Heat Transfer, Vol. 111, No. 4, p. 834.

Duyer, A., and Bober, W., 1984, "The Bottom Heat Loss of a Solar Pond in the Presence of Moving Ground Water," ASME Journal of Solar Energy Engineering, Vol. 106, No. 3, pp. 335-340.

Eckert, E.R.G., and Pfender,E., 1978, "Heat and Mass Transfer in Porous Media with Phase Change," Proc. 6th Int'l Heat Transfer Conference.

Elder, J.W., 1966, New Zealand Department of Science and Industrial Research, Bulletin 169.

Ene, H. I., and Polisevski, D., 1987, Thermal Flow in Porous Media, D. Reidel Publishing Company, Dordrecht, Holland.

FIDAP Revision 4.5, 1989, Fluid Dynamics International, Inc., 1600 Orrington Ave., Suite 400, Evanston, Illinois 60201, April.

File, J., and Considine, D.M., 1977, "Energy," Energy Technology Handbook, D.M. Considine, ed., McGraw Hill Book Co, New York, p. xxvi.

Fulks, W.B., Guenther, R.B., and Roetman, E.L., 1971, "Equations of Motion and Continuity for Fluid Flow in a Porous Medium," Acta Mechanica XII Vol. 11-2, Springer Verlag, pp. 121-129.

Gebhart, B., Jalura, Y.S, Mahajan, R.L., and Sammakia, B., 1988, Buoyancy Induced Flows and Transport, Hemisphere Publishing Corp., Washington, pp. 826-827.

Hart, D.P., and Couvillion, R., 1986, Earth-Coupled Heat Transfer, National Water Well Association, Dublin, OH, pp. 97-107.

Himasekhar, K. and Bau, H.H., 1988, "Thermal Convection around a Heat Source Embedded in a Box Containing a Saturated Porous Medium," ASME Journal of Heat Transfer, Vol. 110, No. 3, p. 650.

Hubbert, M.K., 1940, "The Theory of Ground Water Motion," The Journal of Geology, Vol. XLVIII No. 8, Part 1, pp. 785-944.

Khan, J.A., and Beasley, D.E., 1989, "Two Dimensional Effects of the Response of Packed Bed Regenerators," ASME Journal of Heat Transfer, Vol. 112, No. 2, p. 329.

Kladias, N. and Prasad, V., 1989, "Convective Instabilities in Horizontal Porous Layers Heated Form Below: Effects of Grain Size and Its Properties," Heat Transfer in Convective Flows, ASME HTD-Vol 107, Aug 6-9, pp. 369-379.

Krarti, M., and Claridge, D.E., 1988, "Analytical Calculation Procedure for Underground Heat Losses," ASHRAE Transactions, Vol. 96, Pt. 1.

Krarti, M., Claridge, D., and Kreider, J., 1985, "Interzone Temperature Profile Estimation — Slab-On-Grade Heat Transfer Results," Heat Transfer in Buildings and Structures, P. Bishop, ed., HTD-V, 41, ASME, New York, pp. 11-20.

Krarti, M., Claridge, D.E., and Kreider, J.F., 1990, "ITPE Technique Applications to Time Varying Three-Dimensional Ground-Coupling Problems," ASME Journal of Heat Transfer, Vol. 112, No. 4, pp. 849-856.

Kusuda, T., and Achenbach, T.R., 1963, "Numerical Analysis of the Thermal Environment of Occupied Underground Spaces with Finite Cover Using a Digital Computer," ASHRAE Transactions, 69, pp. 439-462.

Kusuda, T., and Bean, J.W., 1984, "Simplified Methods for Determining Seasonal Heal Loss for Uninsulated Slab-On-Grade Floors," ASHRAE Transactions, Vol. 90, Pt. 1-B, pp. 622-632.

Kusuda, T., Piet, O., and Bean, J.W., 1983, "Annual Variation of Temperature Field and Heat Transfer Under Heated Ground Surfaces (Slab-on-Grade Floor Heat Loss Calculation)," NBS Building Science Series, No. 156, June.

Kwok, L.P., and Chen, C.F., 1987, "Stability of Thermal Convection in a Vertical Porous Layer," ASME Journal of Heat Transfer, Vol. 109, No. 4, pp. 890-892.

Lachenbruch, A.H., 1957, "Three Dimensional Heat Conduction in Perma-Frost Beneath Heated Buildings," U.S. Geological Survey Bulletin 1052-B, U.S. GPO, Washington, D.C.

Lapwood, E.R., 1948, "convection of a Fluid in a Porous Medium," Proceedings of the Cambridge Philosophical Society, 44, pp. 508-521.

Mitalas, G.P., 1982, "Basement Heat Loss Studies at DBR/NRC," DBR Paper No 1045, NRC Canada.

Mitalas, G.P., 1983, Calculation of Basement Heat Loss," ASHRAE Transactions, Vol. 89, Pt. 1B, pp.402-438.

Mitalas, G.P., 1987, "Calculation of Below Grade Heat Loss-Low Rise Residential Building," ASHRAE Transactions, Vol. 93, Part 1, pp. 743-783.

Philip, J.R., and De Vries, D.A., 1975, "Moisture Movement in Porous Media Under Temperature Gradients," Transactions of the American Geophysical Union, Vol. 38, pp. 222-232.

Renken, K.J., and Poulikakos D., 1989, "Experiments on Forced Convection From a Horizontal Heated Plate in a Bed of Glass Spheres," ASME Journal of Heat Transfer, Vol. 111, No. 1, p. 59.

Rust, W.W., and Roberts, A.S., Jr., 1990, "Porous Media Heat Transfer Experiment and Theoretical Model Analysis," Proceedings of the Symposium on Mixed Convection and Environmental Flows, Winter Annual Meeting, ASME HTD-Vol 152, Dallas TX, Nov 25-30, pp. 61-68.

Shen, L.S., Poliakova, J., and Huang, Y.J., 1988, "Calculation of Building Foundation Heat Loss Using Superposition and Numerical Scaling," ASHRAE Transactions, Vol. 94, Pt. 2.

Spiegel M.R., 1964, Complex Variables With an Introduction to Conformal Mapping and Its Applications, McGraw-Hill Book Company, New York, p. 120.

Sun Zu-Shung, Tien Chi, and Yen Yin-Chao, 1970, "Onset of Convection in Porous Medium Containing Liquid With a Density Maximum," International Conference of Heat Transfer, 4th, Versailles, pap N.C. 3-11.

Threlkeld, J.L., 1970, Thermal Environmental Engineering, Prentice-Hall, Inc, Englewood Cliffs, N.J., pp. 196-198.

Witherspoon, P.A., S.P. Neldman, Sorey, M.L., and Lippman, M.J., 1975, Lawrence Berkeley Laboratory Report No. 3263.

Yoshino, H., Matsumoto, S., Hasegawa, F., and Nagamoto, M., 1990, "Effects of Thermal Insulation Located in the Earth Around a Semi-Underground Room: A Two Year Measurement in a Twin Type Test House Without Auxiliary Heating," ASHRAE Transactions, Vol. 96, Pt 2.

Zhang, X., and Nguyen, T.H., 1990, "Development of Convection Flow During the Melting of Ice in Porous Media Heated From Above," Proceedings of the Symposium on Heat Transfer in Porous Media, Winter Annual Meeting, ASME HTD-Vol 156, Dallas Tx, Nov 25-30, pp. 1 - 6.

APPENDIX A

ANALYTICAL DEVELOPMENT OF THE TWO DIMENSIONAL SLAB

A.1 Temperature Field for a Constant Temperature Slab

The slab may be idealized as a plane surface where the actual thickness of the slab is small compared to some characteristic dimension. In the two-dimensional case, the edge of the ideal slab appears as a line segment on the semi-infinite X-Y plane. The slab is heated to some temperature T_1 while the remainder of the X axis is held at temperature T_2. The Temperature field in the semi-infinite plane (designated as Ω) must satisfy the heat equation and also conditions on the boundary (designated as Γ).

On Ω:

$$\nabla^2 T = \frac{1}{a}\frac{\partial T}{\partial t} \tag{A.1.1}$$

On Slab:

$$T(x,0)=T_1,\ -L/2 < x < L/2 \tag{A.1.2}$$

On Γ:

$$T(x,0)=T_2,\ -L/2 > x, \text{ and } L/2 < x \tag{A.1.3}$$

$$T(x,\infty)=T_2. \tag{A.1.4}$$

Let:

$$T = T_{steady} + T_{periodic}, \text{ then} \tag{A.1.5}$$

$$\nabla^2 T_S + \nabla^2 T_p = \frac{1}{a}\frac{\partial T}{\partial t}p \tag{A.1.6}$$

$$\nabla^2 T_s = 0 \tag{A.1.7}$$

and

$$\nabla^2 T_p = \frac{1}{a}\frac{\partial T}{\partial t} \tag{A.1.8}$$

In this section attention will be focused on the steady condition described by Eq. (A.1.7). Changing variables as indicated in in Chap. 4 results in the following:

On Ω:

$$\nabla^2 \Theta_s = 0 \tag{A.1.9}$$

On Slab:

$$\Theta(x^*,0)=1,\ -1/2 < x^* < 1/2 \tag{A.1.10}$$

On Γ:

$$\Theta(x^*,0)=0,\ -1/2 > x^*,\ \text{and}\ 1/2 < x^* \tag{A.1.11}$$

$$\Theta(x^*,\infty)=0. \tag{A.1.12}$$

Solving Eq. (A.1.9) with the boundary conditions can be accomplished by a straight forward application of Poission's Integral Formula for the half plane (Spiegel, 1964). All coordinates will be considered nondimensional and the asterisk notation dropped for brevity.

$$\Theta(x,y) = \frac{1}{\pi}\int\left[\frac{y\ \Theta(x,0)}{(x-\xi)^2+\ y^2}\right]dx \tag{A.1.13}$$

For the particular conditions noted,

$$\Theta(x,y) = \frac{1}{\pi}\int_{-.5}^{+.5}\left[\frac{y}{(x-\xi)^2+\ y^2}\right]\ dx \tag{A.1.14}$$

After integration the result is:

$$\Theta(x,y) = \frac{1}{\pi}\ \arctan\ \frac{y}{x^2+y^2\ -\ .25} \tag{A.1.15}$$

Equation (A.1.15) is the equation of the isotherms when Θ is fixed at a specific value. A graphic representation of Eq. (A.1.15) is illustrated in Fig. 2.1.

A.2 Temperature Field for a Constant Temperature Slab In the Presence of Constant Opposing Heat Flux

The solution to this problem may be found by superposing the solution of the constant temperature slab and the solution of the constant flux temperature fields.

The temperature field for a constant surface temperature slab is given in Appendix A.1 by

$$\Theta'(x,y) = \frac{1}{\pi} \arctan \frac{y}{x^2+y^2 - .25} \tag{A.2.1}$$

The heat flux in a constant opposing flux field is by definition

$$-k\frac{\partial T''}{\partial y} = - q_{crust}\, \mathbf{j} \tag{A.2.2}$$

In nondimensional terms,

$$\frac{\partial \Theta''}{\partial y} = q_{crust} \frac{L}{\lambda \Delta T}\mathbf{j} \tag{A.2.3}$$

Let

$$\tilde{q} = q_{crust} \frac{L}{\lambda \Delta T} \tag{A.2.4}$$

$$\Theta'' = \tilde{q}\, y \tag{A.2.5}$$

By superposition, the temperature field becomes

$$\Theta = \Theta' + \Theta'' \tag{A.2.6}$$

$$\Theta(x,y) = \frac{1}{\pi} \arctan \frac{y}{x^2+y^2 -.25} + \tilde{q}\, y \tag{A.2.7}$$

To find the isotherms, the following relations for heat flux are invoked:

$$\mathbf{q} = -k\Delta T\ \nabla\Theta \tag{A.2.8}$$

$$\mathbf{q} \cdot \mathbf{ds} = 0 \tag{A.2.9}$$

where **ds** is the differential surface element vector which is normal to the constant temperature surface. In two dimensions, this is represented by:

$$\mathbf{ds} = \mathbf{dxi} + \mathbf{dyj} \tag{A.2.10}$$

Combining Eqs. (A.2.8) and (A.2.9) and taking the scalar product results in the following expression:

$$\frac{dy}{dx} = -\frac{\partial\Theta}{\partial x} \Big/ \frac{\partial\Theta}{\partial y} \tag{A.2.11}$$

Differentiating Eq. (A.2.7) and substituting into Eq. (A.2.11) yields the following differential equation:

$$\frac{dy}{dx} = \frac{2xy}{\tilde{\pi q}(x^2+y^2-.25)^2+x^2+(\tilde{\pi q}-1)y^2-.25} \tag{A.2.12}$$

To find the equations for the adiabats, the same procedure is used except the desired expression must be normal to the equation (A.2.11). In two dimensions this may be accomplished by taking the scalar product of the heat flux and the tangent vector along the surface such that:

$$\mathbf{q} \cdot \mathbf{dt} = 0 \tag{A.2.13}$$

where

$$\mathbf{dt} = \mathbf{ds} \times \mathbf{k} \tag{A.2.14}$$

$$\mathbf{dt} = \mathbf{dyi} - \mathbf{dxj} \tag{A.2.15}$$

The result is:

$$\frac{dy}{dx} = \frac{\partial\Theta}{\partial y} \Big/ \frac{\partial\Theta}{\partial x} \tag{A.2.16}$$

The equations for the lines of flux satisfy the following differential equation

$$\frac{dy}{dx} = -\left[\frac{2xy}{\tilde{\pi q}(x^2+y^2-.25)^2+x^2+(\tilde{\pi q}-1)y^2-.25}\right]^{-1} \qquad (A.2.17)$$

A.3 Periodic Heat Flow Through any Point In a One-Dimensional Body

The purpose of this section is to show that a one dimensional body, also known as a semi-infinite slab, when heated at one surface with a periodic surface temperature has zero net flux over any integer multiple of periods for any point in the slab. The following conditions exist:

$$\nabla^2 T_p = \frac{1}{a}\frac{\partial T}{\partial t}p \qquad (A.3.1)$$

$$T_p(0,Y,t) = T_2 \qquad (A.3.2)$$

$$\frac{\partial T}{\partial Y}(X,Y) = 0 \text{ everywhere} \qquad (A.3.3)$$

$$T_p(L,Y,t) = T_1 F(\omega t) \qquad (A.3.4)$$

Where $F(\omega t)$ is a twice differentiable Fourier Series of unit amplitude. The above equations are made nondimensional by defining a time scale such that

$$t^* = t(\ \rho cL^2/\lambda\ )^{-1} \qquad (A.3.5)$$

$$\omega^* = \omega(\ \rho cL^2/\lambda\ )$$

and the length scale previously defined in Chap. 4. The following set of equations results:

On Ω:

$$\frac{\partial^2 \otimes}{\partial x^{*2}} = \frac{\partial \otimes}{\partial t^*} \qquad (A.3.6)$$

On Γ:

$$\Theta(0,t^*) = 0 \qquad (A.3.7)$$

$$\Theta(1,t^*) = F(\omega^* t^*) \qquad (A.3.8)$$

The asterisk notation will be dropped and all variables considered to be nondimensional. Equations (A.3.6) – (A.3.8) may be solved by

using the Laplace transforms to convert the partial differential equation and boundary conditions to an ordinary differential equation. The procedure yields the following equations, where $\hat{\Theta}$ is the transformed temperature function, "D" is the derivative operator and "s" is a complex transform variable:

$$(D^2 - s)_x \hat{\Theta} = 0 \tag{A.3.9}$$

$$\hat{\Theta}(1) = \hat{F} \tag{A.3.10}$$

$$\hat{\Theta}(0) = 0 \tag{A.3.11}$$

the solution of Eqs. (A.3.9) — (A.3.11) is

$$\hat{\Theta} = \hat{F}\,\frac{\sinh(x\sqrt{s})}{\sinh(L\sqrt{s})} \tag{A.3.12}$$

To transform Eq. (A.3.12) back to the time domain, the convolution theorem is used. If

$$\hat{\Theta} = \hat{f}\,\hat{g}\ , \text{ then} \tag{A.3.13}$$

$$\Theta = \int_{\sigma\,=\,0}^{t} f(\sigma)\ g(t-\sigma)\ d\sigma \tag{A.3.14}$$

When applied to this problem

$$\Theta(x,t) = \tag{A.3.15}$$

$$\int_{\sigma\,=\,0}^{t} F(\omega\sigma)\left[\frac{2\pi}{L^2} - \sum_{n=1}^{\infty} n(-1)^n \sin\left(\frac{n\pi x}{L}\right)\exp\left(-n^2\pi^2(t-\sigma)/L^2\right)\right]d\sigma$$

Collecting terms and interchanging the order of integration and summation,

$$\Theta(x,t) = \tag{A.3.16}$$

$$\frac{2\pi}{L^2} - \sum_{n=1}^{\infty} n(-1)^n \sin\left(\frac{n\pi x}{L}\right)\int_{\sigma\,=\,0}^{t} F(\sigma)\left[\exp\left(-n^2\pi^2(t-\sigma)/L^2\right)\right]d\sigma$$

Define a function, $\zeta(x)$ such that

$$\zeta(x) = \frac{2\pi}{L^2} - \sum_{n=1}^{\infty} n(-1)^n \sin\left(\frac{n\pi x}{L}\right) \tag{A.3.17}$$

then

$$\frac{\partial\Theta}{\partial x} = \frac{d\zeta}{dx}\int_{\sigma=0}^{t} F(\omega\sigma)\left[\exp(-n^2\pi^2(t-\sigma)/L^2)\right]d\sigma \tag{A.3.18}$$

The form of $F(\omega t)$ has been assumed to be represented by the Fourier Series

$$F(\omega t) = \sum_{j=1}^{\infty} \{(a_j \cos(j\omega t) + b_j \sin(j\omega t)\} \tag{A.3.19}$$

The sine and cosine terms in the above series will be separated and inserted individually into Eq. (A.3.18). Upon substitution of sine terms from Eq. (A.3.18) into Eq. (A.3.19), the integral becomes

$$\frac{\partial\Theta}{\partial x_j} = \frac{d\zeta}{dx} b_j \int_{\sigma=0}^{t} \sin(j\omega\sigma)\left[\exp(-n^2\pi^2(t-\sigma)/L^2)\right]d\sigma \tag{A.3.20}$$

Let $c = (n\pi/L)^2$ and $d = j\omega$. Then the standard solution for the integral yields

$$I = \int\left[\sin(d\sigma)\exp(c\sigma)d\sigma\right]\exp(-ct)$$

$$= \exp(c(\sigma-t))(c\cdot\sin(d\sigma) - d\cdot\cos(d\sigma))/(c^2 + d^2) \tag{A.3.21}$$

Furthermore, if the following trigonometric substitution is made,

$$\cos\phi = c/(c^2 + d^2)^{0.5} \tag{A.3.22}$$

and $$\sin\phi = d/(c^2 + d^2)^{0.5}$$

This substitution makes the integral in Eq. (A.3.21) become

$$I = \exp(c(\sigma-t))\sin(d\sigma + \phi)/(c^2 + d^2)^{0.5}\Big]_{\sigma=0}^{t} \tag{A.3.23}$$

$$= (\sin(dt - \phi) + e^{-ct}\sin\phi)/(c^2 + d^2)^{0.5} \tag{A.3.24}$$

The final result for the j^{th} sine component of the heat flux is

$$\frac{\partial \Theta}{\partial x_j} = \frac{d\zeta}{dx} b_j (\sin(dt - \phi) + e^{-ct}\sin\phi)/(c^2 + d^2)^{0.5} \qquad (A.3.25)$$

After a sufficiently long time, the exponential term dies out leaving the sine term. The integral of the sine over one period or multiple of periods is zero. The same method applies to the cosine terms. For the j^{th} cosine term, the result is

$$\frac{\partial \Theta}{\partial x_j} = \frac{d\zeta}{dx} a_j (\sin(dt + \phi) + e^{-ct}\sin\phi)/(c^2 + d^2)^{0.5} \qquad (A.3.26)$$

Again, the exponential term vanishes after sufficient time.

Seasonal periodicity is a reasonable approximation to weather patterns which influence the building environment. This analysis indicates that only the steady problem affects the heat transfer from a seasonal perspective as discussed in Chap. 3.

APPENDIX B

FINITE DIFFERENCE APPROXIMATIONS

B.1 The Governing Equations

The governing equations, Eqs. (4.43), (4.44) and (4.46), are appropriate for describing thermally induced porous media flow. For the particular case of a two dimensional, rectangular domain and the gravity vector oriented in the negative y direction, the nondimensional equations can be written in component form as

$$u\frac{\partial\Theta}{\partial x} + v\frac{\partial\Theta}{\partial y} = \frac{\partial^2\Theta}{\partial x^2} + \frac{\partial^2\Theta}{\partial y^2} \tag{B.1.1}$$

letting $\Phi = \mathfrak{R}\, P_D$, then

$$\frac{\partial^2\Phi}{\partial x^2} + \frac{\partial^2\Phi}{\partial y^2} = \frac{\partial\nu}{\partial\Theta}\left(\frac{\partial^2\Phi}{\partial x^2} + \frac{\partial^2\Phi}{\partial y^2}\right) - \mathfrak{R}\,\frac{\partial\rho}{\partial\Theta}\,\frac{\partial\Theta}{\partial y} \tag{B.1.2}$$

and

$$u = -\frac{\partial\Phi}{\partial x}/\nu \tag{B.1.3}$$

$$v = -[\frac{\partial\Phi}{\partial y} + \mathfrak{R}\,(\rho - 1)]/\nu \tag{B.1.4}$$

Equations (5.10)—(5.14) define the operators to be used to form the difference equations. For convenience, the central difference operator will be redefined as:

$$\delta_x^2\, u_{i,j} = -2I_u + 0_{x,u} = (-2I + 0_x)_u \tag{B.1.5}$$

where

$$I_u = u_{i,j} = u(i,j), \text{ and}$$

$$0_{x,u} = u(i+1,j) + u(i-1,j)$$

Using the above notation,

$$u = -\delta_x\Phi/(2\Delta x\nu) \tag{B.1.6}$$

$$v = -[\delta_y\Phi/(2\Delta y) + \Re\,(\rho - 1)]/\nu \tag{B.1.7}$$

$$(-2I + 0_x)_\Theta/\Delta x^2 + (-2I + 0_y)_\Theta/\Delta y^2 = u(\delta_x\Theta)/(2\Delta x) + v\,(\delta_y\Theta)/(2\Delta y), \text{ and} \tag{B.1.8}$$

$$(-2I + 0_x)_\Phi\Delta x^2 + (-2I + 0_y)_\Phi/\Delta y^2 = \frac{\partial\nu}{\partial\Theta}\,[(-2I + 0_x)_\Theta/\Delta x^2 + (-2I + 0_y)_\Theta/\Delta y^2] + \Re\,\frac{\partial\rho}{\partial\Theta}\,(\delta_y\Theta)/(2\Delta y) \tag{B.1.9}$$

For uniform grid spacing, $\Delta x = \Delta y$. Combining terms, Eq. (B.1.8) becomes

$$(-4I + 0_x + 0_y)_\Theta/\Delta y^2 = [u(\delta_x\Theta) + v\,(\delta_y\Theta)]/(2\Delta y), \tag{B.1.10}$$

and Eq. (B.1.9) becomes

$$(-4I + 0_x + 0_y)_\Phi/\Delta y^2 = \frac{\partial\nu}{\partial\Theta}\,(-4I + 0_x + 0_y)_\Theta/\Delta y^2 + \Re\,\frac{\partial\rho}{\partial\Theta}\,(\delta_y\Theta)/(2\Delta y) \tag{B.1.11}$$

where

$$u = -(\Phi(i+1,j) - \Phi(i-1,j))/(2\Delta x\nu) \tag{B.1.12}$$

$$v = -[(\Phi(i,j+1) - \Phi(i,j-1))/(2\Delta y) + \Re\,(\rho - 1)]/\nu \tag{B.1.13}$$

These equations can be made tridiagonal if the off diagonal terms are treated as known values. The initial solution is found for no mass flow in the media.

$$(-4I + 0_x + 0_y)_\Theta = 0 \tag{B.1.14}$$

This may be solved by lines by re-arranging the Eq. (B.1.14)

$$(4I - 0_x)_\Theta = 0_{y,\Theta} \tag{B.1.15}$$

$$(4I - 0_y)_\Theta = 0_{x,\Theta} \tag{B.1.16}$$

subject to the thermal boundary conditions. These results are fed into Eqs. (B.1.11)—(B.1.13) and solved in a similar manner as Eqs. (B.1.15) and (B.1.16).

B.2 The Boundary Conditions

The thermal and velocity boundary conditions for this problem are grouped into two classes. Class I represents the conditions associated the impermeable domain and are delineated as follows:

1. Convective heat transfer at the slab and earth/air interface.
2. Adiabatic condition at the remote earth and symmetry boundary.
3. Impermeable surface surrounding the entire domain so that no mass flux is possible.

Case II represents the condition where evapotranspiration is allowed and will be modeled specifically for evaporation at the earth surface. These conditions are summarized as follows:

1. Convective heat transfer at the slab and earth/air interface.
2. Evaporation at the earth/air interface.
3. Adiabatic condition at remote earth and symmetry boundary.
4. Permeable boundary over some portion of the domain limits to allow for the steady flow of water.

The thermal equations may be generalized from Eq. (7.14) for any location as

$$\frac{\partial \Theta}{\partial y} + Bi\Theta = Bi\Theta_{\infty} - 1.171(Bi/Ste)(\omega - \omega_2) \qquad (B.2.1)$$

For the slab surface: $Bi = Bi_1$; $\Theta_{\infty} = 1$; and, $\omega(\Theta) = \omega_2$. For adiabatic boundaries: $Bi = 0$ and $\omega(\Theta) = \omega_2$. For the earth surface, the conditions are selected by choosing the Biot number, ω and Θ_{∞} for the appropriate case. In Chaps. 5 and 6, $Bi = Bi_2$ and $\Theta_{\infty} = 0$. These conditions were relaxed in Chap. 7 at the earth surface for the particular case where $Bi_2 = 30$, $\Theta_{\infty} = .1$ and $\omega = \omega(\Theta)$. For example, when made discrete for the slab surface, Eq. (B.2.1) becomes

$$-4\Theta(i,j-1) + (3 + \Delta y Bi_1)\Theta(i,j) + \Theta(i,j-2) = 2\Delta y Bi_1$$

For the velocity conditions in the x and y directions,

$$\nu u = \frac{\partial \Phi}{\partial x}, \text{ and}$$

$$\nu v = -(\frac{\partial \Phi}{\partial y} + \Re(\rho-1))$$

These are made discrete at a boundary as follows:

$$-4\Phi(i+1,j) + 3\Phi(i,j) + \Phi(i+2,j) = -2\Delta x \nu u$$

$$-4\Phi(i,j+1) + 3\Phi(i,j) + \Phi(i,j+2) = -2\Delta y(\nu v + \Re(\rho-1))$$

For an impermeable boundary, the appropriate velocity is set to zero.

B.3 The SLAB Code

The SLAB code is the title for a series of programs used to compute data for porous media flow. The essential feature of SLAB is that temperature and pressure fields are computed iteratively by lines in alternating directions and successively over-relaxed.

After the initial physical parameters and geometric data are entered into the data files, SLAB produces a pressure and temperature solution set and stores this data for post-processing. Figure B.1 illustrates the logic flow for this program. The post-processing is performed by a series of programs, the function of which is briefly outlined here:

MESH is a program designed to improve accuracy of the solution sets by decreasing the step size in each direction by half. The output from MESH is a new, intermediate solution set that can re-processed by SLAB main data program for a more accurate solution.

VELOCITY is a program that may be invoked to post-process the solution set and produce flow data. These data are used in conjunction with the temperature and pressure solution sets as input to STREAM

program. STREAM is designed to compute the streamfunction of the flow field. The streamfunction is a helpful way to visualize two dimensional flow fields.

Graphical numerical analysis and presentation were produced by "AXUM", under license agreement to TriMetrix, Inc., 444 N.E. Ravenna Blvd., Suite 210, Seattle, WA 98115.

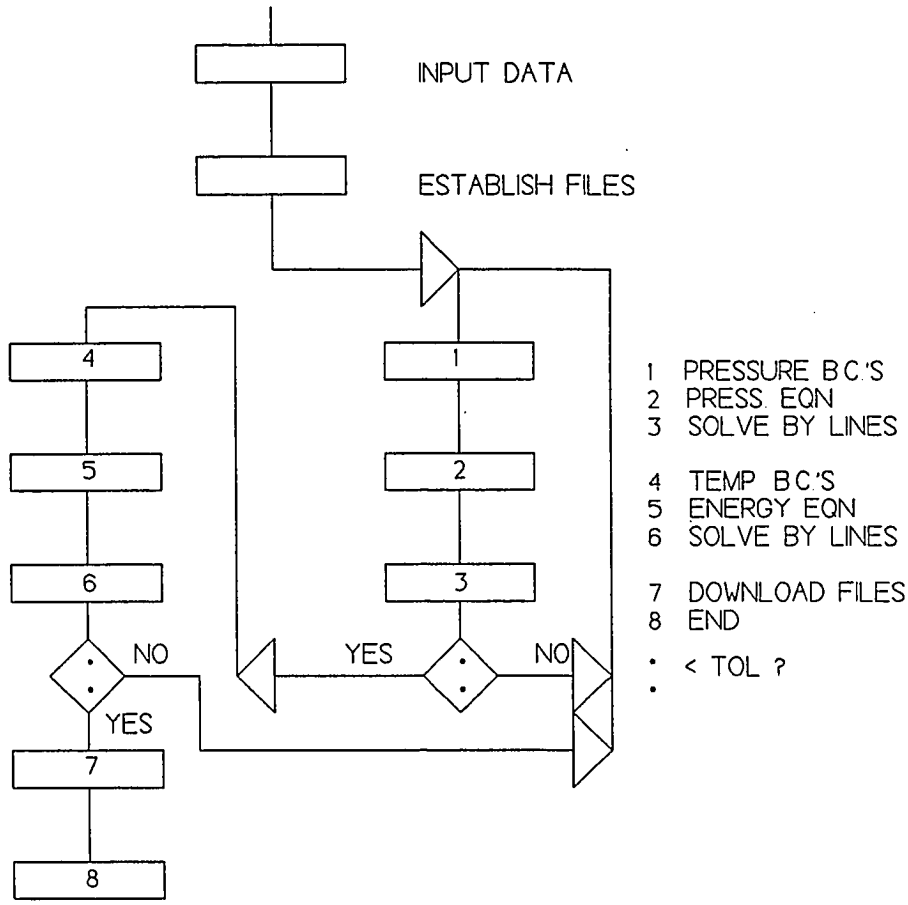

Fig. B.1 Logic diagram for SLAB code.

PROGRAM LISTING

```
10   REM PROGRAM NAME:  SLAB BY W.W. RUST
20   PRINT "ENTER THE NAME OF THE DATA FILES LESS SPECIFIER"
30   LINE INPUT "INPUT ROOT NAME OF DATA FILE,NOT INCLUDING
     SPECIFIER.:"; F$
40   LINE INPUT "READ DATA OR START FROM SCRATCH? <FILE> <SCRATCH>"; G$
50   IF G$ = "F" OR G$ = "f" THEN GOSUB 2160: GOTO 120
60   IF G$ = "S" OR G$ = "s" THEN GOSUB 2090: GOTO 120
70   GOTO 40
80   IF M > N THEN V = M ELSE V = N
90   DIM P(M, N), T(M, N), B(M, N), C(M, N), A1(V), B1(V), C1(V), D1(V),
     TT(V)
100  RETURN
110  REM  SHAPE DATA *****
120  GG = INT(10*.5/L*M + .5)/10
130  TOL = .001: TR = (T1 + T2)/2: T3 = .1
140  REM NUMERICS *****
150  W = 1.75
160  B$ = RIGHT$(F$, 1)
170  REM IF B$ = "2" OR B$ = "3" OR B$ = "4" THEN W = 1.75
180  REM DEFINE PROPERTIES *****
190  NU1 = .568887: NU2 = .200372683#
200  DEF FNNU (I, J) = 1 - NU1*(T(I, J) - .5) + NU2*(T(I, J) - .5) ^ 2
210  DEF FNDNU (I, J) = -NU1 + 2*NU2*(T(I, J) - .5)
220  RHO1 = .001587423#: RHO2 = .00279274#
230  DEF FNRHO (I, J) = -RHO1*(T(I, J) - .5) - RHO2*(T(I, J) - .5) ^ 2
240  DEF FNDRHO (I, J) = -RHO1 - 2*RHO2*(T(I, J) - .5)
250  DEF FNW (X) = -.5076 + 4.307*X + 7.6902*X ^ 2: REM 2C AT 50%rh
260  DEF FNEVAP (X) = 2.8128E-04*BI*R*FNW(X)
270  REM COMPUTING APPROXIMATIONS *****
280  DEF FNU (I, J) = -(P(I + 1, J) - P(I - 1, J))/2/DX/FNNU(I, J)
290  DEF FNV (I, J) = -((P(I, J + 1) - P(I, J - 1))/2/DY + RB*FNRHO(I,
     J))/FNNU(I, J)
300  DEF FNA (I, J) = FNU(I, J)*(T(I + 1, J) - T(I - 1, J))*DX/2
310  DEF FNB (I, J) = FNV(I, J)*(T(I, J + 1) - T(I, J - 1))*DY/2
320  DEF FNT (I, J) = -FNDNU(I, J)*(T(I + 1, J) + T(I - 1, J) - 4*T(I,
     J) + T(I, J + 1) + T(I, J - 1))
330  DEF FNS (I, J) = -RB*FNDRHO(I, J)*(T(I, J + 1) - T(I, J - 1))*DY/2
340  DEF FNDY (I, J) = (3*T(I, J) + T(I, J - 2) - 4*T(I, J - 1))/2: REM
     y derivative top surface
350  DEF FNDX (I, J) = (T(I + 1, J) - T(I - 1, J))/2
360  DEF FNQ (I, J) = -FNDX(I, J) + FNU(I, J)*T(I, J)*DY
370  GOSUB 1670: REM LOAD TEMP COMP MATRIX
380  GOSUB 2560: REM FILL IN CORNERS
390  GOSUB 1210: REM FORWARD ADI TEMP
400  GOSUB 1280: REM BACKWARD ADI TEMP
410  GOSUB 3010: GOSUB 3590: REM HEAT FLUX
420  GOSUB 3300: REM FORWARD ADI PRESSURE
430  GOSUB 3770: REM INLET VELOCITY COMPUTATION
440  GOSUB 2950: REM FILL IN CORNERS
450  GOSUB 1880: REM CHECK PREVIOUS VALUES OF PRESSURE
```

```
460  IF EE > 1*TOL THEN PRINT EE: GOTO 420
470  GOSUB 2560: REM FILL IN CORNERS
480  GOSUB 1670: REM CHECK PREVIOUS VALUES OF TEMPERATURE
490  IF EE > TOL THEN PRINT EE: GOTO 390
500  GOSUB 1210: GOSUB 3300: REM FINAL ITERATION
510  GOSUB 2560: GOSUB 2950: REM FILL IN CORNERS
520  GOSUB 2380: REM SAVE DATA TO DISK
560  END
570  REM ESTABLISH THERMAL CONDITIONS X DIRECTION
580  XX = M
590  D1(0) = 3: A1(0) = -4: C1(0) = 0: B1(0) = 1: REM lHS
600  D1(XX) = 3: B1(XX) = -4: C1(XX) = 0: A1(XX) = 1: REM RHS
610  A = -1: B = -1: D = 4
620  FOR K = 1 TO XX - 1
630  D1(K) = D
640  A1(K) = A
650  B1(K) = B
660  C1(K) = T(K, J + 1) + T(K, J - 1) - (FNA(K, J) + FNB(K, J))
670  NEXT K
680  RETURN
690  REM BOUNDARY CONDITIONS IN Y DIRECTION ON TEMPERATURE
700  XX = N
710  D1(0) = 3: A1(0) = -4: C1(0) = 0: B1(0) = 1
720  IF I < GG THEN D1(XX) = 3 + 2*DX*BI: A1(XX) = 1: C1(XX) = 2*DX*BI:
     B1(XX) = -4: GOTO 750
730  IF I > GG THEN D1(XX) = 3 + 2*DX*R*BI: A1(XX) = 1: C1(XX) =
     2*DX*BI*R*(T3 - .14434*FNW(T(I, XX))): B1(XX) = -4: GOTO 750
740  D1(XX) = 3: A1(XX) = 1: C1(XX) = 0: B1(XX) = -4: REM I=gg
750  A = -1: B = -1: D = 4
760  FOR K = 1 TO XX - 1
770     D1(K) = D
780     A1(K) = A
790     B1(K) = B
800     C1(K) = T(I + 1, K) + T(I - 1, K) - (FNA(I, K) + FNB(I, K))
810  NEXT K
820  RETURN
830  REM SOLVER ALGORITHM
840  REM ENTER WITH TT(I) DEPENDENT VARIABLE
850  REM 0=< K<= XX
860  FOR K = 1 TO XX
870      IF K = 1 THEN GOSUB 980: GOTO 910
880      IF K = XX THEN GOSUB 1060
890      D1(K) = D1(K) - B1(K)*A1(K - 1)/D1(K - 1)
900      C1(K) = C1(K) - B1(K)*C1(K - 1)/D1(K - 1)
910  NEXT K
920  TT(XX) = C1(XX)/D1(XX)
930  FOR K = XX - 1 TO 0 STEP -1
940      IF K = 0 THEN GOSUB 1030: GOTO 960
950      TT(K) = (C1(K) - A1(K)*TT(K + 1))/D1(K)
960  NEXT K
970  RETURN
980  REM FIRST "ZEROTH" ROW
990  D1(1) = D1(1) - B1(1)*A1(0)/D1(0)
1000 A1(1) = A1(1) - B1(1)*B1(0)/D1(0)
```

```
1010 C1(1) = C1(1) - B1(1)*C1(0)/D1(0)
1020 RETURN
1030 REM BACK SUBSTITUTION ON FIRST ROW
1040 TT(0) = (C1(0) - A1(0)*TT(1) - B1(0)*TT(2))/D1(0)
1050 RETURN
1060 REM LAST ROW WITH EXTRA TERM
1070 B1(XX) = B1(XX) - A1(XX - 2)*A1(XX)/D1(XX - 2)
1080 C1(XX) = C1(XX) - C1(XX - 2)*A1(XX)/D1(XX - 2)
1090 RETURN
1100 REM SUBSTITUTE IN X DIRECTION ON TEMPERATURE
1110 FOR K = 0 TO M
1120   T(K, J) = TT(K)
1130 NEXT K
1140 RETURN
1150 REM SUBSTITUTE IN Y DIRECTION ON TEMPERATURE
1160 FOR K = 0 TO N
1170   T(I, K) = TT(K)
1180 NEXT K
1190 RETURN
1210 REM THERMAL ADI ROUTINE
1220 PP = 1: QQ = 1: I = 1: J = 1
1230 FOR ADI = 1 TO V*2
1240    IF ADI = 2*INT(ADI/2) THEN GOSUB 1350: GOTO 1260
1250    GOSUB 1460
1260 NEXT ADI
1270 RETURN
1280 REM THERMAL ADI ROUTINE BACKWARDS
1290 PP = N - 1: QQ = M - 1: I = M - 1: J = N - 1
1300 FOR ADI = V*2 TO 1 STEP -1
1310    IF ADI = 2*INT(ADI/2) THEN GOSUB 1410: GOTO 1330
1320    GOSUB 1520
1330 NEXT ADI
1340 RETURN
1350 REM X DIRECTION ADI
1360    IF PP > N - 1 THEN PP = 1
1370    J = PP
1380    GOSUB 1570
1390    PP = PP + 1
1400 RETURN
1410 REM X DIRECTION ADI BACKWARDS
1420    IF PP < 1 THEN PP = N - 1
1430    GOSUB 1570
1440    PP = PP - 1
1450 RETURN
1460 REM ADI Y DIRECTION
1470 IF QQ > M - 1 THEN QQ = 1
1480    I = QQ
1490    GOSUB 1620
1500    QQ = QQ + 1
1510 RETURN
1520 REM ADI Y DIRECTION BACKWARDS
1530    IF QQ < 1 THEN QQ = M - 1
1540    GOSUB 1620
1550    QQ = QQ - 1
```

```
1560 RETURN
1570 REM WORKING SUBROUTINE
1580 GOSUB 570
1590 GOSUB 830
1600 GOSUB 1100
1610 RETURN
1620 REM WORKING SUBROUTINE
1630 GOSUB 690
1640 GOSUB 830
1650 GOSUB 1150
1660 RETURN
1670 REM TEMPERATURE RELAXATION
1680 EE = 0: RR = RR + 1
1690 FOR I = 0 TO M
1700    FOR J = 0 TO N - 1
1710    IF RR > 1 THEN T(I, J) = B(I, J) + W*(T(I, J) - B(I, J))
1720    EF = ABS(T(I, J) - B(I, J))
1730    IF EF > EE THEN EE = EF
1740    B(I, J) = T(I, J)
1750    NEXT J
1760 NEXT I
1770 RETURN
1880 REM PRESSURE RELAXATION
1890 EE = 0
1900 FOR I = 0 TO M
1910    FOR J = 0 TO N
1920    IF RR > 1 THEN P(I, J) = C(I, J) + .85*(P(I, J) - C(I, J))
1930    EF = ABS(P(I, J) - C(I, J))
1940    C(I, J) = P(I, J)
1950    IF EF > EE THEN EE = EF
1960    NEXT J
1970 NEXT I
1980 RETURN
2090 REM SCRATCH ROUTINE
2100 M = 8: N = 8
2110 L = 1: H = 1
2120 DX = L/M: DY = H/N
2130 T1 = 1: T2 = 0: RB = 0: BI = 30: R = 1
2140 GOSUB 80
2150 RETURN
2160 REM DATA INPUT FROM FILE
2170 OPEN "I", 1, F$ + "T.DAT"
2180 OPEN "I", 2, F$ + "P.DAT"
2190 INPUT #1, M, N, DX, DY, T1, T2, RB, BI, R
2200 L = M*DX: H = N*DY
2210 GOSUB 80
2220 FOR I = 0 TO M
2230     FOR J = 0 TO N
2240     INPUT #1, T(I, J)
2250     NEXT J
2260 NEXT I
2270 CLOSE
2280 OPEN "I", 2, F$ + "P.DAT"
2290 INPUT #2, M, N, DX, DY, T1, T2, RB, BI, R
```

```
2300 FOR I = 0 TO M
2310     FOR J = 0 TO N
2320     INPUT #2, B
2330     P(I, J) = B
2340     NEXT J
2350 NEXT I
2360 CLOSE
2370 RETURN
2380 REM SAVE DATA TO DISK
2390 OPEN "O", 1, F$ + "T.DAT"
2400 PRINT #1, M, N, DX, DY, T1, T2, RB, BI, R
2410 FOR I = 0 TO M
2420    FOR J = 0 TO N
2430     PRINT #1, T(I, J);
2440    NEXT J
2450 NEXT I
2460 CLOSE
2470 OPEN "O", 2, F$ + "P.DAT"
2480 PRINT #2, M, N, DX, DY, T1, T2, RB, BI, R
2490 FOR I = 0 TO M
2500    FOR J = 0 TO N
2510     PRINT #2, P(I, J);
2520    NEXT J
2530 NEXT I
2540 CLOSE
2550 RETURN
2560 REM FILL IN CORNERS
2570 T(0, 0) = (4*T(1, 0) - T(2, 0))/3: T(0, N) = (4*T(1, N) - T(2,
     N))/3
2580 T(M, 0) = (4*T(M - 1, 0) - T(M - 2, 0))/3: T(M, N) = (4*T(M - 1, N)
     - T(M - 2, N))/3
2590 RETURN
2600 REM BOUNDARY CONDITIONS X DIRECTION ON PRESSURE
2610 XX = M
2620 D1(0) = 3: A1(0) = -4: C1(0) = 0: B1(0) = 1: REM lHS
2630 D1(XX) = 3: B1(XX) = -4: C1(XX) = 2*DY*UU*FNNU(XX, J): A1(XX) = 1:
     REM RHS
2640 A = -1: B = -1: D = 4
2650 FOR K = 1 TO XX - 1
2660 D1(K) = D
2670 A1(K) = A
2680 B1(K) = B
2690 C1(K) = P(K, J + 1) + P(K, J - 1) - FNT(K, J) - FNS(K, J)
2700 NEXT K
2710 RETURN
2720 REM BOUNDARY CONDITIONS IN Y DIRECTION ON PRESSURE
2730 XX = N
2740 D1(0) = 3: A1(0) = -4: C1(0) = -2*DY*(-RB*FNRHO(I, 0)): B1(0) = 1
2750 D1(XX) = 3: A1(XX) = 1: C1(XX) = -2*DY*(FNEVAP(T(I, XX)) +
     RB*FNRHO(I, XX)): B1(XX) = -4
2760 A = -1: B = -1: D = 4
2770 FOR K = 1 TO XX - 1
2780    D1(K) = D
2790    A1(K) = A
```

```
2800     B1(K) = B
2810     C1(K) = P(I + 1, K) + P(I - 1, K) - FNT(I, K) - FNS(I, K)
2820 NEXT K
2830 RETURN
2840 REM SOLVER ALGORITHM
2850 REM SUBSTITUTE IN X DIRECTION ON PRESSURE
2860 FOR K = 0 TO M
2870   P(K, J) = TT(K)
2880 NEXT K
2890 RETURN
2900 REM SUBSTITUTE IN Y DIRECTION ON PRESSURE
2910 FOR K = 0 TO N
2920   P(I, K) = TT(K)
2930 NEXT K
2940 RETURN
2950 REM FILL IN CORNERS
2960 P(0, 0) = (P(0, 1) + P(1, 0) - DY*R*FNRHO(0, 0))/2
2970 P(0, N) = (P(M, 1) + P(M - 1, 0) - DY*R*FNRHO(M, 0))/2
2980 P(M, 0) = (P(0, N - 1) + P(1, N) + DY*R*FNRHO(0, N))/2
2990 P(M, N) = (P(M, N - 1) + P(M - 1, N) + DY*R*FNRHO(M, N))/2
3000 RETURN
3010 REM COMPUTE HEAT LOST UNDER SURFACES
3020 GOSUB 3240: REM INSPECT SURFACE NODES
3030 PRINT "HOT SIDE"
3040 SS = 0: YY = 0: XX = 0: ZZ = 0
3050 AA = 0: BB = GG
3060 GOSUB 3120
3070 SS = 0: YY = 0: XX = 0: ZZ = 0
3080 AA = GG: BB = M
3090 PRINT "COLD SIDE"
3100 GOSUB 3120
3110 RETURN
3120 REM INTEGRATING SUBROUTINE
3130 FOR I = AA + 1 TO BB - 1
3140    XX = XX + 1
3150    SS = SS + FNDY(I, N)
3160    IF XX = 2*INT(XX/2) THEN YY = YY + FNDY(I, N) ELSE ZZ = ZZ +
    FNDY(I, N)
3170 NEXT I
3180 IF XX = 2*INT(XX/2) THEN GOSUB 3220 ELSE GOSUB 3200
3190 RETURN
3200 PRINT "SIMPSON'S RULE"; (FNDY(AA, N) + FNDY(BB, N) + 2*YY + 4*ZZ)/3
3210 RETURN
3220 PRINT "TRAPEZOIDAL RULE"; (FNDY(AA, N) + FNDY(BB, N))/2 + SS
3230 RETURN
3240 REM INSPECT SURFACE NODES
3250 FOR I = 0 TO M
3260    PRINT USING " #.###"; T(I, N);
3270 NEXT I
3280 PRINT
3290 RETURN
3300 IF RB = 0 THEN RETURN: REM PRESSURE ADI ROUTINE
3310 PP = 1: QQ = 1: I = 1: J = 1
3320 FOR ADI = 1 TO V*2
```

```
3330    IF ADI = 2*INT(ADI/2) THEN GOSUB 3370: GOTO 3350
3340    GOSUB 3430
3350 NEXT ADI
3360 RETURN
3370 REM X DIRECTION ADI
3380    IF PP > N - 1 THEN PP = 1
3390    J = PP
3400    GOSUB 3490
3410    PP = PP + 1
3420 RETURN
3430 REM ADI Y DIRECTION
3440 IF QQ > M - 1 THEN QQ = 1
3450    I = QQ
3460    GOSUB 3540
3470    QQ = QQ + 1
3480 RETURN
3490 REM WORKING SUBSUBROUTINE
3500 GOSUB 2600
3510 GOSUB 830
3520 GOSUB 2850
3530 RETURN
3540 REM WORKING SUBROUTINE
3550 GOSUB 2720
3560 GOSUB 830
3570 GOSUB 2900
3580 RETURN
3590 REM CENTRAL HEAT FLUX
3600 PRINT "CENTRAL"
3610 SS = 0: YY = 0: XX = 0: ZZ = 0
3620 AA = 0: BB = N: CC = GG
3630 GOSUB 3650
3640 RETURN
3650 REM INTETRATING SUBROUTINE
3660 FOR J = AA + 1 TO BB - 1
3670    XX = XX + 1
3680    SS = SS + FNQ(CC, J)
3690    IF XX = 2*INT(XX/2) THEN YY = YY + FNQ(CC, J) ELSE ZZ = ZZ +
    FNQ(CC, J)
3700 NEXT J
3710 IF XX = 2*INT(XX/2) THEN GOSUB 3750 ELSE GOSUB 3730
3720 RETURN
3730 PRINT "SIMPSON'S RULE"; (FNQ(CC, AA) + FNQ(CC, BB) + 2*YY + 4*ZZ)/3
3740 RETURN
3750 PRINT "TRAPEZOIDAL RULE"; (FNQ(CC, AA) + FNQ(CC, BB))/2 + SS
3760 RETURN
3770 REM VELOCITY INTETRATING SUBROUTINE
3780 SS = 0: YY = 0: XX = 0: ZZ = 0
3790 AA = GG: BB = M
3800 FOR I = AA + 1 TO BB - 1
3810    XX = XX + 1
3820    SS = SS + FNEVAP(T(I, N))
3830    IF XX = 2*INT(XX/2) THEN YY = YY + FNEVAP(T(I, N)) ELSE ZZ = ZZ
    + FNEVAP(T(I, N))
3840 NEXT I
```

```
3850 IF XX = 2*INT(XX/2) THEN GOSUB 3890 ELSE GOSUB 3870
3860 RETURN
3870 UU = (FNEVAP(T(AA, N)) + FNEVAP(T(BB, M)) + 2*YY + 4*ZZ)/3/N
3880 RETURN
3890 UU = ((FNEVAP(T(AA, N)) + FNEVAP(T(BB, M)))/2 + SS)/N
3900 RETURN
```

APPENDIX C

MATERIAL PROPERTIES AND MEASUREMENTS

Properties used in the experimental work were extracted from various sources. Table C.1 is a listing of pertinent properties of solids. The metric values appear in this tabulation are shown on the upper line and English values are located beneath the line. Properties of water have been approximated using a least squares fit of tabulated data[1].

Viscosity:

$$\nu^* = 1 + a_1(\Theta - .5) + a_2(\Theta - .5)^2, \text{ where} \qquad (C.1)$$

$a_1 = -0.568887$

$a_2 = \ \ 0.200373$

$\nu_r = 13.116 \text{ X } 10^{-7} \text{ m}^2/\text{s}$

Density:

$$\rho^* = 1 + b_1(\Theta - .5) + b_2(\Theta - .5)^2, \text{ where} \qquad (C.2)$$

$b_1 = -0.00158742$

$b_2 = -0.00279274$

$\rho_r = 999.69 \text{ Kg/m}^3$

Table C.2 is a listing of data collected during the calibration procedure for the test apparatus.

---

[1]Liley, P.E., "Thermophysical Properties," **Handbook of Single-Phase Convective Heat Transfer**, S. Kakac, R.K. Shah, and W. Aung, Eds., John Wiley and Sons, New York, 1987, p. 22·30–22·32.

Table C.1 Properties of solids

Material	Density	Specific Heat	Thermal Conductivity
	Kg/m^3 / lb/ft^3	W-s/kg-^{o}K / BTU/lb-^{o}F	W/m-^{o}K / BTUH/ft-^{o}F
Acrylite	1190	1470 / 0.35	0.19 / 0.108 [2]
Styrofoam	1.8-3.5	0.29	0.0167 [3]
Water			0.348 [3]
Glass	154	0.18	0.59 [3]
Glass			0.59(200F) [4]
Glass		673	1.046(20C) [5]
Glass	2500	670	0.74(80C) [6]
Glass	2707	800	.76(20C) [7]

[2]"Physical Properties of Acrylite FF Acrylic Sheet," CYRO Industries, Mt. Arlington, NJ, 1987, p. 6.

[3]"Physical Properties of Materials," **ASHRAE Handbook of Fundamentals, I-P Edition,** American Society of Heating Refrigerating and Air Conditioning Engineers, Inc., Atlanta, GA, 1989, p. 37.1-37.4.

[4]Baumeister, T., ed., **Marks' Standard Handbook for Mechanical Engineers,** McGraw-Hill Book Company, New York, 1967, p. 4-95.

[5]Hodgman, C.D., R.C. Weast, R.S. Shankland, and S.M. Selby, eds., **Handbook of Chemistry and Physics,** The Chemical Rubber Publishing Co., Cleveland, Ohio, 1963, p. 2531.

[6]Isachenko, V.P., V.A. Osipova, and A.S. Sukomel, **Heat Transfer,** Mir Publishers, Moscow, 1980, pp. 477-479.

[7]Eckert, E.R.G., and R.M. Drake, Jr., **Analysis of Heat and Mass Transfer,** McGraw-Hill Book Company, New York, 1972, p. 772-785.

Table C.2 Calibration data for test cell

Time	Cold plate temp at location, deg F			Hot plate temp at location, deg F			Room temp, deg F	Discharge vol, ml
	C1	C2	C3	H1	H2	H3		
0930	33.0	33.0	33.0	38.0	38.0	38.0	68.0	00.00
1100	33.0	33.0	33.0	37.0	37.0	37.0	68.0	10.68
1130	32.0	32.0	32.0	36.0	36.0	36.0	68.0	10.08
1200	33.0	33.0	33.0	36.0	36.0	36.0	69.0	13.41
1230	32.0	32.0	32.0	34.0	34.0	34.0	68.0	22.50
1300	32.0	32.0	32.0	34.0	34.0	34.0	70.0	10.40
1330	33.0	33.0	33.0	35.0	35.0	35.0	68.0	9.08
1400	33.0	32.0	33.0	33.0	33.0	33.0	69.0	20.56
1430	32.0	32.0	32.0	35.0	35.0	35.0	69.0	1.96
1515	32.0	32.0	32.0	35.0	35.0	35.0	69.0	21.63

DATE: 28 Feb 1990

CONFIGURATION: Test cell removed and replaced with one inch styrofoam block. Ice is placed in both the heating and cooling chamber.